University of Stavanger

Faculty of Science and Technology

MASTER'S THESIS

Study program/Specialization: **MSc in Petroleum Engineering / Drilling**	Spring semester, 2017 Open
Writer: **Thomas Horpestad**	..... (Writer's signature)
Supervisor: **Dan Sui**	
Thesis title: **An investigation into the heat transfer process in petroleum wells, and a comprehensive modeling study investigating the temperature distribution in production wells**	
Credits (ECTS): 30	
Key words: **Temperature model** **Heat transfer in production well** **Production well temperature distribution** **Free/natural convection in multiple annulus** **Overall heat transfer coefficient**	Pages: 127 + enclosure: 26 Stavanger, 15/06-2017 Date/year

Frontpage for master's thesis
Faculty of Science and Technology
Decision made by the Dean October 30th 2009

Master's Thesis

An investigation into the heat transfer process in petroleum wells, and a comprehensive modeling study investigating the temperature distribution in production wells

Thomas Horpestad

Faculty of Science and Technology
University of Stavanger

This thesis is submitted for the degree of
Master of Science

June 2017

Acknowledgements

I would like to thank my supervisor, Associate Prof. Dan Sui at the University of Stavanger, for her excellent guidance and our good discussions during this semester.

A big thank you also goes out to my dear Tea Kristina for taking taking extra responsibility for our newborn son during this semester. It was a huge relief, and gave me freedom to focus on the work ahead of me.

Abstract

When producing hot fluid from a reservoir, the production well experiences changing temperatures with depth for the different tubing, casing, cement and wellbore interfaces. To what extent the temperatures change is depending on many factors. The production flow rate, produced fluid specific heat capacity, thermal conductivity and viscosity of the annular fluids, the Joule-Thomson effect on the produced fluid, radius of the wellbore, annular clearance, and production time, are some of the parameters playing an important role in determining the heat transfer across the wellbore between the produced fluid and the formation.

A wellbore heat transfer model for a single phase oil production scenario, based on the wellbore heat transfer model presented by Hasan, Kabir, and Wang (2009), has been implemented in the MATLAB ® software. The model considers a fairly complex wellbore configuration, consisting of five wellbore sections of different configuration, with the possibility of natural/free convection taking place in three brine filled annulus. Correlations taking temperature and/or pressure into consideration has been implemented for all thermophysical properties in the wellbore, such as thermal conductivity of tubing, casing, and cement, specific heat capacity, viscosity, thermal conductivity of annular fluids, and densities of produced and annular fluids, to mention some. The MATLAB program allows for custom well configurations, and is able to calculate the temperatures at all the wellbore, casings and tubing interfaces, and has the ability to use other fluid, casing/tubing, cement and formation properties than the ones used in this study.

Table of contents

List of figures

List of tables

Chapter 1

Introduction

1.1 Reaserch problem

Estimating correct casing and tubing temperatures in completed wells are of great importance for multiple applications. To accurately carry out stress analysis of tubing/-casing, and to select the appropriate materials to use in the wells, are some examples of application areas where we need to have as correct as possible estimates of the temperatures in the well. This is increasingly important as we drill deeper, with margins becoming smaller. Correct temperature estimates are also important for geothermal wells, due to many of the same reasons as for oil wells, but also to maximize the energy extracted from the well.

The intention of this research is to implement a temperature model for a production well into the MATLAB software, and to perform a sensitivity analysis of the finished model to get a better understanding of the mechanisms controlling the heat transfer in a well with a complex configuration consisting of multiple casings, multiple fluid filled annulus, and changing fluid thermophysical properties.

1.2 Literature review

Theoretical models for estimation of wellbore fluid temperatures have been around since the sixties. Ramey (1962) presented the classic model for temperature estimation of fluids, tubing and casing along the wellbore path, with the assumption of steady-state heat transfer in the wellbore, and transient thermal behavior in the formation. The model is simple, considering only single phase fluid or gas production, and neglects thermal resistance of casing and tubing, frictional and kinetic energy effects. Willhite (1967) developed a calculation procedure for wellbore temperature estimation for the case of an injection well with a gas filled annulus, subjected to radiative, conductive and free convection heat transfer mechanisms, also considering the model for transient radial conduction in the formation by Ramey (1962). Willhite introduced natural convection and radiation to the wellbore heat transfer calculations, and developed a general definition for the overall heat transfer coefficient for wellbores. Alves, Alhanati, and Shoham (1992) introduced a mechanistic approach to estimate the Joule-Thomson coefficient, responsible for the heating or cooling of the produced fluid, resulting from the pressure decreases as the produced fluid is transported upwards in the tubing. Hasan and Kabir (1994) presented a model incorporating steady-state two-phase flow. They also presented a new way of solving the transient thermal behavior of the formation, as opposed to that of Ramey (1962). Hasan et al. (2009) presented an analytical steady-state model, able to estimate the wellbore fluid temperature profiles, incorporating wellbore inclination, varying geothermal gradient, and the Joule-Thomson effect.

Common for these studies are that the sample calculations provided assume simple well configurations, negligible thermal resistance of casing/tubing, and constant thermophysical properties for the well. There is lacking publically available literature on simulation models considering free convection in multiple fluid filled annulus for complex well configurations.

1.3 Structure of thesis

Chapter 1 presents the introduction, consisting of the reaserch problem, literature review, and this section. Chapter 2 takes us through the different modes of heat transfer, how to calculate the overall heat transfer coefficient for a given wellbore configuration, an introduction to the thermophysical properties, the Joule-Thomson effect on the produced fluid, formation thermal properties and transient temperature estimation, and the estimation of the convective heat transfer coefficient for forced and free/natural convection. Chapter 3 contains the derivation of the temperature model, the well configuration and the definition of the different overall heat transfer coefficients for the different well sections, the definition of the convective and the free/natural convection coefficients for the tubing and annulus respectively, and the calculation of the wellbore trajectory as function of inclination. It also contains the thermophysical properties used in the model, the calculation procedure to establish the overall heat transfer coefficient for the individual cell, and example calculations of the the temperatures at the different interfaces. Chapter 4 contains the sensitivity analysis of the model. Chapter 5 contains the conclusion. Appendix A presents parts of the MATLAB code, with some essential parts removed due to copy protection, but still deemed sufficient enough to give a rough overview of the calculations carried out.

Chapter 2

Heat transfer theory

2.1 Introduction

Heat transfer can be defined as thermal energy in transit due to a spatial temperature difference to temperature differences (Bergman, Incropera, DeWitt, and Lavine, 2011). As long as the temperature of the systems are unequal, energy exchange takes place, and the internal energy of the objects changes according to the first law of thermodynamics. If there are no temperature differences, there will be no exchange of heat between the systems.

Heat itself is not a measure of energy stored in a system but rather a measure of the quantity of energy being transferred from a system of higher temperature to a system of lower temperature. The heat transfer leads to change in the systems state functions such as temperature and internal energy.

2.2 The different modes of heat transfer

There are three possible means of which heat may be transferred, referred to as modes. The modes are conduction, convection and radiation, explained in the following. The heat transfer rate is generally denoted as Q [W or $\mathrm{J\,s^{-1}}$].

2.2.1 Conduction

Conduction can be defined as the transfer of heat energy through direct contact between substances (solids or stationary fluids) in which there exists a temperature gradient. By transferring heat energy to a system, the systems temperature rises as the vibrational energy of its particles such as atoms or molecules increases. For fluids the temperature gradient will change as the highly vibrating particles collide with nearby lower energy particles. For solids the energy transfer is due to lattice vibrations. The net energy transfer is called diffusion of energy.

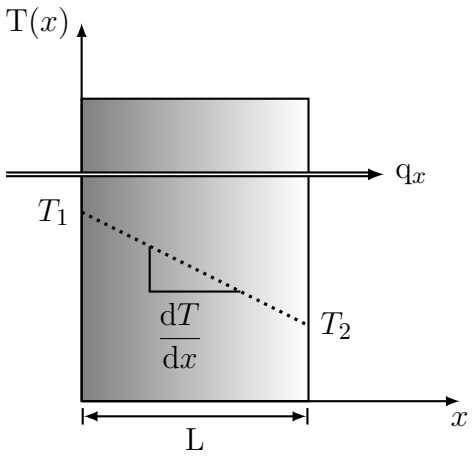

Fig. 2.1. 1-D conduction

The heat flux by conduction in the x-dimension, or rate of heat transferred per unit area, q_x [$\mathrm{W\,m^{-2}}$], through a plane wall as shown in Fig. 2.1 is given as:

$$q_x = -k\frac{\mathrm{d}T}{\mathrm{d}x} \tag{2.1}$$

where $\dfrac{\mathrm{d}T}{\mathrm{d}x}$ is the temperature gradient in x-direction [$\mathrm{K\,m^{-1}}$], A is the area of the surface normal to the direction heat is transferred, and k is the thermal conductivity of the substance [$\mathrm{W\,m^{-1}\,K^{-1}}$], known as the transport property of the substance. This

equation is also known as Fourier's law of heat conduction. The negative sign implies that the direction of heat flow is from hot to cold along the temperature gradient. As the temperature slope $\frac{\mathrm{d}T}{\mathrm{d}x}$ is constant through the plane wall thickness, L, $\frac{\mathrm{d}T}{\mathrm{d}x}$ can be written as $\frac{T_2-T_1}{L-0} = -\frac{T_1-T_2}{L} = -\frac{\Delta T}{L}$, giving:

$$q_x = -\frac{k}{L}\Delta T \tag{2.2}$$

To find the heat rate by conduction for a plane wall, Q [W], one simply multiply the heat flux, q_x by the plane wall area, A, and obtain the following expression:

$$Q = -\frac{kA}{L}\Delta T \tag{2.3}$$

Heat rate transferred through a cylindrical shell geometry such as a pipe or tubing wall is given in a different form, based on inside radius, r_1, and outside radius, r_2, of the pipe or tubing wall. The heat rate conducted radially through the wall is given as (Bergman et al., 2011):

$$Q = -kA\frac{dT}{dr} = -k(2\pi rL)\frac{dT}{dr} \tag{2.4}$$

where $A = 2\pi rL$ is the area normal to the direction of heat transfer. Rearranging and integrating yields:

$$Q = \frac{2\pi Lk(T_1 - T_2)}{\ln\left(\frac{r_2}{r_1}\right)} \tag{2.5}$$

2.2.2 Convection

Convection is the transfer of heat between two surfaces by a fluid in motion through molecular interaction. The heat transfer mechanisms involved are diffusion, as for conduction, and advection, which is energy transfer through fluid bulk movement if a temperature gradient is present. There are two types of convective heat transfer:

1. Forced convection where the fluid flow is forcefully passed by a surface. A typical example is a fan.

2. Natural- or free convection where the cooling or heating of the fluid generates buoyancy effects through change in density due to temperature change. A typical example is heating of water in a pot.

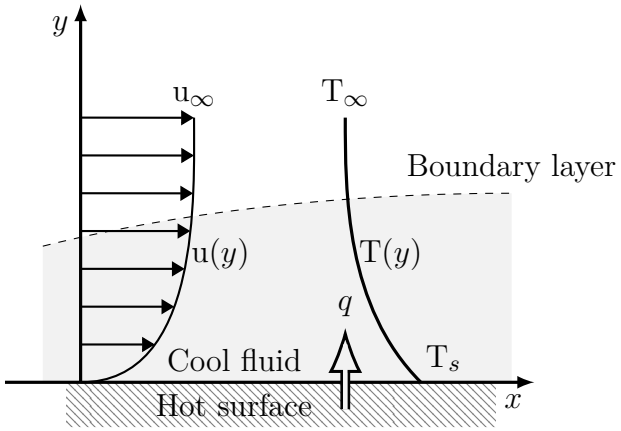

Fig. 2.2. Convective heat transfer with boundary layer

The convective heat flux, q [$\mathrm{W\,m^{-2}}$], is given by:

$$q = h(T_\infty - T_\mathrm{s}) = h\Delta T \tag{2.6}$$

where: T_∞ : Temperature of the free stream outside the velocity boundary layer (°C)
T_s : Temperature of the surface on which convection is considered (°C)

This equation is also known as Newton's law of cooling. The convective heat transfer rate is given as:

$$Q = qA = hA\Delta T \tag{2.7}$$

Here a new term, h [$\mathrm{W\,m^{-2}\,K^{-1}}$], is introduced. It is the convective heat transfer coefficient (CHTC), which depends upon the geometry of the system, the thermodynamic properties of the fluid, the thermal properties of the solid medium and the systems boundary conditions. Estimation of CHTC is explained in section 2.10.1.

Bergman et al. (2011) states that as a fluid moves along a surface there will develop a layer, the velocity boundary layer, where the fluid velocity varies between stagnant at the surface, and increasing outwards from the surface until its velocity is equal to the free stream fluid flow velocity. Further they state that if there exist a temperature difference between the surface and the flowing fluid, a thermal boundary layer must

develop. The temperature profile follows the velocity boundary layer, such that the temperature of the stagnant fluid at the fluid/surface boundary is equal to that of the surface, approaching the flowing fluid temperature as it moves away. This is called the temperature boundary layer. The convection boundary layers are presented in Fig. 2.2, where the layers are of the same magnitude (y in the figure represents the distance inwards from the wall surface on which the boundary layers develop). This is not always the case. The Pr number, presented in Subsubsection 2.10.1.3, gives a measure of the relative thickness of the velocity and thermal boundary layers. The velocity and thermal boundary layer profiles have the same shape, and their relative distance is given by the Pr number. If $Pr = 1$ their thickness is identical. For a $Pr > 1$ the velocity boundary layer is larger than the thermal boundary layer, and vice versa (Bergman et al., 2011).

2.2.2.1 Free/natural convection

Free or natural convection is heat transfer due to internal movement in a fluid due to buoyancy forces driven by a temperature difference. A fluid experiencing heating or cooling will expand or contract respectively. As a fluid is heated and expands, its density is decreased, and vice versa for cooling. If we consider a fluid in a cubic cell where the walls opposite of one another are of different temperatures, the fluid near the hot surface will rise because of buoyancy forces due to decreased density, in agreement with Archimedes' principle. The hot fluid transports the heat energy upwards, exchanging heat energy directly with surrounding colder fluid as it rises, and new cold fluid fills the free space. This new cold fluid is also in turn heated, expands, and rises, and so on. The fluid that was driven up due to bouyancy forces is gradually cooled down to the temperature of its surrounding fluid, and starts descending due to the continuous supply of hot and less dense fluid rising up and taking its space. This pattern will continue as long as there exists a temperature gradient in the fluid, and the result is a circulation of the fluid. The process is shown in Fig. 2.3

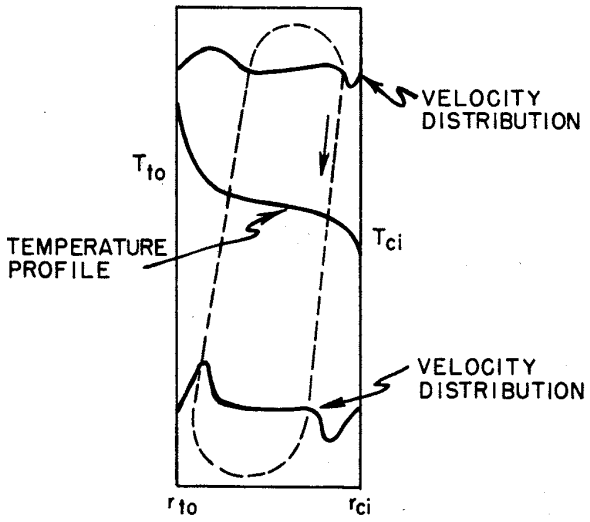

Fig. 2.3. Natural convection in casing annulus (Figure from Willhite (1967))

When comparing the velocity profile from Fig. 2.3 with forced convection velocity boundary layer in Fig. 2.2, there are some distinct differences. The forced convection velocity boundary layer is zero at the wall, increasing outwards. For the natural convection case it is seen that the velocity boundary layer is zero at the wall, increases, and then goes back towards zero again. For the natural convection case this corresponds to the buoyancy effect resulting from heating of fluid close to the wall. Fig. 2.4 shows the flow vectors in an concentric annulus where the inner wall is hotter than the outer wall.

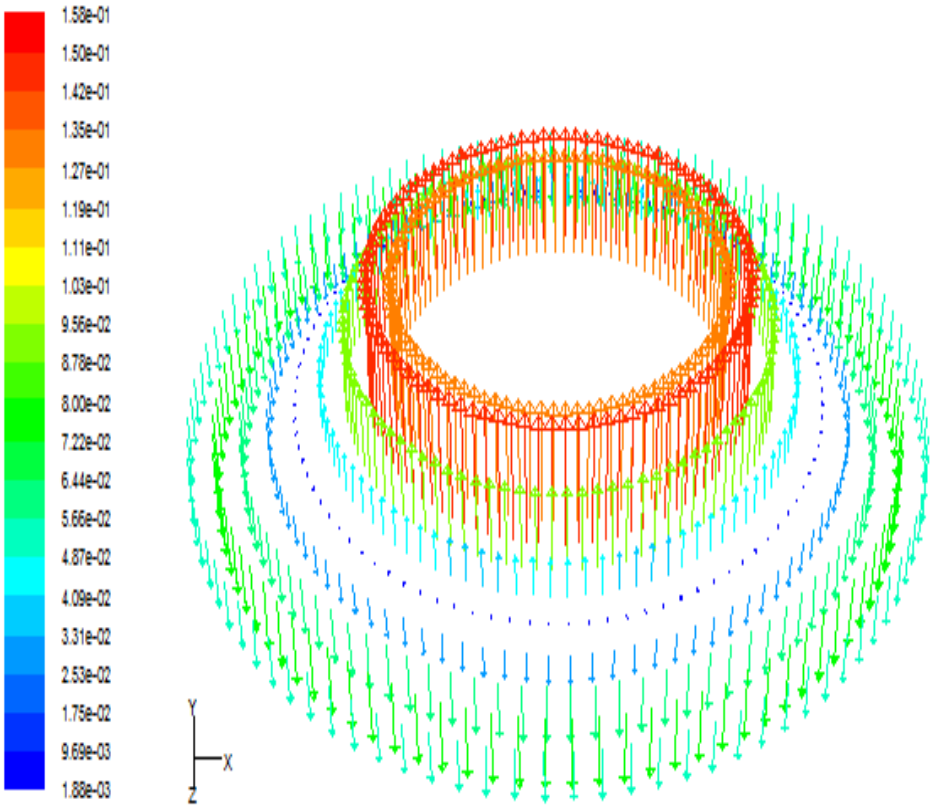

Fig. 2.4. Flow vectors inside an annulus (Figure from Shoushtari, Al-Kayiem, and Aja (2011))

Where the velocity boundary layers for forced convection is constricted to laminar flow, the natural convection boundary layers are not. The flow regime is decided by the relative magnitude of the buoyancy to the viscous forces in the fluid. The shift in flow regimes has a large impact on the heat transfer, and the occurrence of transition between flow regimes can be determined by the Ra number (See Section 2.10 for a definition of Ra number).

2.2.3 Radiation

Where heat conduction and convection happens with the aid of a solid or liquid substance, the radiative heat transfer takes place by electromagnetic radiation through regions with perfect vacuum (Holman, 2010). This electromagnetic radiation, if taking place due to temperature differences between surfaces, is called thermal radiation. A blackbody is considered an ideal thermal radiator. The rate at which energy is emitted from the blackbody is proportional to the fourth power of the absolute temperature of the blackbody, and proportional to the blackbody surface area, and given by the

Stefan-Boltzmann law of thermal radiation (Holman, 2010):

$$Q_{\text{emitted}} = \sigma A T^4 \tag{2.8}$$

where σ is the proportionality constant, also known as the Stefan-Boltzmann constant with a value of 5.669×10^{-8} W/m^2 K^4. A blackbody may for example be a metal piece coated with carbon black, where this black metal piece approximates the blackbody behavior described by the Stefan-Boltzmann law.

When two surfaces exchange radiation, the net radiant exchange is given by (Holman, 2010):

$$\frac{Q_{\text{net exchange}}}{A} \propto \sigma(T_1^4 - T_2^4) \tag{2.9}$$

Surfaces may not be ideal as a blackbody. For such cases as e.g. white or gray coated surfaces with polished or glossy textures, so called gray-body, the radiative behavior described by the Stefan-Boltzmann law, Eq. (2.8), is depending on an additional factor called the emissivity, ϵ. Besides the emissivity, a term called the geometric view factor is added. It accounts for the radiation lost between the surfaces due to the geometry of the objects, as radiation only travels in straight lines. So for gray-bodies, the radiant heat exchange is (Holman, 2010):

$$Q = F_\epsilon F_{\text{G}} \sigma A(T_1^4 - T_2^4) \tag{2.10}$$

where F_ϵ and F_{G} are the emissivity and view factor functions respectively. The emissivity is a material specific property and varies between 0 and 1. Emissivity for a blackbody is 1, whereas polished stainless steel is 0.074, and roofing paper is 0.91 (Holman, 2010).

For the case of a surface, A_s, at temperature T_s, completely covered or surrounded by, or enclosed in a much larger surface, A_surr, at temperature T_surr, the radiant heat exchange is given as (Holman, 2010):

$$Q = \epsilon_s \sigma A_s(T_s^4 - T_{\text{surr}}^4) \tag{2.11}$$

where: A_s : Surface area of the smaller body surrounded by a larger body [m^2].

As thermal radiation hits a surface, some energy is reflected, some is absorbed and some is transmitted through the material, as shown in Fig. 2.5:

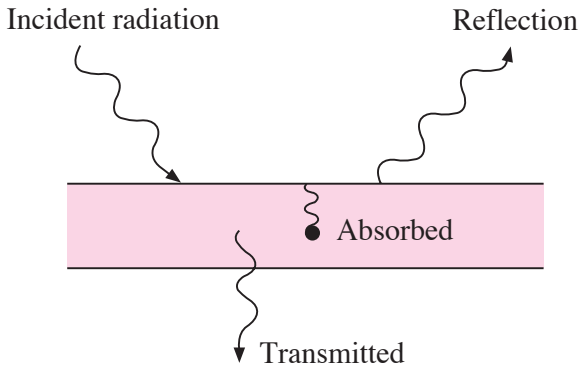

Fig. 2.5. Effect of incident radiation (Figure from Holman (2010, p. 381))

The reflected radiation may be diffuse (reflects in all directions) or specular (the reflection exits at an angle equal to the incident angle), depending on the surface (Holman, 2010). Specular reflection of visible light is what we see in a mirror.

2.3 Thermal resistance analogy

An analogy comparing the conduction of heat with conduction of electricity is often used when studying heat transfer through multiple layers of matter. The resistance of electrical conduction is given by Ohms law as:

$$R = \frac{V}{I} \tag{2.12}$$

where R is the electrical resistance, V is the voltage, and I is the electrical current. When comparing to 1-D heat transfer, the heat flux, q, is the analogue to the electrical current, I. For the case of conduction, given by Eq. (2.3), the thermal resistance through a solid, R is given as:

$$R_{\text{cond}} = \frac{\Delta T}{Q} = \frac{L}{kA} \tag{2.13}$$

which gives:

$$Q_{\text{conv}} = \frac{1}{R_{\text{cond}}} \Delta T \tag{2.14}$$

Similarly the convective heat transfer by a liquid, given by Eq. (2.7), can be written in terms of R:

$$R_{\text{conv}} = \frac{\Delta T}{Q} = \frac{1}{hA} \tag{2.15}$$

which gives:

$$Q_{\text{conv}} = \frac{1}{R_{\text{conv}}} \Delta T \tag{2.16}$$

Just as combining a series of resistances in an electrical circuit will lower the electrical current which can be easily calculated, combining different thermal resistances, in the form of fluid or solid layers, will affect the rate of heat transfer. The heat transfer rate through an object, e.g. a plate separating opposite hot and cold fluid flows, is depending on the thermophysical properties of the materials through which the heat is transferred, and of the fluid transferring heat to and away from the plate.

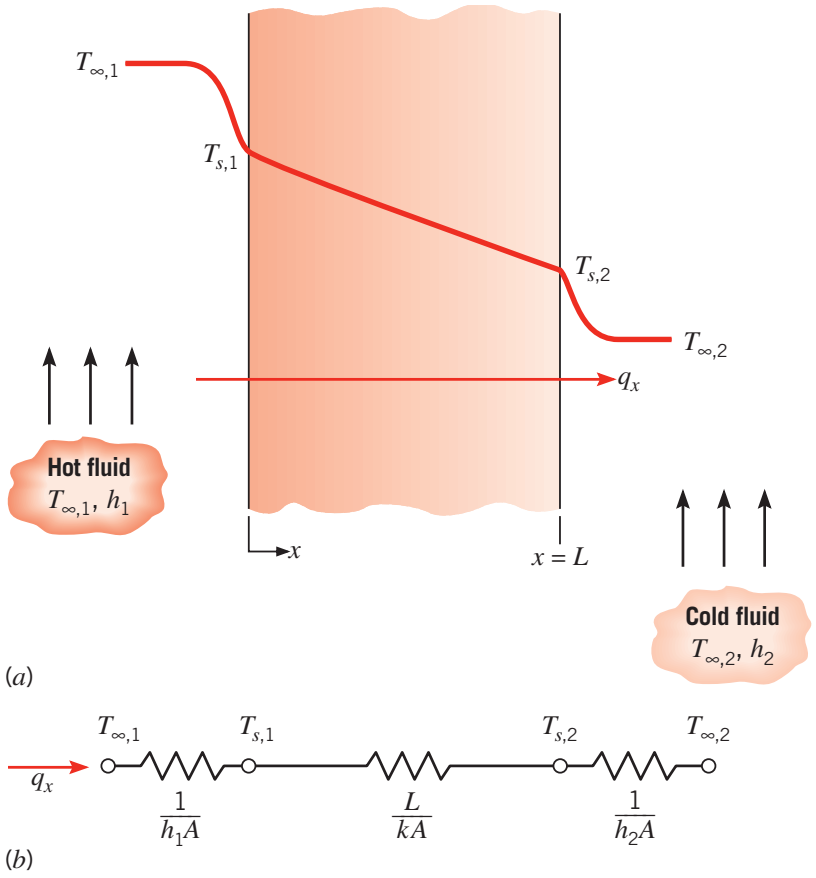

Fig. 2.6. Thermal resistance analogy (b) for heat transfer through a plane wall (a) (Figure from Bergman, Incropera, DeWitt, and Lavine (2011, p. 113))

Assuming no heat generation or storage in the system, the heat transfer is constant. Considering a system consisting of, from left to right, convection by hot fluid, conduction through solid, and convection by cold fluid:

$$Q = \frac{T_{\infty,1} - T_{s,1}}{1/h_1 A} = \frac{T_{s,1} - T_{s,2}}{L/kA} = \frac{T_{s,2} - T_{\infty,2}}{1/h_2 A} \tag{2.17}$$

When considering the total thermal resistance, the systems heat transfer can be expressed as:

$$Q = \frac{T_{\infty,1} - T_{\infty,2}}{R_{\text{total}}} \tag{2.18}$$

where the total heat transfer resistance, R_{total}, is given by

$$R_{\text{total}} = \frac{1}{h_1 A} + \frac{L}{kA} + \frac{1}{h_2 A} \tag{2.19}$$

With each new layer of matter considered, a new resistance term must be added to R_{total}.

We may write R_{total} as:

$$R_{\text{total}} = \sum R = \frac{\Delta T}{Q} = \frac{1}{UA} \tag{2.20}$$

where: U : Overall heat transfer coefficient $[\mathrm{W\,m^{-2}\,K^{-1}}]$

2.4 Overall heat transfer coefficient

To make calculations more manageable when considering heat transfer through a system of several different layers, like a composite wall, it is favorable to define an overall heat transfer coefficient, U, analogous to Newton's law of cooling, and defined by (Bergman et al., 2011):

$$Q \equiv UA\Delta T \tag{2.21}$$

where from Eq. (2.20), we have:

$$U = \frac{1}{R_{\text{total}}A} \tag{2.22}$$

2.4.1 Overall heat transfer coefficient for plane wall geometry

For the case of a plane wall geometry where the area of the plane wall, A, is constant throughout the wall, we see that U, by Eq. (2.19) and Eq. (2.22) is given by:

$$U = \frac{1}{R_{\text{total}}A} = \left[\frac{1}{h_1} + \frac{L}{k} + \frac{1}{h_2}\right]^{-1} \tag{2.23}$$

2.4.2 Overall heat transfer coefficient for cylindrical geometry

For cylindrical geometry, U is obtained in a similar fashion. Considering the radial heat flow across a pipe due to fluids of different temperature flowing along the axial direction of the pipe both inside and outside, the conductive heat transfer through the pipe can be expressed as (See Section 2.5 for definition of conductivity, k):

$$Q = \frac{2\pi Lk\Delta T}{\ln\left(\frac{r_2}{r_1}\right)} \tag{2.24}$$

which gives the following expression for the conductive resistance, R_{cond}, for radial geometry:

$$R_{\text{cond}} = \frac{\Delta T}{Q} = \frac{\ln\left(\frac{r_2}{r_1}\right)}{2\pi r_1 Lk} \tag{2.25}$$

Similarly the convective resistance, R_{conv}, for radial geometry:

$$R_{\text{conv}} = \frac{\Delta T}{Q} = \frac{1}{hA} = \frac{1}{2\pi r L h} \tag{2.26}$$

where the area, A, is the surface at which the convection is considered, e.g. pipe inside or outside area.

The total radial heat transfer rate through the pipe can now be expressed as:

$$Q = \frac{\Delta T}{R_{\text{total}}} = \frac{T_{\infty,1} - T_{\infty,2}}{\frac{1}{2\pi r_1 L h_1} + \frac{\ln(r_2/r_1)}{2\pi L k} + \frac{1}{2\pi r_2 L h_2}} \tag{2.27}$$

where $T_{\infty,1}$ and $T_{\infty,2}$ is the inside and outside average flow temperatures.

The overall heat transfer coefficient, U, in this case defined in terms of pipe inside area, $A_1 = 2\pi r_1 L$, may be expressed as:

$$U_1 = \frac{1}{R_{\text{total}} A_1} = \left[\frac{1}{h_1} + \frac{r_1 \ln\left(\frac{r_2}{r_1}\right)}{k} + \frac{r_1}{r_2}\frac{1}{h_2} \right]^{-1} \tag{2.28}$$

For each additional layer considered, a new resistance term is added in a similar fashion, and the respective overall heat transfer coefficient, U, is obtained.

2.5 Thermophysical properties

The thermophysical properties are the properties of the matter that changes with temperature. Thermophysical properties may be categorized in transport properties and thermodynamic properties. Viscosity and thermal conductivity are transport properties, while density and specific heat are thermodynamic properties which describe the state of a system (Bergman et al., 2011). The knowledge of how these properties vary with temperature is of prime importance as they are present in heat transfer calculations. Neglecting the temperature dependence may lead to inaccurate calculations.

2.5.1 Thermal conductivity

Thermal conductivity is a material specific transport property which is included in Fourier's law, and in that context tells us something about the energy transfer rate in the diffusion process (Bergman et al., 2011). According to Bergman and Incropera the thermal conductivity of matter may vary with both pressure and temperature, and its behavior is decided by the physical structure of the material related to the state of matter. The thermal conductivity, k, is given as:

$$k = -\frac{q}{\partial T/\partial x} \tag{2.29}$$

which for an isotropic material is the same in all directions. If the thermal conductivity increases, so does the heat flux, q. According to Bergman et al. (2011), the thermal conductivity may vary greatly with the state of matter. Generally speaking, the thermal conductivity of a solid is larger than a liquid, and that of a liquid larger than that of a gas. Bergman and Incropera also states that the energy transport is less effective in fluids and gases, largely due to a larger intermolecular distance and more random movement of molecules, separating fluid and gas states from the solid state when considering energy transport.

For the solid state, the energy transport happens by lattice vibrational waves and migration of free electrons. For gases he relates the thermal conductivity behavior to the kinetic theory of gases, which gives a directly proportional relationship between the thermal conductivity and the gas density, the mean molecular speed, and the average distance a molecule can travel before colliding with an other molecule, namely the mean free path. The physics behind thermal conductivity of fluids are not well understood (Bergman et al., 2011).

The thermal conductivity behavior with changing temperature for some alloys, and for water and engine oil, are presented in Fig. 2.7 and Fig. 2.8 respectively. The thermal conductivity of fluids is said to decrease with both increasing molecule weight and temperature, with water and engine oil being amongst the exceptions for the latter (Bergman et al., 2011).

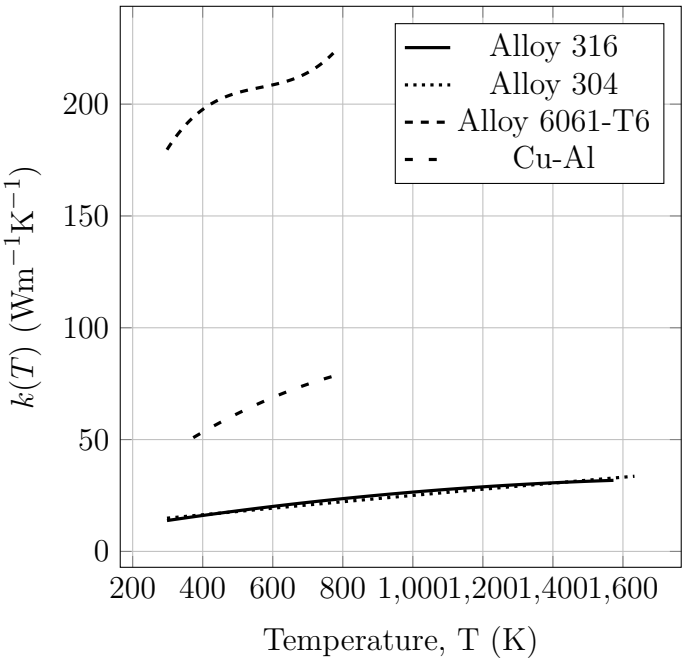

Fig. 2.7. Thermal conductivity temperature dependence for some alloys (Plot created with correlations from Furrer and Semiatin (2010))

2.5.2 Specific Heat Capacity

The specific heat capacity, c_p, of a material is related to its ability to store heat as kinetic or vibrational energy on an atomic level. There are a lot of factors to be considered when talking about the specific heat capacity of solids; lattice vibration spectrum, electron distribution, interaction of particles and phase transitions (Reed, 1983), but that is out of the scope of this thesis. Fig. 2.9 shows the temperature effect on the c_p for some alloys.

The specific heat capacity is an intensive property, which means that it does not change with the size of the system or the amount of material present in the system. It is defined as the amount of energy needed to raise the temperature of 1 gram of a substance by 1 K, and has the units $\mathrm{J\,kg^{-1}\,K^{-1}}$. The relationship is commonly referred

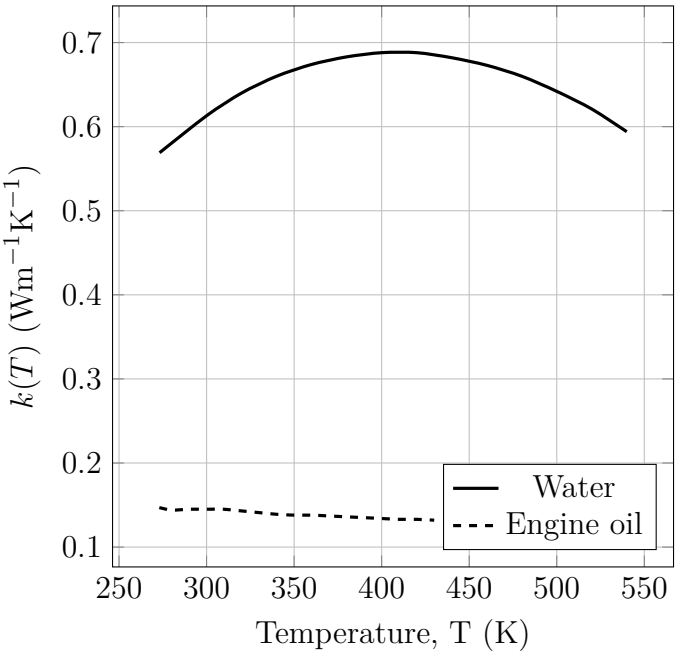

Fig. 2.8. Thermal conductivity temperature dependence for some liquids (Plot created with tabulated values from Bergman, Incropera, DeWitt, and Lavine (2011))

to as the simplified steady-flow thermal energy equation:

$$Q = c_{\mathrm{pm}} \Delta T \tag{2.30}$$

The heat capacity of gases and solids are well understood and documented in literature, but the physics behind the heat capacity of liquids is not really understood (Bergman et al., 2011). A liquid has strong molecular and system specific interactions, which depend on the type of liquid, thus making calculation in general form impossible (Bolmatov, Brazhkin, and Trachenko, 2012). Therefor we mostly have to rely on empirical correlations obtained through experiments when calculating the specific heat capacity for liquids subjected to different temperatures and pressures.

At room temperature and 1 atm pressure (101325 Pa), water has a c_{p} of 4181 $\mathrm{J\,kg^{-1}\,K^{-1}}$, and unused engine oil has a c_{p} of around 1888 $\mathrm{J\,kg^{-1}\,K^{-1}}$. Fig. 2.10 shows a comparison between saturated water and engine oil specific heat capacities, and how they vary as a function temperature.

As an example we will see what role the specific heat capacity plays, and what the temperature decreases to if we remove 4000 joules of heat energy from 1 kg of engine oil vs 1 kg of water at 25 °C (298.15 K). From Eq. (2.30):

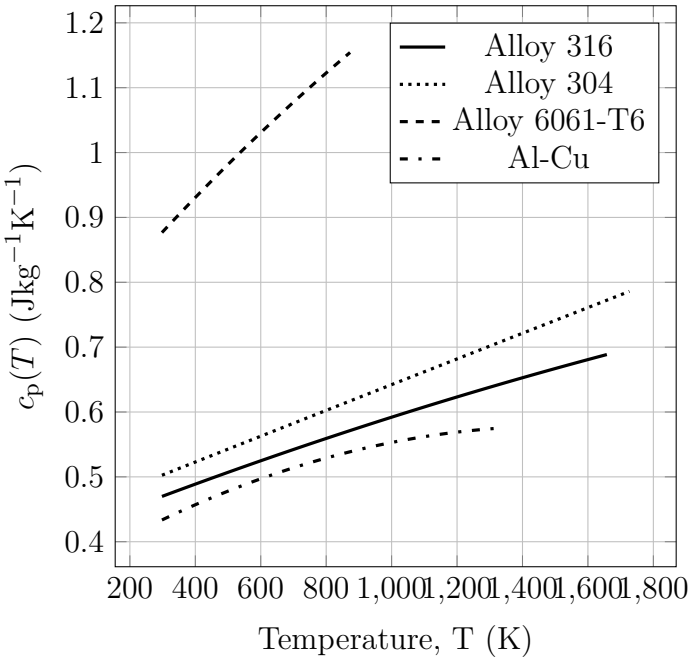

Fig. 2.9. c_p vs temperature for some alloys (Correlations from Furrer (2010))

Engine oil:

$$T_2 = \frac{Q}{c_{p(Engine\,oil)} m} + T_1 = \frac{-4000\,\text{joules}}{1888\ \text{Jkg}^{-1}\text{K}^{-1} \times 1\ \text{kg}} + 298.15\ \text{K} = 296\ \text{K} = 23\ ^\circ\text{C}$$

Water:

$$T_2 = \frac{Q}{c_{P(Water)} m} + T_1 = \frac{-4000\,\text{joules}}{4181\ \text{Jkg}^{-1}\text{K}^{-1} \times 1\ \text{kg}} + 298.15\ \text{K} = 297.19\ \text{K} = 24\ ^\circ\text{C}$$

It is clear from this example that water, due to its high specific heat capacity, can give away more energy with less impact on its initial temperature compared to engine oil.

It is sometimes useful to speak of the heat capacity per unit volume of a substance, which is termed the volumetric heat capacity, c_V, and has the units $\text{J}\,\text{m}^{-3}\,\text{K}^{-1}$. It may also be expressed as the product of the density and the specific heat capacity, ρc_p. In chemistry applications the molar heat capacity, c_{mol} ($\text{J}\,\text{mol}^{-1}\,\text{K}^{-1}$) is often used.

The specific or volumetric heat capacity is not to be confused with heat capacity, C, which is the ratio of heat added or removed from a system to the resulting change of temperature. The heat capacity is an extensive property, i.e. changing with system size, and is measured in joules per kelvin, $\text{J}\,\text{K}^{-1}$.

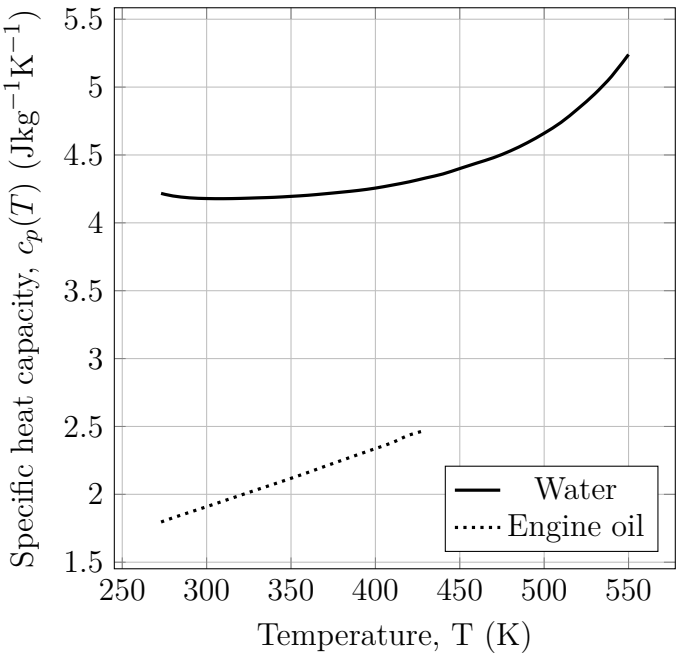

Fig. 2.10. c_p vs temperature for some saturated liquids (Plot created with tabulated values from Bergman, Incropera, DeWitt, and Lavine (2011))

2.5.3 Thermal diffusivity

According to Bergman et al. (2011), thermal diffusivity is defined as the ratio of thermal conductivity to the product of the density and specific heat capacity (also known as the volumetric heat capacity, c_V), which is basically the materials ability to conduct energy relative to its ability to store energy. It gives a measure of the heat transfer rate through a material, and is measured in m^2/s.

$$\alpha = \frac{k}{\rho c_p} \tag{2.31}$$

A material with a small α implies its ability to store energy is dominating (ρc_p is larger), and for large α its ability to conduct energy is dominating (k is larger). When the ability to store energy is dominating (small α), the material respond slowly to changes in temperature. When the ability to conduct energy is dominating (large α), the material may respond quickly to temperature changes.

2.5.4 Viscosity

The viscosity is an important parameter of fluids as it expresses its resistance to flow. The rheological behavior of a fluid system, and thus the viscosity, depends upon the particles suspended in it. A fluid system with suspended unsymmetrical particles will have a viscosity depending on the fluid velocity, said to behave non-Newtonian, while a simple and clean fluid system composed of particles no bigger than molecule size particles will behave as a Newtonian fluid (Skjeggestad, 1989). The viscosity of a fluid is given by its ratio of shear stress, τ (Pa), to the share rate, $\dot{\gamma}$ (1/s):

$$\mu = \frac{\tau}{\dot{\gamma}} \tag{2.32}$$

where: μ : Viscosity [Pa s]

Fluids may be described by two ideal theoretical fluid behaviors, namely Newtonian and Bingham plastic, which may be described by simple models (Skjeggestad, 1989). For Newtonian fluids the viscosity does not change and stays the same for all shear rates. For Bingham plastic fluids the viscosity is not linearly related to the shear rate (Skalle, 2015), because the fluid is required to overcome an initial shear stress, a yield point, to start moving. After passing the yield point it behaves like a Newtonian fluid. A Newtonian fluid can also be shear thickening or shear thinning, which means that it experiences increased or decreased resistance to move with shear rate. Similarly a Bingham fluid experiencing a shear thinning with shear rate is called a Bingham pseudoplastic fluid. These fluid behaviors can be seen in Fig. 2.11.

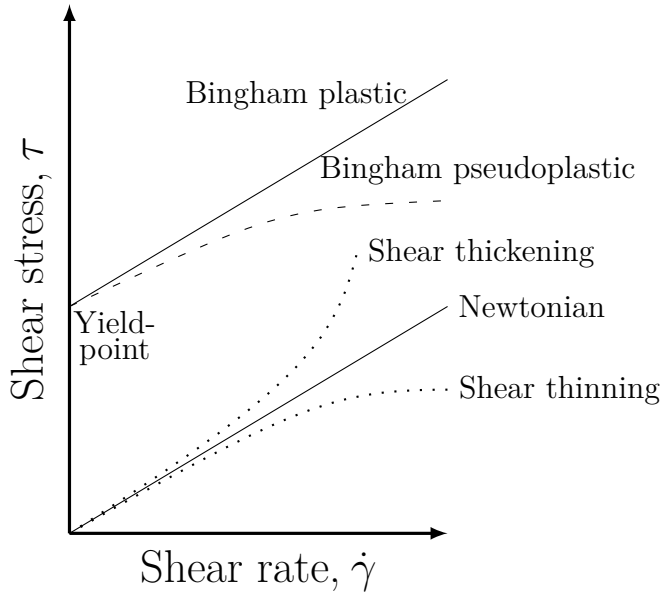

Fig. 2.11. Typical behavior Newtonian and non-Newtonian fluids

For drilling applications, rheological models have been developed to closely describe a drilling fluids non-Newtonian behavior under different shear rates. The most common models are (Skalle, 2015):

- Newtonian model

$$\tau = \mu\dot{\gamma} \tag{2.33}$$

- Bingham plastic model

$$\tau = \tau_y + \mu_{pl}\dot{\gamma} \tag{2.34}$$

- Power law model

$$\tau = K\dot{\gamma}^n \tag{2.35}$$

- Herschel & Bulkley model

$$\tau = \tau_y + K\dot{\gamma}^n \tag{2.36}$$

The model characteristics are shown in Fig. 2.12.

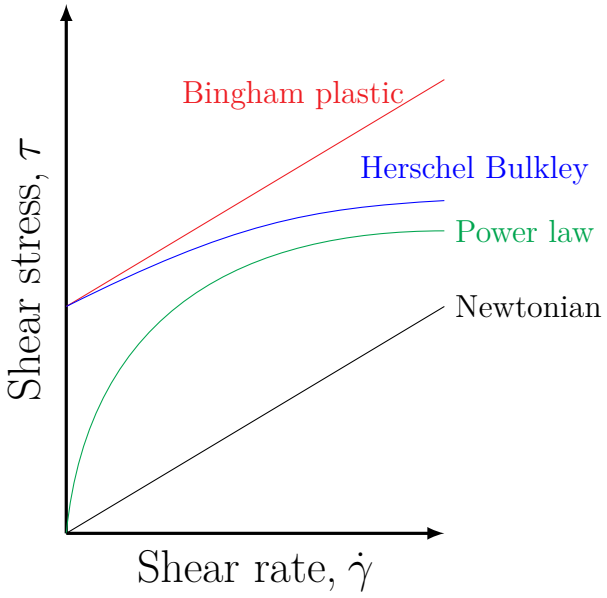

Fig. 2.12. Common drilling fluid rheology models

2.5.5 Density

The density, ρ, of a substance is the rato of its mass, m, to its volume, V:

$$\rho = \frac{m}{V} \tag{2.37}$$

where: ρ : Density [kg m^{-3}]
m : Mass [kg]
V : Volume [m^3]

For a homogenous material, the density is defined as the volumetric mass density like we have just seen. For e.g. a porous material, its density is really the density of the substance filling the pore space plus the porous material. This is defined as the bulk density. The bulk density may as well be a fluid composed of multiple phases such as a water/oil mixture with gas bubbles, or a drilling fluid with suspended particles such as barite.

Different materials have different densities which vary with both temperature and pressure. Increasing the pressure will compress the material such that it has less volume but the same mass, thus increasing its density. Increasing the temperature of a material generally increases its volume, reducing its density.

If we assume a density, ρ, equal to the average density of a fluid column, the hydrostatic pressure at the bottom may be calculated as:

$$P = \rho g z \tag{2.38}$$

where: P : Pressure [Pa]
g : Gravitational acceleration [$\mathrm{m\,s^{-2}}$]
z : Height of fluid column [m]

As the fluid is heated, the density decreases, and thus the hydrostatic pressure at the bottom of the fluid column also decreases.

2.6 Joule-Thomson effect

2.6.1 Pressure loss calculations in the wellbore

Now considering a small differential fluid element, $\mathrm{d}L$, in the flow along the stream lines through the tubing, at steady state, considered Newtonian and incompressible over the element, with no work done, and at an inclination θ from the vertical. Assuming mechanical energy conservation over the element, the change in energy:

$$\frac{\mathrm{d}p}{\rho} + \frac{\mathrm{d}v^2}{2} + g\cos\theta \mathrm{d}L = -f_\mathrm{D}\frac{dL}{d}\frac{v^2}{2} \tag{2.39}$$

where: p : Pressure [Pa]
ρ : Fluid density [$\mathrm{kg\,m^{-3}}$]
v : Fluid velocity [$\mathrm{m\,s^{-1}}$]
z : Vertical displacement over the element [m]
f_D : Darcy friction factor
d : Inside diameter of pipe [$\mathrm{m^2}$]

The terms, left to right respectively, is: Pressure, kinetic, potential and frictional energy changes through the fluid element. As $\frac{\mathrm{d}v^2}{2} = v\mathrm{d}v$, solving for $\frac{\mathrm{d}P}{\mathrm{d}L}$ gives:

$$-\frac{\mathrm{d}p}{\mathrm{d}L} = \frac{f_\mathrm{D}v^2\rho}{2d} + \rho v\frac{\mathrm{d}v}{dL} + \rho g\cos\theta \tag{2.40}$$

The left hand side is the total pressure loss for fluid flowing upwards through the tubing, which is equal to the right hand side terms, given as friction, momentum and static pressure losses respectively:

$$\left(\frac{\mathrm{d}p}{\mathrm{d}L}\right)_\mathrm{Total} = \left(\frac{\mathrm{d}p}{\mathrm{d}L}\right)_\mathrm{Friction} + \left(\frac{\mathrm{d}p}{\mathrm{d}L}\right)_\mathrm{Static} + \left(\frac{\mathrm{d}p}{\mathrm{d}L}\right)_\mathrm{Momentum} \tag{2.41}$$

2.6.2 The Joule-Thomson coefficient

The enthalpy (H) of a fluid flowing through a restriction such as a throttling valve may be considered to remain approximately unchanged ($H \approx$ constant). The fluid experiences a pressure drop and a change in temperature. The temperature may decrease, remain unchanged or increase. As the reservoir fluid moves up the tubing towards the surface, the surrounding pressure decreases and a resulting temperature

change takes place. This effect is called the Joule-Thomson effect, defined as (Cengel and Boles, 2006):

$$\mu_{\mathrm{JT}} = \left(\frac{\partial T}{\partial P}\right)_H \tag{2.42}$$

where: μ_{JT} : Joule-Thomson coefficient [$\mathrm{K\,Pa^{-1}}$]

Whether the temperature increases or decreases depends on the composition of the fluid. Real gases generally tend to cool as the pressure drops, while the opposite is generally said to be happening to fluids (Cengel et al., 2006). A mixture of oil and gas may experience heating from the oil phase, and cooling from the gas phase. Depending on the mixture volume fractions of each component, and their response to pressure changes, a net temperature increase or decrease may take place (Hasan et al., 2009).

$$\mu_{\mathrm{JT}} \begin{cases} < 0 & \text{temperature increases} \\ = 0 & \text{no temperature change} \\ > 0 & \text{temperature decreases} \end{cases} \tag{2.43}$$

The expression for μ_{JT}, Eq. (2.42), represents the slopes of the constant enthalpy lines on a P-T diagram (Cengel et al., 2006). From Fig. 2.13 (note that h in the figure is the same as enthalpy H as defined in this text) it is seen that the slopes of some of the lines are zero at some point. By passing a line through these points of zero slope, the inversion line, we define the values (P,T) for which a negative μ_{JT} exists. Any temperature where the constant enthalpy lines intersects with the inversion line is called the inversion temperature. The upper intersection point at zero pressure is called the maximum inversion temperature.

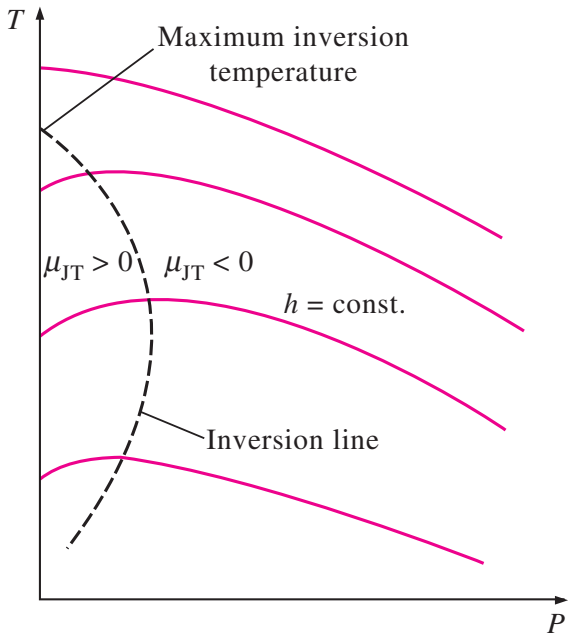

Fig. 2.13. "Constant-enthalpy lines of a substance on a T-P diagram" (Cengel and Boles, 2006)

Considering a fluid experiencing a decreasing pressure, it is expected to experience heating as long as we are to the right of the inversion line ($\mu_{JT} < 0$). As seen from the figure, the inversion line is not always crossed.

2.7 Formation thermal properties

The thermal conductivity of North Sea sedimentary rocks was measured by Evans (1977). The rock samples taken was both from washed cutting and core samples, and the results for the wells are presented in Fig. 2.14. From Fig. 2.14 and Fig. 2.15 it is obvious that the thermal conductivity is not constant throughout the wellbore, and differ quite a bit depending on lithology. Evans (1977) points out an increase in conductivity with depth for the chalk due to burial diagenesis, hardening and loss of porosity, and also a similar trend for the sequence between Jurassic and Triassic.

Age	Formation	Dominant Lithology	7/3-1	WELL-X	27/3-1	Weighted Mean ($W \cdot m^{-1} \cdot K^{-1}$)
Post Paleocene	-	clay	1.76 ± .52(51)	No Samples	No Samples	1.74
Paleocene	-	shale	1.47 ± .03(3)	Absent	Absent	
U. Cretaceous	-	chalk	2.16 ± .14(16)	2.08 ± .33(17)	No Samples	2.07
L. Cretaceous	-	shale/marl	1.76 ± .21(7)	2.37 ± .36(2)	No Samples	
Jurassic	-	shale/sst	1.41 ± .33(4)	1.51 ± .32(13)	Absent	1.49
U. Triassic	Keuper	shale/marl	Absent	1.84 ± .28(5)	No Samples	2.10
M. Triassic	Muschelkalk	evap./shale	Absent	2.05(1)	No Samples	
L. Triassic	Bunter	sst/shale	Absent	2.19 ± .31(15)	No Samples	
U. Permian	Zechstein	evap./carb.	4.53 ± .84(11)	3.94 ± .56(17)	5.45(1)	4.22
L. Permian	Rotleigendes	sandstone	2.50 ± .89(7)	4.41 ± .55(2)	Absent?	2.92
Carbonifer.	Coal Measures	shale/sst	-	2.82 ± 1.23(9)	Absent?	2.82
L. Paleozoic	-	lst./sst./ metamorph.	-	-	3.89 ± .47(10)	3.89

Fig. 2.14. Thermal conductivity of formation for North Sea sedimentary rocks (Figure from Evans (1977))

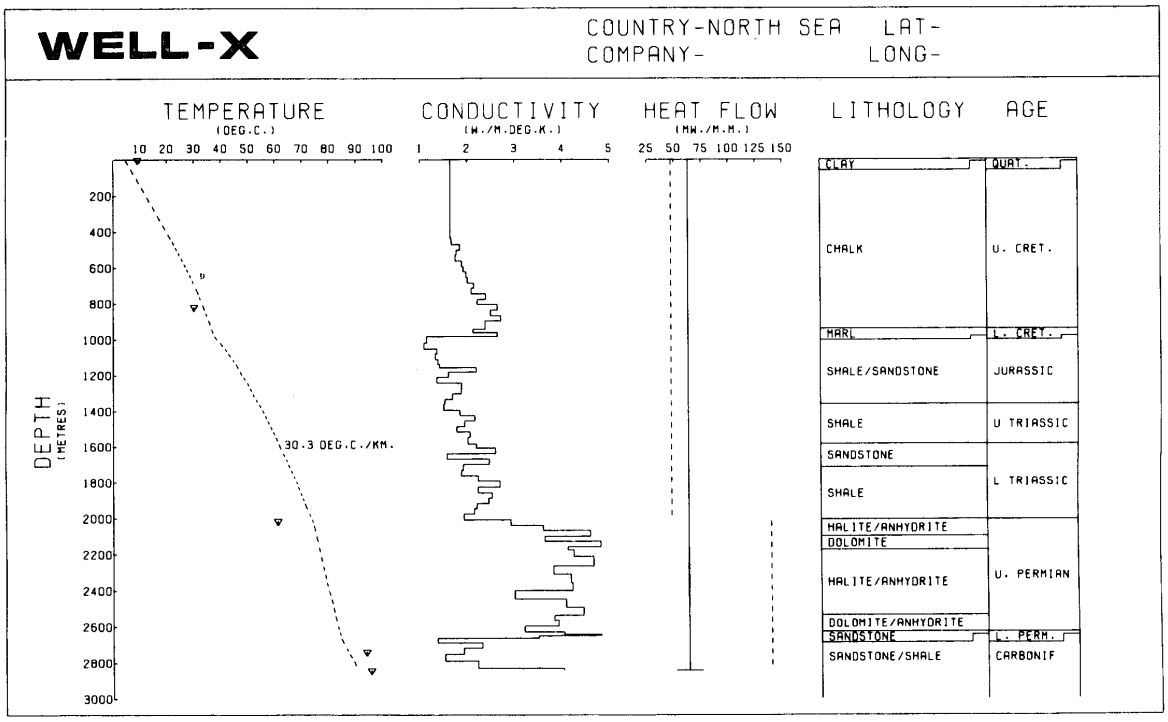

Fig. 2.15. Composite temperature-conductivity-heat flow-lithology plot (Figure from Evans (1977))

2.8 Formation temperature

As hot fluid is produced and transported up the tubing, and as time goes, it will heat up the formation surrounding the well. Heat diffusion in the formation is a three-dimensional problem. By assuming symmetry around the heat source, being the heated wellbore, it may be treated as a two-dimensional problem (Hasan and Kabir, 1991). By also considering a considerable small increment in the axial direction, the problem further reduces to a one-dimensional one. The resulting problem is a one-dimensional diffusion problem, as vertical heat diffusion is ignored due to the assumption of very small axial increments.

Assuming constant heat flux from the wellbore, and considering very a small section of the wellbore, in a short time step, the 1-D radial heat diffusion problem is given by the following partial differential equation in cylindrical coordinates:

$$\frac{\partial^2 T_\mathrm{e}}{\partial r^2} + \frac{1}{r}\frac{\partial T_\mathrm{e}}{\partial r} = \frac{c_e \rho_\mathrm{e}}{k_\mathrm{e}}\frac{\partial T_\mathrm{e}}{\partial t} \tag{2.44}$$

where: t : Time [s]
T_e : Formation temperature at time t (°C)
r : Radial distance from the center of the wellbore [m]
c_e : Specific heat capacity of formation [$\mathrm{J\,kg^{-1}\,K^{-1}}$]
ρ_e : Density of formation [$\mathrm{kg\,m^{-3}}$]
k_e : Thermal conductivity of formation [$\mathrm{W\,m^{-1}\,K}$]
$\frac{c_e \rho_r}{k_\mathrm{e}}$: Thermal diffusivity of formation, α_e [$\mathrm{m^2\,s^{-1}}$]

The dimensionless radius and time are defined as, respectively:

$$r_\mathrm{D} = \frac{r}{r_\mathrm{wb}} \tag{2.45}$$

$$t_\mathrm{D} = \frac{\alpha_\mathrm{e} t}{r_\mathrm{wb}^2} \tag{2.46}$$

where: r_wb : Wellbore radius [m]

The initial formation temperature at any depth is constant, giving:

$$\lim_{t \to 0} T_\mathrm{e} = T_\mathrm{ei} \tag{2.47}$$

where: T_ei : Far away undisturbed formation temperature (°C)

The undisturbed formation temperature at the outer temperature boundary does not change with radial distance from the well:

$$\lim_{r\to\infty}\frac{\partial T_{\mathrm{e}}}{\partial r}=0 \tag{2.48}$$

The heat flow rate from produced fluid per unit length of the well:

$$Q=-\frac{2\pi k_{\mathrm{e}}}{w}\frac{r\partial T_{\mathrm{e}}}{\partial r}|_{r=r_{\mathrm{wb}}} \tag{2.49}$$

where: w : Mass flow rate of produced fluid $[\mathrm{kg\,s^{-1}}]$

Now applying dimensional variables and boundary conditions, Eq. (2.44) can be rewritten:

$$\frac{\partial^2 T_{\mathrm{e}}}{\partial r_{\mathrm{D}}^2}+\frac{1}{r_{\mathrm{D}}}\frac{\partial T_{\mathrm{e}}}{\partial r_{\mathrm{D}}}=\frac{\partial T_{\mathrm{e}}}{\partial t_{\mathrm{D}}} \tag{2.50}$$

Eq. (2.48) and Eq. (2.49) becomes:

$$\lim_{r_{\mathrm{D}}\to\infty}\frac{\partial T_{\mathrm{e}}}{\partial r_{\mathrm{D}}}=0 \tag{2.51}$$

$$\frac{\partial T_{\mathrm{e}}}{\partial r_{\mathrm{D}}}|_{r_{\mathrm{D}}=1}=-\frac{wQ}{2\pi k_{\mathrm{e}}} \tag{2.52}$$

Applying Laplace transform to solve the equations, wellbore interface temperature is given as:

$$T_{\mathrm{wb}}=T_{\mathrm{ei}}+\frac{wQ}{\pi^2 k_{\mathrm{e}}}I \tag{2.53}$$

$$I=\int_0^\infty\frac{1-e^{-u^2 t_{\mathrm{D}}}}{u^2}\frac{Y_1(u)-J_1(u)Y_0(u)}{J_1^2(u)+Y_1^2(u)}du \tag{2.54}$$

where: u : Dummy variable
J_0, J_1 : Zero and first-order Bessel functions of first kind
Y_0, Y_1 : Zero and first-order modified Bessel functions of first kind

Dimensionless temperature is now defined as:

$$T_{\mathrm{D}} = -\frac{2\pi k_{\mathrm{e}}}{wQ}(T_{\mathrm{wb}} - T_{\mathrm{ei}}) \tag{2.55}$$

Now Eq. (2.53) can be rewritten:

$$T_{\mathrm{D}} = -\frac{2I}{\pi} \tag{2.56}$$

Hasan and Kabir applied the principle of superposition to the wellbore, thus reducing I and T_{wb} expressions (Eq. (2.53) and Eq. (2.54) respectively) from integrals involving Bessel functions of zero and first orders over the limit of zero to infinity for u, to definite integrals as a function of t_{D} alone. They evaluated T_{D} vs t_{D} and found the following relations: For small t, T_{D} is proportional to the square root of the dimensionless time, t_{D}, and for large t_{D}, T_{D} is log-linear with t_{D}. The following expressions define T_{D} for small and large values of t_{D} respectively:

$$T_{\mathrm{D}} = 1.1281\sqrt{t_{\mathrm{D}}}[1 - 0.3]\sqrt{t_{\mathrm{D}}} \qquad \text{if } t_{\mathrm{D}} \leq 1.5 \tag{2.57}$$

$$T_{\mathrm{D}} = [0.4063 + 0.5\ln(t_{\mathrm{D}})]\left[1 + \frac{0.6}{t_{\mathrm{D}}}\right] \qquad \text{if } t_{\mathrm{D}} > 1.5 \tag{2.58}$$

These expressions are discontinuous, and as a result Hasan and Kabir later formulated an improved continuous expression which they have been using more recently (Izgec, Hasan, Lin, and Kabir, 2010):

$$T_{\mathrm{D}} = \ln[e^{-0.2t_{\mathrm{D}}} + (1.5 - 0.3719e^{-t_{\mathrm{D}}})\sqrt{t_{\mathrm{D}}}] \tag{2.59}$$

Fig. 2.16 shows the solutions plotted vs t_{D}.

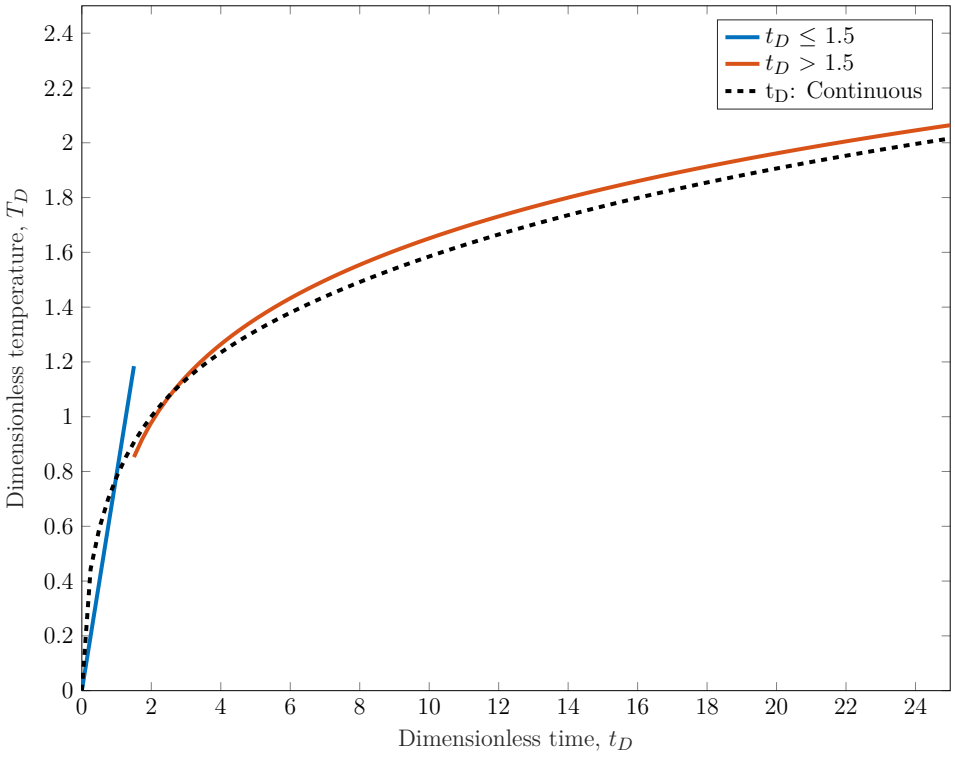

Fig. 2.16. Dimensionless temperatures

2.9 Relaxation distance

As fluid is produced at some depth and flows up through the tubing, it cools by heat loss to the surroundings. After some distance it will be close to, or reach equilibrium, thus approaching an asymptote parallel to the geothermal gradient (Ipek, Smith, and Bassiouni, 2002). The relaxation distance, A_{d}, is the distance between the point at which the flowing temperature gradient can first be estimated by the geothermal gradient, and the point of production/inflow. This asymptote offset from the geothermal gradient is controlled by flowing fluid thermal properties, flow rate, how long time the well have been producing, and well geometry (Ipek et al., 2002). The asymptote is shown in Fig. 2.17a, and the relaxation distance is shown in Fig. 2.17b. The relaxation distance appears in the equation for the produced fluid temperature, Eq. (3.37), and is defined in Eq. (3.21)

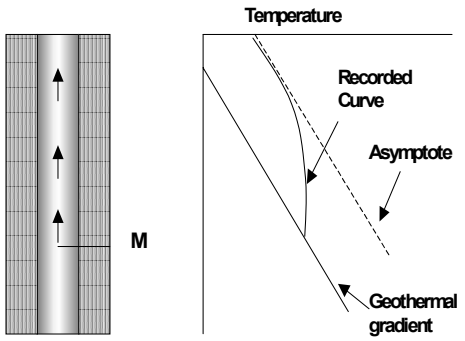

(a) Temperature profile in producing well

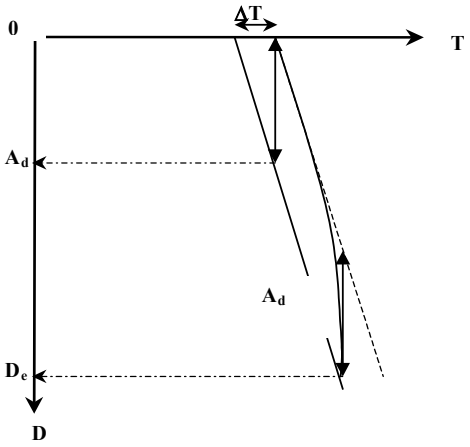

(b) Relaxation distance

Fig. 2.17. Temperature profile and relaxation distance in a producing well (Figures from Ipek, Smith, and Bassiouni (2002))

2.10 Heat transfer in wellbore

When considering heat transfer in a fluid filled wellbore, heat transfer by radiation may be neglected as the contribution from conduction and convection transfer modes are considered to be dominating. The contribution from radiative heat transfer is only meaningful in gas filled annuli (Zhou and Zheng, 2015).

2.10.1 Convective Heat Transfer Coefficient

The Nusselt (Nu) number and its associated Prandtl (Pr), Reynolds (Re) and Rayleigh (Ra) numbers are all dimensionless numbers used in solving convective (forced and naturaal/free) heat transfer problems. In the following their definitions are presented and their significance discussed.

2.10.1.1 Nusselt number

The Nusselt number, Nu, is the ratio of total to conductive heat transfer rate (Santoyo-Gutierrez, 1997). According to Bergman et al. (2011) "*the Nusselt number is to the thermal boundary layer what the friction coefficient is to the velocity boundary layer*". For forced convection it is a function of the Reynold's, Re, and the Prandtl, Pr, numbers. For free convection it is a function of the Grashof, Gr, and the Pr numbers. The Nu is often estimated by correlations obtained experimentally or analytically.

The Nu for forced convection in circular pipes is related to the CHTC in the following way (Bergman et al., 2011):

$$Nu = \frac{\text{Total heat transfer}}{\text{Conductive heat transfer}} \tag{2.60}$$

$$Nu = \frac{h2r}{k} \tag{2.61}$$

where: h : Conductive heat transfer coefficient [$\mathrm{W\,m^{-2}\,K^{-1}}$]
r : Pipe wall inside radius at which the heat transfer is considered [m]
k : Thermal conductivity of the fluid [$\mathrm{W\,m^{-1}\,K^{-1}}$]

The Nu for free convection in concentric pipe annulus is related to the CHTC in the following way (Hasan et al., 2009):

$$Nu = \frac{h}{k} r_i \ln\left(\frac{r_o}{r_i}\right) \tag{2.62}$$

where: $r_{(i,o)}$: Inner and outer radius of the annulus [m]

To obtain the equation for the CHTC for pipe (Eq. (2.63)), and concentric pipe annulus (Eq. (2.64)), respectively, Eq. (2.61) is solved for h, and the appropriate Nu correlation is used.

$$h = \frac{k}{2r} Nu \tag{2.63}$$

$$h = \frac{k}{r_i \ln\left(\frac{r_o}{r_i}\right)} Nu \tag{2.64}$$

A recent study (García, Santoyo, and Espinosa, 2006) observed large differences in CHTC between Newtonian and non-Newtonian fluids, and underlines the importance of using non-Newtonian viscosity Nu correlations when estimating the CHTC for such fluid systems.

The convective heat transfer can be due to free/natural or forced convection, and correlations to estimate their coefficient is presented in Subsubsection 2.10.1.7.

2.10.1.2 Reynold's number

The Reynold's number, Re, is used to predict the flow behavior of the fluid, or rather the onset of laminar, transitional or turbulent flow. The laminar region is for $Re \leq 2300$, the transitional region is for $2300 < Re \leq 4000$, and the turbulent region is for $Re > 4000$. The Re number is the ratio of inertia to viscous force and is defined as (Bergman et al., 2011):

$$Re = \frac{\rho v D}{\mu} \tag{2.65}$$

where: μ : Dynamic fluid viscosity [Pa]
D : Hydraulic diameter ($d_\mathrm{o} - d_\mathrm{i}$ for annulus, d_i for pipe) [m]
ρ : Fluid density [$\mathrm{kg\,m^{-3}}$]

2.10.1.3 Prandtl number

The Prandtl number, Pr, is the ratio of momentum diffusion rate to thermal diffusion rate. It is fully a fluid property, and it is given as (Bergman et al., 2011):

$$Pr = \frac{\nu}{\alpha} = \frac{\mu/\rho}{k/c_p\rho} = \frac{\mu c_p}{k} \tag{2.66}$$

where: ν : Fluid momentum diffusivity (kinematic viscosity) [$\mathrm{m^3\,s^{-1}}$]
α : Fluid thermal diffusivity [$\mathrm{m^3\,s^{-1}}$]

2.10.1.4 Grashof number

The Grashof number, Gr, is a measure of the ratio of the buoyancy forces to the viscous forces in the velocity boundary layer. When it comes to determination of flow regime in natural convection, the Gr number is for free convection what the Re number is for forced convection. Comparing two fluids at the same temperature, the more viscous fluid, implying restricted movement, will have a smaller Gr number. The Gr number is given as (Bergman et al., 2011):

$$\frac{g\beta(T_s - T_\infty)\rho^2 L^3}{\mu^2} \tag{2.67}$$

where: β : Thermal expansion coefficient [$\mathrm{K^{-1}}$]
L : Characteristic length [m]
T_s : Surface temperature (°C)
T_∞ : Fluid temperature just outside the boundary layer (°C)

2.10.1.5 Rayleigh number

The Ra number is associated with free/natural convection, and tells us how the transfer of heat throughout a fluid occurs. Fluid can only transfer heat through conduction and convection in the presence of a temperature gradient. The Ra number tells us which of the modes dominates the heat transfer. If Ra number is less than critical value the heat transfer happens through conduction, and if the Ra number is higher the heat transfer happens through convection. It is given as (Bergman et al., 2011):

$$Ra = GrPr \tag{2.68}$$

2.10.1.6 Correlations for the convective heat transfer coefficient

The relationship between convection and conduction for fluid flow through circular tubes, where there exists a temperature difference between the flowing fluid temperature and the tube walls, may be estimated through correlations obtained experimentally. Such correlations have been made out for various flow conditions and geometry. The most common CHTC correlations for forced convection in circular tubes are presented in Table 2.1, both for turbulent and laminar flow regimes.

Nusselt correlation	**Author**	**Parameter and flow conditions**
Turbulent flow:		
$Nu = 0.023Re^{4/5}Pr^{n}$	Dittus and Boelter (1930)	$0.7 \leq Pr \leq 160$ $Re \geq 10000$ $L/D \geq 10$
$Nu = 0.027Re^{4/5}Pr^{1/3}\left(\frac{\mu}{\mu_s}\right)^{0.14}$	Seider and Tate (1936)	$0.7 \leq Pr \leq 16700$ $Re \geq 10000$ $L/D \geq 10$
$Nu = \frac{(f_{\mathrm{D}}/8)(Re-1000)Pr}{1+12.7(f_{\mathrm{D}}/8)^{1/2}\left(Pr^{2/3}-1\right)}$	Gnielinski (1976)	$0.5 < Pr < 2000$ $2300 < Re < 5 \times 10^{6}$
Laminar flow:		
$Nu = 4.36$		$Re < 2300$

Table 2.1. Various forced convection correlations for circular tubes (Correlations presented in (Bergman, Incropera, DeWitt, and Lavine, 2011))

Dittus and Boelter correlation:

- Based on whether the fluid is subjected to heating or cooling, the correlation coefficient n is defined respectively as n = 0.4 (for surface temperature larger than mean fluid bulk temperature, $T_s > T_m$) or 0.3 (for mean fluid bulk temperature

larger than surface temperature, $T_s < T_m$). This correlation may be applicable for small to moderate temperature differences. The fluid properties should be evaluated at T_m. Errors may be as large as 25%. (Bergman et al., 2011)

Sieder and Tate correlation:

- Applicable for larger temperature differences than the Dittus and Boelter. It includes a term, $\left(\frac{\mu}{\mu_s}\right)^{0.14}$, which accounts for viscosity variations between the pipe wall temperature, T_s and the mean bulk fluid temperature, T_m. μ_s is evaluated at T_s. All other properties evaluated at mean bulk temperature T_m. Errors may be as large as 25%. (Bergman et al., 2011).

Gnielinski correlation:

- Applicable for both turbulent and the transition flow regime (large Re range), and with lower errors (less than 10%) than Dittus and Boelter and the Seider and Tate correlations. The fluid properties should be evaluated at T_m. (Bergman et al., 2011)

2.10.1.7 Correlations for free/natural convective heat transfer coefficient in enclosed spaces

The Dropkin and Somerscales correlation (Dropkin and Somerscales, 1965) have been used in natural convection calculations in annulus (Hasan et al. (1994), Willhite (1967), Zhou et al. (2015) amongst others), and are presented in Table 2.2. Developed for liquids (experiment conducted on water and silicone oil) confined between two parallel plates at varying angles of inclination, the correlations are of the form $Nu = C(Ra)^{1/3}(Pr)^{0.074}$ where C is the coefficient of inclination.

Nusselt correlation	**Inclination θ**	**Parameter and flow conditions**
$Nu = 0.049(Ra)^{1/3}Pr^{0.074}$	0 deg	$0.02 \leq Pr \leq 11560$ $5 \times 10^4 < Ra < 2.5 \times 10^8$
$Nu = 0.057(Ra)^{1/3}Pr^{0.074}$	30 deg	$0.02 \leq Pr \leq 11560$ $1.5 \times 10^5 < Ra < 2.5 \times 10^8$
$Nu = 0.059(Ra)^{1/3}Pr^{0.074}$	45 deg	$0.02 \leq Pr \leq 11560$ $1.5 \times 10^5 < Ra < 2.5 \times 10^8$
$Nu = 0.065(Ra)^{1/3}Pr^{0.074}$	60 deg	$0.02 \leq Pr \leq 11560$ $1.5 \times 10^5 < Ra < 2.5 \times 10^8$
$Nu = 0.069(Ra)^{1/3}Pr^{0.074}$	90 deg	$0.02 \leq Pr \leq 11560$ $1.5 \times 10^5 < Ra < 7.5 \times 10^8$

Table 2.2. Compilation of the free/natural convection correlations for concentric annulus for various inclinations (Equations from Dropkin and Somerscales (1965))

The lower value of the Ra range is where the flow is transitioning from turbulent to transient flow. For lower Ra values than the specified range, other correlations may be used. According to Holman (2010), for $Ra < 2000$, the internal movement in the fluid is very low, meaning that the heat transfer is mainly conduction through the fluid.

For $10^4 < Ra < 10^7$ and $1 < Pr < 2 \times 10^4$, Holman (2010) recommends using:

$$Nu = 0.42(Ra)^{1/4}(Pr)^{0.012}(\frac{L}{\delta})^{-0.30} \tag{2.69}$$

where: δ : Annular clearance, $r_o - r_i$ [m]

Further, in lack of correlations incorporating inclination, he suggests to substitute g for g' in the grashof number, where:

$$g' = g \sin\theta \tag{2.70}$$

where: θ : The horizontal projection of the heated surface

The pitfall by using this correlation is the small δ range. Validity outside this range is questionable.

To use correlations developed for free convection between plates, one must neglect the curvature of the annulus, such that the general expression for the CHTC for annular geometry, may be expressed as:

$$h_{ca} = \frac{k_a Nu}{r_i \ln \frac{r_i}{r_o}} \tag{2.71}$$

where: $_{(i,o)}$: Inner and outer walls of the annulus respectively

Common for these kinds of correlations are the use of equivalent thermal conductivity (See Subsection 3.2.4).

Chapter 3

Temperature model

3.1 Temperature model for production scenario

We now consider a small control volume, $\mathrm{d}z$, in the wellbore at a distance z from the top of the well ($z = 0$ at the top of the well, and $z = z_{\mathrm{bh}}$ at the bottom of the well), spanning between z and $(z - \Delta z)$. The heat transfer across the wellbore is considered constant, and the heat transfer from formation is considered transient. As the hot reservoir fluid is produced, considered single phase, it rises up along the tubing. The produced fluid, assumed to be hotter than the temperature across the annulus, casing, cement and formation at all depths except at the bottom point of the well, transports heat, $Q_{(z)}$, in to the control volume at z, and heat out of the control volume, $Q_{(z-\Delta z)}$, at distance $z - \mathrm{d}z$. The difference in heat in and out of the control volume must be equal to the amount of heat transferred to the formation.

$$Q_{\mathrm{in}} - Q_{\mathrm{out}} = \text{Heat transferred to the formation} \tag{3.1}$$

The heat transferred to the formation, Q, is equal to the change in internal heat of the control volume. The heat change over $\mathrm{d}z$ is given as:

$$Q_{(z)} - Q_{(z-\Delta z)} = Q \tag{3.2}$$

The energy balance for the system, assuming steady state, can be written as:

$$\Big[(wH)_z - (wH)_{z-\Delta z}\Big] + \frac{1}{2}\Big[(wv^2)_z - (wv^2)_{z-\Delta z}\Big] +$$

$$\left[z(wg\cos\theta)_z - (z-\Delta z)(wg\cos\theta)_{z-\Delta z}\right] = Q\Delta z \tag{3.3}$$

where: w : Rate of mass flow per unit area [$\mathrm{kg\,s^{-1}}$]
H : Fluid enthalpy [J]
v : Fluid velocity [$\mathrm{m\,s^{-1}}$]
g : Gravitational accelerations, 9.81 [$\mathrm{m\,s^{-2}}$]
θ : Inclination from vertical (Degrees)
Δz : Control volume length [m]
Q : Heat transferred to the formation [J]

By dividing Eq. (3.3) by Δz and evaluating the expression as $\lim_{\Delta z \to 0}$, and rearranging, we obtain the following expression:

$$\frac{\mathrm{d}H}{\mathrm{d}z} + g\cos\theta + v\frac{\mathrm{d}v}{\mathrm{d}z} = \frac{Q}{w} \tag{3.4}$$

The $\dfrac{Q}{w}$ expresses the heat transfer rate from the produced fluid.

The generalized relation for enthalpy change is given as (Cengel et al., 2006):

$$\mathrm{d}H = c_{\mathrm{pl}}\mathrm{d}T + \left[V - T\left(\frac{\partial V}{\partial T}\right)_P\right]\mathrm{d}P \tag{3.5}$$

where: c_{pl} : Specific heat capacity of the produced fluid [$\mathrm{J\,kg^{-1}\,K^{-1}}$]
V : Specific volume, or the inverse of density of the produced fluid [$\mathrm{m^3\,kg^{-1}}$]

The Joule-Thomson coefficient, μ_{JT}, is defined as:

$$\mu_{\mathrm{JT}} = \left(\frac{\partial T}{\partial P}\right)_H = -\frac{1}{c_{\mathrm{pl}}}\left[V - T\left(\frac{\partial V}{\partial T}\right)_P\right] \tag{3.6}$$

Assuming that the fluid does not undergo any change of phase during its rise towards the surface, enthalpy for the fluid as a function of temperature and pressure is thus given by:

$$\mathrm{d}H = c_{\mathrm{pl}}\mathrm{d}T - c_{\mathrm{pl}}\mu_{\mathrm{JT}}\mathrm{d}P \tag{3.7}$$

Inserting Eq. (3.7) in to Eq. (3.4) and rearranging to give the expression for the change of fluid temperature, T_f with depth, z:

$$\frac{\mathrm{d}T_\mathrm{f}}{\mathrm{d}z} = \mu_\mathrm{JT}\frac{\mathrm{d}p}{\mathrm{d}z} + \frac{1}{c_\mathrm{pl}}\left(\frac{Q}{w} - g\cos\theta - v\frac{\mathrm{d}v}{\mathrm{d}z}\right) \tag{3.8}$$

where: T_f : Temperature of the produced fluid (°C)

The heat transferred from the formation to the wellbore is given as (Hasan et al., 1994):

$$Q = -\frac{2\pi k_\mathrm{e}}{T_\mathrm{D}}(T_\mathrm{wb} - T_\mathrm{ei}) \tag{3.9}$$

where: T_ei : Far away undisturbed earth temperature at the considered depth (°C)
T_wb : Temperature at the wellbore interface (°C)
T_D : Dimensionless temperature

The algebraic approximation of T_D in Eq. (3.9) is given by the continuous formation temperature approximation Eq. (2.59):

$$T_\mathrm{D} = \ln[e^{-0.2t_\mathrm{D}} + (1.5 - 0.3719e^{-t_\mathrm{D}})\sqrt{t_\mathrm{D}}] \tag{3.10}$$

where t_D is dimensionless time, given as:

$$t_\mathrm{D} = \frac{\alpha_\mathrm{e} t}{r_\mathrm{wb}^2} \tag{3.11}$$

where: α_e : Thermal diffusion of the formation [$\mathrm{m^3\,s^{-1}}$]
t : Time [s]

α_e is given as:

$$\alpha_\mathrm{e} = \frac{k_\mathrm{e}}{\rho_\mathrm{e} c_\mathrm{pe}} \tag{3.12}$$

where: k_e : Thermal conductivity of formation [$\mathrm{W\,m^{-1}\,K^{-1}}$]
ρ_e : Density of formation [$\mathrm{kg\,m^{-3}}$]
c_pe : Specific heat capacity of formation [$\mathrm{J\,kg^{-1}\,K}$]

The total heat transferred across the well from the wellbore interface to the tubing fluid is given as:

$$Q_{\text{total}} = -2\pi L r_{\text{ti}} U_{\text{ti}} (T_{\text{f}} - T_{\text{wb}}) \tag{3.13}$$

where: Q_{total} : Total heat flow rate per unit length of well [$\text{J}\,\text{s}^{-1}\,\text{m}^{-1}$]
r_{ti} : Tubing inside area [m]
U_{ti} : Overall heat transfer coefficient based on tubing inside area [$\text{W}\,\text{m}^{-2}\,\text{K}^{-1}$]
L : Wellbore length [m]

Assuming the heat transferred from the formation to the wellbore (Eq. (3.9)) is equal to the total heat transferred across the well from the wellbore interface to the tubing (Eq. (3.13)), such that:

$$Q_{\text{total}} = Q = -2\pi r_{\text{ti}} U_{\text{ti}} (T_{\text{f}} - T_{\text{wb}}) = -\frac{2\pi k_{\text{e}}}{T_{\text{D}}} (T_{\text{wb}} - T_{\text{ei}}) \tag{3.14}$$

$$Q_{\text{total}} - Q = -2\pi r_{\text{ti}} U_{\text{ti}} (T_{\text{f}} - T_{\text{wb}}) + \frac{2\pi k_{\text{e}}}{T_{\text{D}}} (T_{\text{wb}} - T_{\text{ei}}) = 0 \tag{3.15}$$

Cancelling out and rearranging:

$$-r_{\text{ti}} U_{\text{ti}} T_{\text{D}} T_{\text{f}} + r_{\text{ti}} U_{\text{ti}} T_{\text{D}} T_{\text{wb}} + k_e T_{\text{wb}} - k_{\text{e}} T_{\text{ei}} = 0 \tag{3.16}$$

The wellbore temperature, T_{wb}, is now given by:

$$T_{\text{wb}} = \frac{k_{\text{e}} T_{\text{ei}} + r_{\text{ti}} U_{\text{ti}} T_{\text{D}} T_{\text{f}}}{k_{\text{e}} + r_{\text{ti}} U_{\text{ti}} T_{\text{D}}} \tag{3.17}$$

Inserting Eq. (3.17) in to Eq. (3.9) removes the T_{wb} term, yielding the following expression for total heat conducted from the formation to the produced fluid:

$$Q = -\frac{2\pi k_{\text{e}}}{T_{\text{D}}} (T_{\text{wb}} - T_{\text{ei}}) \tag{3.18}$$

$$= \frac{2\pi k_{\text{e}}}{T_{\text{D}}} \left(T_{\text{ei}} - \frac{k_{\text{e}} T_{\text{ei}} + r_{\text{ti}} U_{\text{ti}} T_{\text{D}} T_{\text{f}}}{k_{\text{e}} + r_{\text{ti}} U_{\text{ti}} T_{\text{D}}} \right) \tag{3.19}$$

$$Q = \frac{2\pi r_{\text{ti}} U_{\text{ti}} k_{\text{e}}}{k_{\text{e}} + r_{\text{ti}} U_{\text{ti}} T_{\text{D}}} (T_{\text{ei}} - T_{\text{f}}) \tag{3.20}$$

Defining A_{d} as:

$$A_{\mathrm{d}} = \frac{c_{\mathrm{pl}} w}{2\pi}\left[\frac{k_{\mathrm{e}} + (r_{\mathrm{ti}} U_{\mathrm{ti}} T_{\mathrm{D}})}{r_{\mathrm{ti}} U_{\mathrm{ti}} k_{\mathrm{e}}}\right] \tag{3.21}$$

where: A_{d} : The relaxation distance (See Section 2.9) [m]

The flowing fluid specific heat capacity, c_{pl}, is in the case of water cut, given as:

$$c_{\mathrm{pl}} = \left(\frac{q_{\mathrm{o}}}{q_{\mathrm{o}}+q_{\mathrm{w}}}\right) c_{\mathrm{po}} + \left(1 - \frac{q_{\mathrm{o}}}{q_{\mathrm{o}}+q_{\mathrm{w}}}\right) c_{\mathrm{pw}} \tag{3.22}$$

For single phase oil, assuming no water cut, $c_{\mathrm{pl}} = c_{\mathrm{po}}$

Equation Eq. (3.20) and Eq. (3.21) can now be put into Eq. (3.8). We get the following expression:

$$\frac{\mathrm{d}T_{\mathrm{f}}}{\mathrm{d}z} = \frac{T_{\mathrm{ei}} - T_{\mathrm{f}}}{A_{\mathrm{d}}} - \frac{g\cos\theta}{c_{\mathrm{pl}}} + \mu_{\mathrm{JT}}\frac{\mathrm{d}p}{\mathrm{d}z} - \frac{v}{c_{\mathrm{pl}}}\frac{\mathrm{d}v}{\mathrm{d}z} \tag{3.23}$$

If we now assume that the last two terms of Eq. (3.23) does not vary with depth within the considered control volume, $\mathrm{d}z$, we obtain the following linear differential equation:

$$\frac{\mathrm{d}T_{\mathrm{f}}}{\mathrm{d}z} = \frac{T_{\mathrm{ei}} - T_{\mathrm{f}}}{A_{\mathrm{d}}} - \frac{g\cos\theta}{c_{\mathrm{pl}}} + \phi \tag{3.24}$$

where ϕ is assumed constant throughout the small control element, and given by:

$$\phi = \mu_{\mathrm{JT}}\frac{\mathrm{d}p}{\mathrm{d}z} - \frac{v}{c_{\mathrm{pl}}}\frac{\mathrm{d}v}{\mathrm{d}z} \tag{3.25}$$

The Joul-Thomson coefficient, μ_{JT}, is for a single phase fluid, defined as Eq. (3.6):

$$\mu_{\mathrm{JT}} = -\frac{1}{c_{\mathrm{pl}}}\left[V - T\left(\frac{\partial V}{\partial T}\right)_P\right] \tag{3.26}$$

It can be expressed as:

$$\mu_{\mathrm{JT}} = -\frac{V}{c_{\mathrm{pl}}}(1 - T\beta) \tag{3.27}$$

where: V : Fluid specific volume [$\mathrm{m^3\,kg^{-1}}$]
β : Thermal expansion coefficient of the produced fluid [$\mathrm{K^{-1}}$]
T : Temperature (°C)

β is given as:

$$\beta \equiv -\frac{1}{\rho}\left(\frac{\partial \rho}{\partial T}\right)_P \tag{3.28}$$

and can be estimated by two different density values at different temperatures for constant pressure.

According to Hasan et al. (2009), when considering single phase liquid flow, the product $T\beta$ in Eq. (3.27) may be neglected, which would further simplify Eq. (3.27):

$$\mu_{\mathrm{JT}} \approx -\frac{1}{\rho c_{\mathrm{pl}}} \tag{3.29}$$

Even though the approximation of the $T\beta$ term being very small and nearly constant may be useful for simple and fast calculations, this simplification is not implemented in the model.

The ϕ parameter may now be calculated by:

$$\phi = -\frac{1}{c_{\mathrm{pl}}}\left[V(1-T\beta)\frac{\mathrm{d}p}{\mathrm{d}z} + v\frac{\mathrm{d}v}{\mathrm{d}z}\right] \tag{3.30}$$

where the pressure losses up along the tubing is given by:

$$-\frac{\mathrm{d}p}{\mathrm{d}z} = \left(\frac{\mathrm{d}p}{\mathrm{d}z}\right)_{\mathrm{Friction}} + \left(\frac{\mathrm{d}p}{\mathrm{d}z}\right)_{\mathrm{Static}} + \left(\frac{\mathrm{d}p}{\mathrm{d}z}\right)_{\mathrm{Momentum}} \tag{3.31}$$

where the friction, static and momentum pressure losses are given as, respectively (See Subsection 2.6.1):

$$\left(\frac{\mathrm{d}p}{\mathrm{d}z}\right)_{\mathrm{Friction}} = \frac{f_{\mathrm{D}} v^2 \rho}{2d} \tag{3.32}$$

$$\left(\frac{\mathrm{d}p}{\mathrm{d}z}\right)_{\mathrm{Static}} = \rho g \cos\theta \tag{3.33}$$

$$\left(\frac{\mathrm{d}p}{\mathrm{d}z}\right)_{\mathrm{Momentum}} = \rho v \frac{\mathrm{d}v}{\mathrm{d}z} \tag{3.34}$$

where: f_{D} : Darcy-Weisbach friction factor

According to Hasan et al. (2009) the density of single phase oil does not vary significantly with depth, resulting in a negligible static-head change with depth, such that we may neglect the kinetic-energy loss term in Eq. (3.25), which would lead to ϕ being approximated by:

$$\phi = \mu_{\mathrm{JT}} \left[\left(\frac{\mathrm{d}p}{\mathrm{d}z} \right)_F + \left(\frac{\mathrm{d}p}{\mathrm{d}z} \right)_H \right] \tag{3.35}$$

Even though this approximation yields faster calculations, it is not implemented in the model.

As we are calculating from the bottom towards the top, the undisturbed formation temperature in the current cell, $T_{\mathrm{ei}}(i)$, is equal to that of the previous cell, $(i-1)$, minus the temperature reduction given by the geothermal gradient. The $\cos\theta$ term takes care of the inclination of the wellbore:

$$T_{\mathrm{ei}}(i) = T_{\mathrm{ei}}(i-1) - g_{\mathrm{G}} \cos\theta(i) \mathrm{d}z \tag{3.36}$$

This expression is valid for varying inclination and geothermal gradient.

Assuming all terms but T_{f} is staying unchanged along the length of the considered control volume, $\mathrm{d}z$, Eq. (3.24) can be integrated with appropriate boundary conditions applied, yielding an equation of the following form (Hasan et al., 1994):

$$\begin{aligned} T_{\mathrm{f}}(i) = T_{\mathrm{ei}}(i) + A_{\mathrm{d}}(i) \left[1 - e^{-\mathrm{d}z/A_{\mathrm{d}}(i)} \right] \left(g_G \cos\theta(i) + \phi(i) - \frac{g \cos\theta(i)}{c_{\mathrm{pl}(i)}} \right) \\ + e^{-\mathrm{d}z/A_{\mathrm{d}}(i)} \left(T_{\mathrm{f}}(i-1) - T_{\mathrm{ei}}(i-1) \right) \end{aligned} \tag{3.37}$$

This is a bottom-up calculation, where each subsequent calculation step is based on the fluid temperature of the former step as a boundary condition. The first step starting from the bottom of the well assumes the temperature of the produced fluid to be equal to the in-situ formation temperature, $T_{\mathrm{f}} = T_{bh} = T_{\mathrm{ei}}$, thus eliminating the last term of Eq. (3.37) for the first cell.

The parameters $c_{\mathrm{pl}}(i)$, $\phi(i)$ and the relaxation distance for the current cell, $A_{\mathrm{d}}(i)$, is evaluated at the previous cell conditions. The same is true for $c_{\mathrm{pl}}(i)$. The current cell inclination, $\theta(i)$, is calculated for each cell prior to the temperature calculations. The geothermal gradient, g_{G}, is assumed constant with depth in the model. The

thermophysical properties used in the model is given in Section 3.3. See also Section 3.4 for details of the calculation procedure.

3.2 Model parameters for simulating production scenario

3.2.1 The well configuration

To calculate the heat transfer throughout the well, some assumptions regarding the well configuration is made:

- The well consists of 5 casings and one production tubing.
- The casing strings are numbered from 1 to 5, with 1 being the deepest set casing.
- All casing strings are suspended within the wellhead.
- All casing strings are cemented at least up to the previous casing shoe.
- All casing strings are considered to be made of the same alloy.
- The three innermost annulus are considered to be filled with 3.5%wt NaCl brine.
- Pressure build-up in annulus is not considered.
- Any changes in well configuration dimensions due to temperature changes are not considered.
- Natural or free convection is considered to take place in the three fluid filled annulus, if the temperature conditions allow for such conditions are to arise.
- The three outermost casing strings are cemented to surface.

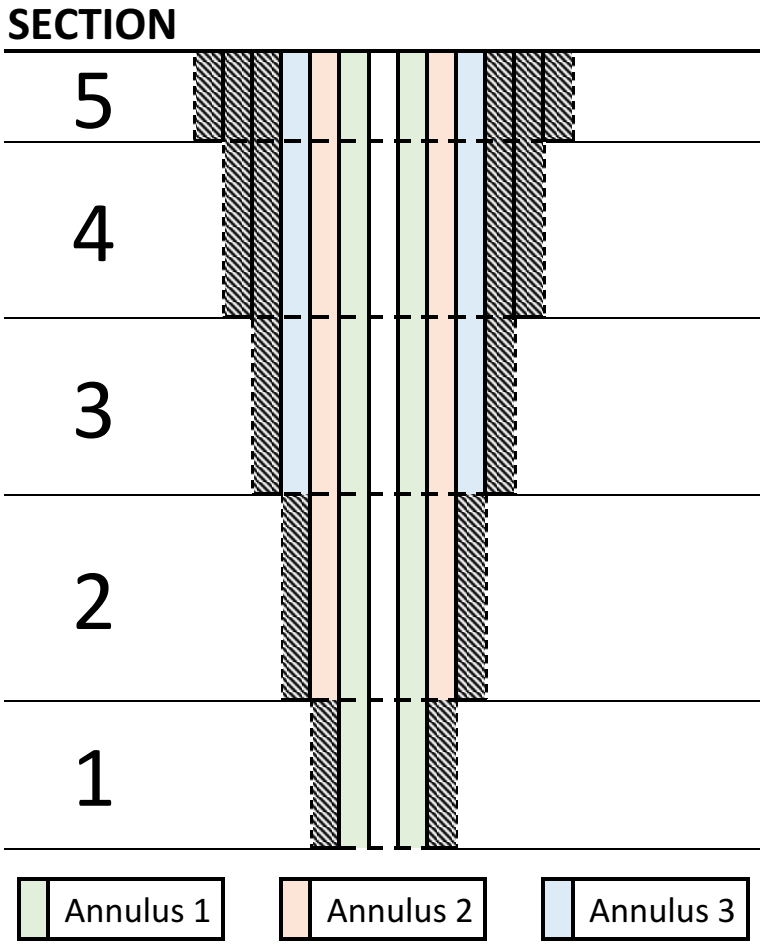

Fig. 3.1. Well configuration

As it is the lateral lineup of resistance terms that dictates the U_{ti}, a new U_{ti} have to be defined for each section where there is a change in well configuration, such as an additional casing, cement, etc. To calculate the U_{ti} for the entire length of the well, the well is divided into 5 sections:

1. Casing shoe 1 to casing shoe 2
2. Casing shoe 2 to casing shoe 3
3. Casing shoe 3 to casing shoe 4
4. Casing shoe 4 to casing shoe 5
5. Casing shoe 5 to top of well (wellhead)

3.2.2 Calculation of the overall heat transfer coefficient for the different well sections

Following is the definitions of U_{ti} given for each section. The parameters used in the definitions are:

h_{ti} : Tubing CHTC [$\mathrm{W\,m^{-2}\,K^{-1}}$]
k_{tbg} : Thermal conductivity of the tubing [$\mathrm{W\,m^{-1}\,K^{-1}}$]
$h_{ca(1,2,3)}$: Annulus 1, 2 and 3 natural CHTC [$\mathrm{W\,m^{-2}\,K^{-1}}$]
$k_{csg(1,2,3,4,5)}$: Thermal conductivity of the casing [$\mathrm{W\,m^{-1}\,K^{-1}}$]
$k_{cem(1,2,3,4,5)}$: Cement layer thermal conductivity [$\mathrm{W\,m^{-1}\,K^{-1}}$]
r_{ti} : Tubing wall inside radius [m]
r_{to} : Tubing wall outside radius [m]
$r_{ci(1,2,3,4,5)}$: Casing wall inside radius [m]
$r_{co(1,2,3,4,5)}$: Casing wall outside radius [m]
$r_{wb(1,2,3,4,5)}$: Wellbore wall radius [m]
$_{1,2,3,4,5}$: Subscripts for element representing its position in the wellbore

3.2.2.1 Section 1 (casing shoe 1 to casing shoe 2)

Section 1 consist of the following resistances, left to right:

(i) The thin stagnant fluid film on the inside of the production tubing

(ii) The tubing wall

(iii) The fluid in annulus 1

(iv) The casing 1 wall

(v) The cement 1 sheath

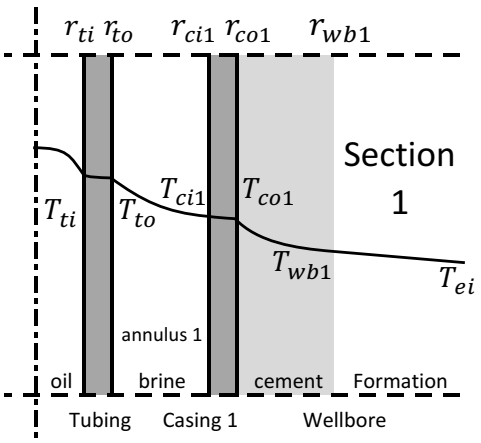

Fig. 3.2. Temperature distribution throughout the wellbore cross section for section 1

$$R_{\text{total1}} = \frac{1}{2\pi r_{\text{ti}} L h_{\text{ti}}} + \frac{\ln\left(\frac{r_{\text{to}}}{r_{\text{ti}}}\right)}{2\pi L k_{\text{tbg}}} + \frac{1}{2\pi r_{\text{to}} L h_{\text{ca1}}} + \frac{\ln\left(\frac{r_{\text{co1}}}{r_{\text{ci1}}}\right)}{2\pi L k_{\text{csg1}}} + \frac{\ln\left(\frac{r_{\text{wb1}}}{r_{\text{co1}}}\right)}{2\pi L k_{\text{cem1}}} \tag{3.38}$$

Thus, U_{ti1} is given as:

$$U_{\text{ti1}} = \frac{1}{R_{\text{total1}} A_{\text{ti}}}$$

$$U_{\text{ti1}} = \left[\frac{1}{h_{\text{ti}}} + \frac{r_{\text{ti}} \ln\left(\frac{r_{\text{to}}}{r_{\text{ti}}}\right)}{k_{\text{tbg}}} + \frac{r_{\text{ti}}}{r_{\text{to}} h_{\text{ca1}}} + \frac{r_{\text{ti}} \ln\left(\frac{r_{\text{co1}}}{r_{\text{ci1}}}\right)}{k_{\text{csg1}}} + \frac{r_{\text{ti}} \ln\left(\frac{r_{\text{wb1}}}{r_{\text{co1}}}\right)}{k_{\text{cem1}}}\right]^{-1} \tag{3.39}$$

3.2.2.2 Section 2 (casing shoe 2 to casing shoe 3)

Section 2 consist of the following resistances, left to right:

(i) The thin stagnant fluid film on the inside of the production tubing

(ii) The tubing wall

(iii) The fluid in annulus 1

(iv) The casing 1 wall

(v) The fluid in annulus 2

(vi) The casing 2 wall

(vii) The cement 2 sheath

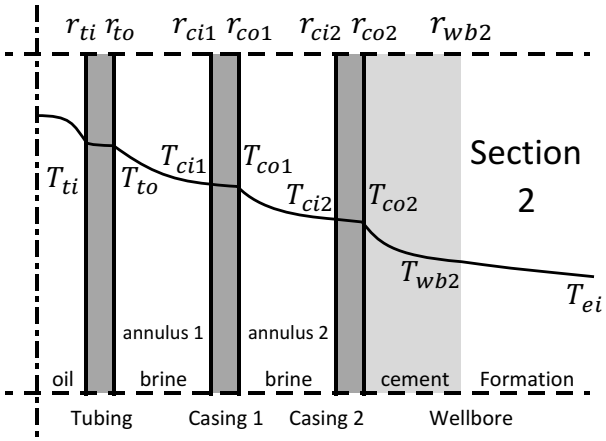

Fig. 3.3. Temperature distribution throughout the wellbore cross section for section 2

$$\begin{aligned} R_{\text{total2}} =& \frac{1}{2\pi r_{\text{ti}} L h_{\text{ti}}} + \frac{\ln\left(\frac{r_{\text{to}}}{r_{\text{ti}}}\right)}{2\pi L k_{\text{tbg}}} + \frac{1}{2\pi r_{\text{to}} L h_{\text{ca1}}} + \frac{\ln\left(\frac{r_{\text{co1}}}{r_{\text{ci1}}}\right)}{2\pi L k_{\text{csg1}}} \\ &+ \frac{1}{2\pi r_{\text{co1}} L h_{\text{ca2}}} + \frac{\ln\left(\frac{r_{\text{wb2}}}{r_{\text{co2}}}\right)}{2\pi L k_{\text{cem2}}} \end{aligned} \tag{3.40}$$

Thus, U_{ti2} is given as:

$$\begin{aligned} U_{\text{ti2}} =& \frac{1}{R_{\text{total2}} A_{\text{ti}}} \\ U_{\text{ti2}} =& \left[\frac{1}{h_{\text{ti}}} + \frac{r_{\text{ti}} \ln\left(\frac{r_{\text{to}}}{r_{\text{ti}}}\right)}{k_{\text{tbg}}} + \frac{r_{\text{ti}}}{r_{\text{to}} h_{\text{ca1}}} + \frac{r_{\text{ti}} \ln\left(\frac{r_{\text{co1}}}{r_{\text{ci1}}}\right)}{k_{\text{csg1}}} \right. \\ &\left. + \frac{r_{\text{ti}}}{r_{\text{co1}} h_{\text{ca2}}} + \frac{r_{\text{ti}} \ln\left(\frac{r_{\text{co2}}}{r_{\text{ci2}}}\right)}{k_{\text{csg2}}} + \frac{r_{\text{ti}} \ln\left(\frac{r_{\text{wb2}}}{r_{\text{co2}}}\right)}{k_{\text{cem2}}} \right]^{-1} \end{aligned} \tag{3.41}$$

3.2.2.3 Section 3 (casing shoe 3 to casing shoe 4)

Section 3 consist of the following resistances, left to right:

(i) The thin stagnant fluid film on the inside of the production tubing

(ii) The tubing wall

(iii) The fluid in annulus 1

(iv) The casing 1 wall

(v) The fluid in annulus 2

(vi) The casing 2 wall

(vii) The fluid in annulus 3

(viii) The casing 3 wall

(ix) The cement 3 sheath

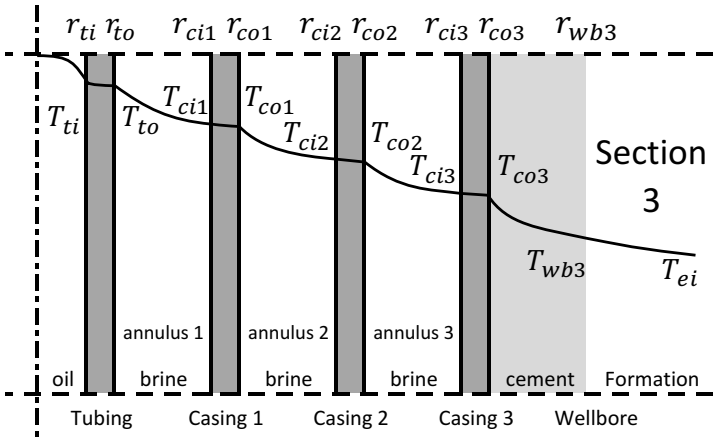

Fig. 3.4. Temperature distribution throughout the wellbore cross section for section 3

$$\begin{aligned} R_{\text{total3}} = & \frac{1}{2\pi r_{\text{ti}} L h_{\text{ti}}} + \frac{\ln\left(\frac{r_{\text{to}}}{r_{\text{ti}}}\right)}{2\pi L k_{\text{tbg}}} + \frac{1}{2\pi r_{\text{to}} L h_{\text{ca1}}} + \frac{\ln\left(\frac{r_{\text{co1}}}{r_{\text{ci1}}}\right)}{2\pi L k_{\text{csg1}}} \\ & + \frac{1}{2\pi r_{\text{co1}} L h_{\text{ca2}}} + \frac{\ln\left(\frac{r_{\text{co2}}}{r_{\text{ci2}}}\right)}{2\pi L k_{\text{csg2}}} + \frac{1}{2\pi r_{\text{co2}} L h_{\text{ca3}}} + \frac{\ln\left(\frac{r_{\text{co3}}}{r_{\text{ci3}}}\right)}{2\pi L k_{\text{csg3}}} \\ & + \frac{\ln\left(\frac{r_{\text{wb3}}}{r_{\text{co3}}}\right)}{2\pi L k_{\text{cem3}}} \end{aligned} \tag{3.42}$$

Thus, U_{ti3} is given as:

$$U_{\text{ti3}} = \frac{1}{R_{\text{total3}} A_{\text{ti}}}$$

$$U_{\mathrm{ti3}} = \left[\frac{1}{h_{\mathrm{ti}}} + \frac{r_{\mathrm{ti}} \ln\left(\frac{r_{\mathrm{to}}}{r_{\mathrm{ti}}}\right)}{k_{\mathrm{tbg}}} + \frac{r_{\mathrm{ti}}}{r_{\mathrm{to}} h_{\mathrm{ca1}}} + \frac{r_{\mathrm{ti}} \ln\left(\frac{r_{\mathrm{co1}}}{r_{\mathrm{ci1}}}\right)}{k_{\mathrm{csg1}}} + \frac{r_{\mathrm{ti}}}{r_{\mathrm{co1}} h_{\mathrm{ca2}}} + \frac{r_{\mathrm{ti}} \ln\left(\frac{r_{\mathrm{co2}}}{r_{\mathrm{ci2}}}\right)}{k_{\mathrm{csg2}}} + \frac{r_{\mathrm{ti}}}{r_{\mathrm{co2}} h_{\mathrm{ca3}}} + \frac{r_{\mathrm{ti}} \ln\left(\frac{r_{\mathrm{co3}}}{r_{\mathrm{ci3}}}\right)}{k_{\mathrm{csg3}}} + \frac{r_{\mathrm{ti}} \ln\left(\frac{r_{\mathrm{wb3}}}{r_{\mathrm{co3}}}\right)}{k_{\mathrm{cem3}}} \right]^{-1} \tag{3.43}$$

3.2.2.4 Section 4 (casing shoe 4 to casing shoe 5)

Section 4 consist of the following resistances, left to right:

(i) The thin stagnant fluid film on the inside of the production tubing

(ii) The tubing wall

(iii) The fluid in annulus 1

(iv) The casing 1 wall

(v) The fluid in annulus 2

(vi) The casing 2 wall

(vii) The fluid in annulus 3

(viii) The casing 3 wall

(ix) The cement 3 sheath

(x) The casing 4 wall

(xi) The cement 4 sheath

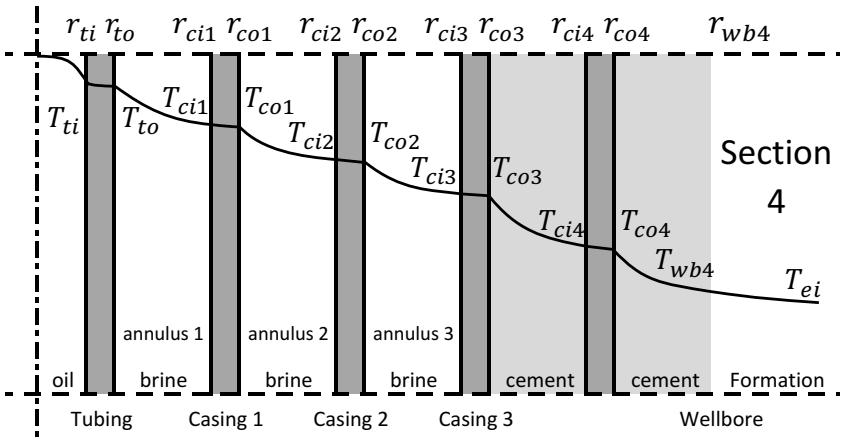

Fig. 3.5. Temperature distribution throughout the wellbore cross section for section 4

$$
\begin{aligned}
R_{\text{total4}} =& \frac{1}{2\pi r_{\text{ti}} L h_{\text{ti}}} + \frac{\ln\left(\frac{r_{\text{to}}}{r_{\text{ti}}}\right)}{2\pi L k_{\text{tbg}}} + \frac{1}{2\pi r_{\text{to}} L h_{\text{ca1}}} + \frac{\ln\left(\frac{r_{\text{co1}}}{r_{\text{ci1}}}\right)}{2\pi L k_{\text{csg1}}} \\
&+ \frac{1}{2\pi r_{\text{co1}} L h_{\text{ca2}}} + \frac{\ln\left(\frac{r_{\text{co2}}}{r_{\text{ci2}}}\right)}{2\pi L k_{\text{csg2}}} + \frac{1}{2\pi r_{\text{co2}} L h_{\text{ca3}}} \\
&+ \frac{\ln\left(\frac{r_{\text{co3}}}{r_{\text{ci3}}}\right)}{2\pi L k_{\text{csg3}}} \\
&+ \frac{\ln\left(\frac{r_{\text{ci4}}}{r_{\text{co3}}}\right)}{2\pi L k_{\text{cem3}}} + \frac{\ln\left(\frac{r_{\text{co4}}}{r_{\text{ci4}}}\right)}{2\pi L k_{\text{csg4}}} + \frac{\ln\left(\frac{r_{\text{wb4}}}{r_{\text{co4}}}\right)}{2\pi L k_{\text{cem4}}}
\end{aligned}
\tag{3.44}
$$

Thus, U_{ti4} is given as:

$$
\begin{aligned}
U_{\text{ti4}} =& \frac{1}{R_{\text{total4}} A_{\text{ti}}} \\
U_{\text{ti4}} =& \left[\frac{1}{h_{\text{ti}}} + \frac{r_{\text{ti}} \ln\left(\frac{r_{\text{to}}}{r_{\text{ti}}}\right)}{k_{\text{tbg}}} + \frac{r_{\text{ti}}}{r_{\text{to}} h_{\text{ca1}}} + \frac{r_{\text{ti}} \ln\left(\frac{r_{\text{co1}}}{r_{\text{ci1}}}\right)}{k_{\text{csg1}}} \right. \\
&+ \frac{r_{\text{ti}}}{r_{\text{co1}} h_{\text{ca2}}} + \frac{r_{\text{ti}} \ln\left(\frac{r_{\text{co2}}}{r_{\text{ci2}}}\right)}{k_{\text{csg2}}} + \frac{r_{\text{ti}}}{r_{\text{co2}} h_{\text{ca3}}} + \frac{r_{\text{ti}} \ln\left(\frac{r_{\text{co3}}}{r_{\text{ci3}}}\right)}{k_{\text{csg3}}} \\
&\left. + \frac{r_{\text{ti}} \ln\left(\frac{r_{\text{ci4}}}{r_{\text{co3}}}\right)}{k_{\text{cem3}}} + \frac{r_{\text{ti}} \ln\left(\frac{r_{\text{co4}}}{r_{\text{ci4}}}\right)}{k_{\text{csg4}}} + \frac{r_{\text{ti}} \ln\left(\frac{r_{\text{wb4}}}{r_{\text{co4}}}\right)}{k_{\text{cem4}}} \right]^{-1}
\end{aligned}
\tag{3.45}
$$

3.2.2.5 Section 5 (casing shoe 5 to wellhead)

Section 5 consist of the following resistances, left to right:

(i) The thin stagnant fluid film on the inside of the production tubing

(ii) The tubing wall

(iii) The fluid in annulus 1

(iv) The casing 1 wall

(v) The fluid in annulus 2

(vi) The casing 2 wall

(vii) The fluid in annulus 3

(viii) The casing 3 wall

(ix) The cement 3 sheath

(x) The casing 4 wall

(xi) The cement 4 sheath

(xii) The casing 5 wall

(xiii) The cement 5 sheath

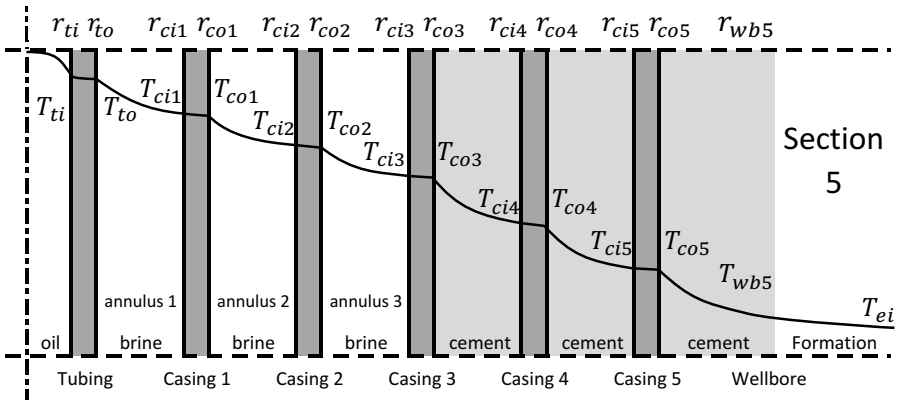

Fig. 3.6. Temperature distribution throughout the wellbore cross section for section 5

$$
\begin{aligned}
R_{\text{total5}} =& \frac{1}{2\pi r_{\text{ti}} L h_{\text{ti}}} + \frac{\ln\left(\frac{r_{\text{to}}}{r_{\text{ti}}}\right)}{2\pi L k_{\text{tbg}}} + \frac{1}{2\pi r_{\text{to}} L h_{\text{ca1}}} + \frac{\ln\left(\frac{r_{\text{co1}}}{r_{\text{ci1}}}\right)}{2\pi L k_{\text{csg1}}} \\
&+ \frac{1}{2\pi r_{\text{co1}} L h_{\text{ca2}}} + \frac{\ln\left(\frac{r_{\text{co2}}}{r_{\text{ci2}}}\right)}{2\pi L k_{\text{csg2}}} + \frac{1}{2\pi r_{\text{co2}} L h_{\text{ca3}}} + \frac{\ln\left(\frac{r_{\text{co3}}}{r_{\text{ci3}}}\right)}{2\pi L k_{\text{csg3}}} \\
&+ \frac{\ln\left(\frac{r_{\text{ci4}}}{r_{\text{co3}}}\right)}{2\pi L k_{\text{cem3}}} + \frac{\ln\left(\frac{r_{\text{co4}}}{r_{\text{ci4}}}\right)}{2\pi L k_{\text{csg4}}} + \frac{\ln\left(\frac{r_{\text{ci5}}}{r_{\text{co4}}}\right)}{2\pi L k_{\text{cem4}}} + \frac{\ln\left(\frac{r_{\text{co5}}}{r_{\text{ci5}}}\right)}{2\pi L k_{\text{csg5}}} \\
&+ \frac{\ln\left(\frac{r_{\text{wb5}}}{r_{\text{co5}}}\right)}{2\pi L k_{\text{cem5}}}
\end{aligned}
\tag{3.46}
$$

Thus, U_{ti5} is given as:

$$
\begin{aligned}
U_{\text{ti5}} =& \frac{1}{R_{\text{total5}} A_{\text{ti}}} \\
U_{\text{ti5}} =& \left[\frac{1}{h_{\text{ti}}} + \frac{r_{\text{ti}} \ln\left(\frac{r_{\text{to}}}{r_{\text{ti}}}\right)}{k_{\text{tbg}}} + \frac{r_{\text{ti}}}{r_{\text{to}} h_{\text{ca1}}} + \frac{r_{\text{ti}} \ln\left(\frac{r_{\text{co1}}}{r_{\text{ci1}}}\right)}{k_{\text{csg1}}} \right. \\
&+ \frac{r_{\text{ti}}}{r_{\text{co1}} h_{\text{ca2}}} + \frac{r_{\text{ti}} \ln\left(\frac{r_{\text{co2}}}{r_{\text{ci2}}}\right)}{k_{\text{csg2}}} + \frac{r_{\text{ti}}}{r_{\text{co2}} h_{\text{ca3}}} + \frac{r_{\text{ti}} \ln\left(\frac{r_{\text{co3}}}{r_{\text{ci3}}}\right)}{k_{\text{csg3}}} \\
&+ \frac{r_{\text{ti}} \ln\left(\frac{r_{\text{ci4}}}{r_{\text{co3}}}\right)}{k_{\text{cem3}}} + \frac{r_{\text{ti}} \ln\left(\frac{r_{\text{co4}}}{r_{\text{ci4}}}\right)}{k_{\text{csg4}}} + \frac{r_{\text{ti}} \ln\left(\frac{r_{\text{ci5}}}{r_{\text{co4}}}\right)}{k_{\text{cem4}}} + \frac{r_{\text{ti}} \ln\left(\frac{r_{\text{co5}}}{r_{\text{ci5}}}\right)}{k_{\text{csg5}}} \\
&\left. + \frac{r_{\text{ti}} \ln\left(\frac{r_{\text{wb5}}}{r_{\text{co5}}}\right)}{k_{\text{cem5}}} \right]^{-1}
\end{aligned}
\tag{3.47}
$$

3.2.3 The convective heat transfer coefficient for the tubing inside wall

The convective heat transfer coefficient for the tubing inside, h_{ti}, is estimated by the Nu given by the Gnielinski correlation (See Table 2.1).

$$
h_{\text{ti}} = \left[\frac{(f_{\text{D}}/8)(Re - 1000)Pr}{1 + 12.7(f_{\text{D}}/8)^{0.5}\left(Pr^{2/3} - 1\right)} \right] \frac{k_t}{2r_{\text{ti}}} \tag{3.48}
$$

It is valid for $2300 < Re < 5 \times 10^6$ and $0.5 < Pr < 2000$. The Pr for the tubing is given by:

$$Pr_{\mathrm{t}} = \frac{c_{\mathrm{pl}} \mu_{\mathrm{l}}}{k_{\mathrm{l}}} \tag{3.49}$$

where: μ_{l} : Viscosity of the produced fluid [Pa s]
k_{l} : Thermal conductivity of the produced fluid [$\mathrm{W\,m^{-1}\,K^{-1}}$]

The Gnielinski correlation applies to both turbulent and transition flow regimes. For laminar flow, $Re < 2300$, $Nu = 4.36$ (Table 2.1) is used.

3.2.4 The free/natural convective heat transfer coefficient for fluid filled annulus

When calculating free or natural convective heat transfer through annulus it may be beneficial to express the heat transfer in terms of fictitious stationary fluid, where the equivalent thermal conductivity, k_{hc} is used instead of the normal thermal conductivity (Bergman et al., 2011, p. 625). k_{hc} can be defined as:

$$\frac{k_{\mathrm{hc}}}{k_{\mathrm{a}}} = Nu \tag{3.50}$$

Note that there is both conduction through fluid and natural convection taking place in the annulus. The equivalent thermal conductivity, k_{hc}, can not be less than the thermal conductivity of the annulus fluid, k_{a}, alone. Thus k_{hc} must be set equal to k_{a} if $k_{\mathrm{hc}}/k_{\mathrm{a}} < 1$. The heat transfer through this fictitious fluid can be considered to be the same as for the real free convection case (Bergman et al., 2011, p. 625), and thus reducing the case of free convection to a conductive heat transfer problem.

In the following example, equations representing the innermost annulus (1) between the production tubing and casing is presented. The calculations are applicable to all three fluid filled annulus.

The equivalent conductive heat transfer of the fluid filling the annulus between the hot and cold opposite walls (in this example the tubing outside, r_{to} and casing inside r_{ci1} wall respectively) is given as:

$$Q = \frac{2\pi L k_{\mathrm{hc1}} \left(T_{\mathrm{to}} - T_{\mathrm{ci1}}\right)}{\ln\left(\frac{r_{\mathrm{ci1}}}{r_{\mathrm{to}}}\right)} \tag{3.51}$$

The convective heat transfer in annulus 1 is given as:

$$Q = 2\pi r_{\text{to}} L h_{\text{ca1}} \left(T_{\text{to}} - T_{\text{ci1}}\right) \tag{3.52}$$

where: $(2\pi r_{\text{to}} L)$: Tubing outside area (A_{to}) [m^2]

The expression for k_{hc1} can be obtained by combining Eq. (3.51) and Eq. (3.52):

$$h_{\text{ca1}} = \frac{k_{\text{hc1}}}{r_{\text{to}} \ln\left(\frac{r_{\text{ci1}}}{r_{\text{to}}}\right)} \tag{3.53}$$

By substituting the definition of k_{hc1} from Eq. (3.50) into Eq. (3.53), we can see that:

$$h_{\text{ca1}} = \frac{k_{\text{a1}} Nu}{r_{\text{to}} \ln\left(\frac{r_{\text{ci1}}}{r_{\text{to}}}\right)} \tag{3.54}$$

The Nu for free convection is a function of both Gr and Pr numbers, $Nu = f(Gr, Pr)$ (Holman, 2010). By choosing the appropriate free convection correlation, e.g. the Dropkin and Somerscales correlation used by both Hasan et al. (1994) and Willhite (1967), we can find an expression for h_{ca1}. The Dropkin and Somerscales correlation is given as:

$$Nu = C(GrPr)^{1/3} Pr^{0.074} \tag{3.55}$$

where: C : Correction factor for wellbore inclination

See Subsubsection 2.10.1.7 for the inclination correction factors. The correlation is valid in the range $5 \times 10^4 < Ra < 7.5 \times 10^8$ with small variations depending on inclination angle, and $0.02 \leq Pr \leq 11560$ for all inclination angles. Representing the correlation in the form of Eq. (3.54), h_{ca1} is defined as:

$$h_{\text{ca1}} = \frac{k_{\text{a1}} C(Gr_{\text{a1}} Pr_{\text{a1}})^{1/3} Pr_{\text{a1}}^{0.074}}{r_{\text{to}} \ln\left(\frac{r_{\text{ci1}}}{r_{\text{to}}}\right)} \tag{3.56}$$

All parameters are evaluated at $T_{\text{a1}} = (T_{\text{to}} + T_{\text{ci1}})/2$. The Grashof number for the annulus, Gr_{a1}:

$$Gr_{\text{a1}} = \frac{(r_{\text{ci1}} - r_{\text{to}})^3 g \rho_{\text{a1}}^2 \beta \left(T_{\text{to}} - T_{\text{ci1}}\right)}{\mu_{\text{a1}}^2} \tag{3.57}$$

where: β_{a1} : Thermal volumetric expansion coefficient of the fluid in annulus 1 [K^{-1}]
ρ_{a1} : Annulus 1 fluid density [$kg\,m^{-3}$]
μ_{a1} : Viscosity of the fluid in annulus 1 [$Pa\,s$]

The Prandtl number for the annulus, Pr_{a1}:

$$Pr_{a1} = \frac{c_{pa1}\mu_{a1}}{k_{a1}} \tag{3.58}$$

where: c_{pa1} : Specific heat capacity of the annulus fluid [$J\,kg^{-1}\,K^{-1}$]
k_{a1} : Thermal conductivity of the annulus fluid [$W\,m^{-1}\,K^{-1}$]

3.2.5 Calculation of the wellbore trajectory

As the model takes into consideration the wellbore inclination angle, there is an option to implement a wellbore trajectory.

For testing the inclination effects on the model, a simple wellbore trajectory is implemented. The wellbore is divided into three sections; a vertical section, followed by a build section, and then a sail section at a constant inclination equal to the dogleg (DL) angle, as shown in Fig. 3.7.

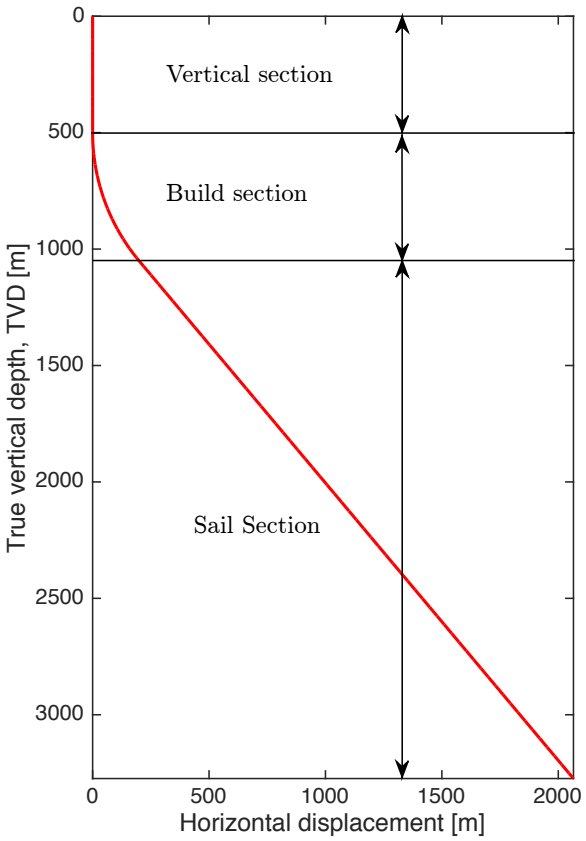

Fig. 3.7. Wellbore trajectory

The wellbore is divided into n cells of measured length, dz, along the wellbore trajectory. Assuming zero azimuth, each cell is considered to have a constant inclination with respect to the vertical, and a true vertical and horizontal length equal to the vertical and horizontal projection of the cell respectively. Cell (i) is presented in Fig. 3.8.

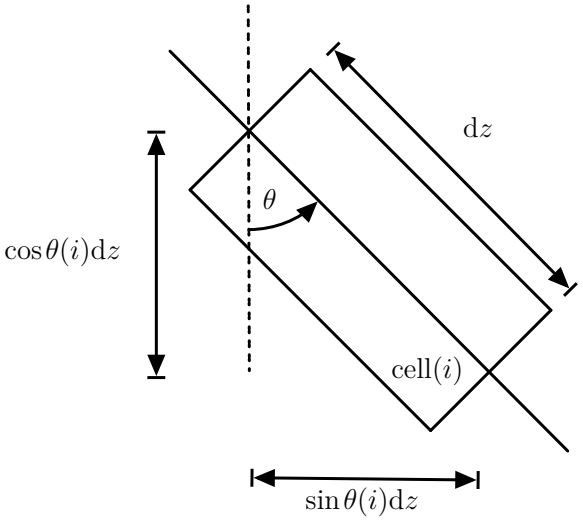

Fig. 3.8. Wellbore cell (i)

After specifying individual section lengths and the DL, the dogleg severity (DLS) is given as:

$$\text{DLS} = \frac{\text{DL (deg)}}{\text{Measured length of bending section}} \tag{3.59}$$

The individual cell inclination in the bending section is given by increasing each consecutive cells inclination by DLS$\times$dz. As an example, the inclination of cell m is given as:

$$\theta(m) = \sum_{i=1}^{m} \text{DLS} \times \text{d}z \tag{3.60}$$

The inclination of the individual cells in the sail section is equal to the DL.

The vertical and horizontal dimensions of each individual cell are calculated, respectively, as:

$$\text{Vertical length}(i) = \cos\theta(i)\text{d}z \tag{3.61}$$

$$\text{Horizontal length}(i) = \sin\theta(i)\text{d}z \tag{3.62}$$

The true vertical depth (TVD) from the top of the well to the bottom of cell (i) is given as the sum of the previous cells vertical extent:

$$\mathrm{TVD}(i) = \sum_{i=1}^{n} \cos\theta(i)\mathrm{d}z \tag{3.63}$$

The true horizontal displacement (THD) of the bottom of cell (i) is given as:

$$\mathrm{THD}(i) = \sum_{i=1}^{n} \sin\theta(i)\mathrm{d}z \tag{3.64}$$

The last cell of the TVD and THD vectors give the target coordinates, (THD(n), TVD(n)).

3.3 Thermophysical properties used in the model

3.3.1 Formation properties

To get values that are representable for formation rock, a dataset from Kutasov and Eppelbaum (2015) (Found in Table 2.7 in the reference) for clay is used to represent formation properties. The values for density, thermal conductivity and specific heat capacity of clay is given as:

$$\rho_{\mathrm{e}} = 2080[\mathrm{kg\,m^{-3}}] \tag{3.65}$$

$$k_{\mathrm{e}} = 1.42[\mathrm{W\,m^{-1}\,K^{-1}}] \tag{3.66}$$

$$c_{\mathrm{pe}} = 2027[\mathrm{J\,kg^{-1}\,K}] \tag{3.67}$$

3.3.2 Properties of fluid in annulus

Following are the temperature correlations for the annular fluid properties. Sadly, some are not given in SI-units. Assuming a Newtonian fluid, similar in composition to seawater to be filling up the annulus, the annular fluid thermal conductivity, k_{a}, and specific heat capacity, c_{pa}, temperature dependency may be approximated by correlations for aqueous NaCl solutions. According to Ozbek and Phillips (1979), the thermal conductivity of aqueous NaCl solutions may be approximated by first calculating the pure water thermal conductivity:

$$\begin{aligned} k_{\mathrm{w}} = -0.92247 + 2.8395 \times \left(\frac{T+273.15}{273.15}\right) - 1.8007 \times \left(\frac{T+273.15}{273.15}\right)^2 \\ +0.52577 \times \left(\frac{T+273.15}{273.15}\right)^3 - 0.07344 \times \left(\frac{T+273.15}{273.15}\right)^4 \end{aligned} \tag{3.68}$$

where: T : Temperature (°C)

k_{w} : Thermal conductivity of pure water $[\mathrm{W\,m^{-1}\,K^{-1}}]$

With the thermal conductivity for pure water, k_{w}, we can calculate the thermal conductivity of the aqueous NaCl solution. The saline solution thermal conductivity, k_{a}, is given by the following correlation (Range of validity: 20 to 330 °C):

$$\begin{aligned} \frac{k_{\mathrm{a}}}{k_{\mathrm{w}}} = 1 - (2.3434 \times 10^{-3} - 7.024 \times 10^{-6} T + 3.924 \times 10^{-8} T^2) C_{\mathrm{S}} \\ +(1.06 \times 10^{-5} - 2 \times 10^{-8} T + 1.2 \times 10^{-10} T^2) C_{\mathrm{S}}^2 \end{aligned} \tag{3.69}$$

where: k_a : Thermal conductivity of aqueous NaCl solution [$\mathrm{W\,m^{-1}\,K^{-1}}$]
T : Temperature (°C)
C_S : Salt concentration, weight percent

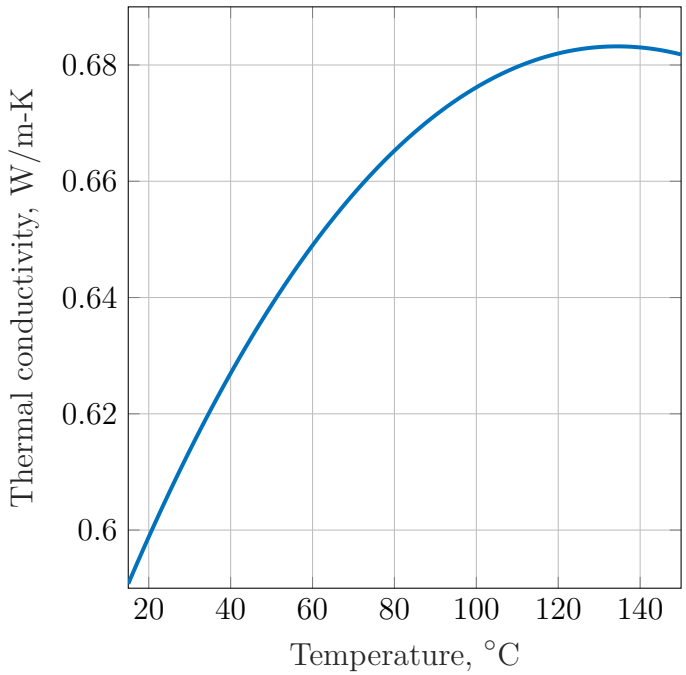

Fig. 3.9. Thermal conductivity of 3.5 wt% NaCl brine vs temperature

The following temperature correlation for sea water specific heat capacity, given by Jamieson, Tudhope, Morris, and Cartwright (1969), is implemented.

$$c_{pa} = (A_1 + A_2 T + A_3 T^2 + A_4 T^3) \times 10^3 \tag{3.70}$$

$$A_1 = 5.328 - 9.76 \times 10^{-2} S + 4.04 * 10^{-4} S^2$$
$$A_2 = -6.913 \times 10^{-3} + 7.351 * 10^{-4} * S - 3.15 * 10^{-6} S^2$$
$$A_3 = 9.6 \times 10^{-6} - 1.927 \times 10^{-6} S + 8.23 \times 10^{-}9 S^2$$
$$A_4 = 2.5 \times 10^{-9} + 1.666 \times 10^{-9} S - 7.125 \times 10^{-12} S^2$$

where: T : Temperature [K]
c_{pa} : Specific heat capacity of NaCl solution [$\mathrm{J\,kg^{-1}\,K^{-1}}$]
S : Salinity of aqueous NaCl solution [g/kg]

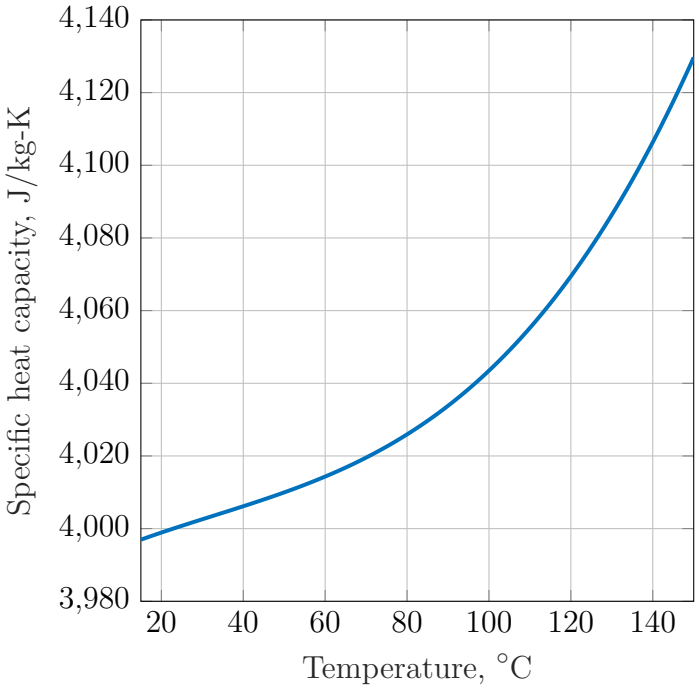

Fig. 3.10. Specific heat capacity of 3.5 wt% NaCl brine vs temperature

The viscosity temperature behavior of brines can be described by a correlation presented by Numbere, Brigham, and Standing (1977). It requires us to first define the pure water viscosity as a function of temperature at saturation pressure. It is given as:

$$\mu_{\mathrm{w}}(T, P_{\mathrm{sat}}) = 241.4 \times 10^{\left[\frac{247.8}{T-140}\right]} \tag{3.71}$$

where: $\mu_{\mathrm{w}}(T, P_{\mathrm{sat}})$: Apparent viscosity of pure water at saturation pressure (cP)
T : Temperature (°F)
P_{sat} : Saturation pressure for pure water (psi)

The viscosity of the aqueous NaCl solution is a function of saturation pressure, given by:

$$P_{\mathrm{sat}} = 0.468 \times \left(\frac{\mathrm{T}}{100}\right)^{4.52} \tag{3.72}$$

where: P_{sat} : Saturation pressure of aqueous NaCl solution (psi)

The viscosity of pure water at elevated pressures (above saturation pressure) is then

given as:

$$\mu_{\mathrm{w}}(T,P) = \left[1 + \frac{P - P_{\mathrm{sat}}}{10^6}\left(1.046T - 319.24\right)\right] \times \mu_{\mathrm{w}}(T, P_{\mathrm{sat}}) \tag{3.73}$$

where: $\mu_{\mathrm{w}}(T,P)$: Viscosity of pure water above saturation pressure (cP)
P : Pressure (psi)

Finally, the viscosity of the brine as a function of salinity and temperature may be calculated from:

$$\begin{aligned}\mu_{\mathrm{s}} = \Bigg(\Big[&-1.87\times10^{-3}C_{\mathrm{S}}^{0.5} + 2.18\times10^{-4}C_{\mathrm{S}}^{2.5} + (T^{0.5} - 1.35\times10^{-2}T) \\ &\times(2.76\times10^{-3}C_{\mathrm{S}} - 3.44\times10^{-4}C_{\mathrm{S}}^{1.5})\Big] + 1\Bigg) \times \mu_{\mathrm{w}}\end{aligned} \tag{3.74}$$

where: μ_{s} : Viscosity of the aqueous NaCl solution brine at P > $\mathrm{P_{sat}}$ (cP)

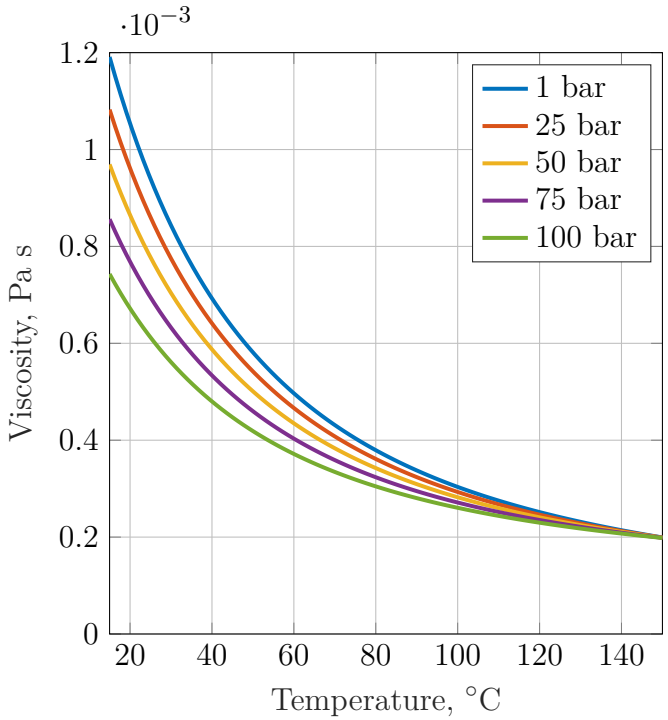

Fig. 3.11. Viscosity of 3.5 wt% NaCl brine vs temperature

The density of the fluid in the annulus as a function of temperature and pressure is modeled by the following equation of state for NaCl brine at high pressure and high

temperature conditions, presented by Kutasov et al. (2015):

$$\rho = \rho_0 \times e^{[\alpha_V P + \beta(T - T_s) + \gamma(T - T_s)^2]} \tag{3.75}$$

where: ρ : Density of brine at P and T (ppg)
α_V : Coefficient of compression (1/psig)
β : Thermal expansion coefficient (1/°F)
γ : Thermal expansion coefficient (1/°F^2)
T : Temperature (°F)
T_s : Temperature at surface (°F)

For details on the calculation of the model coefficients, see Kutasov et al. (2015). The model coefficient values obtained when selecting 3.5 wt% NaCl solution is presented below:

$$\begin{aligned} \rho_0 &= 8.5025 && \text{(ppg)} \\ \alpha &= 4.0770 \times 10^{-6} && \text{(1/psig)} \\ \beta &= -1.6727 \times 10^{-4} && \text{(1/°F)} \\ \gamma &= -4.6568 \times 10^{-7} && \text{(1/°F}^2\text{)} \end{aligned}$$

resulting in the following equation of state for the selected 3.5 wt% NaCl brine:

$$\rho = 8.5025 \times e^{[4.0770 \times 10^{-6} P - 1.6727 \times 10^{-4}(T - T_s) - 4.6568 \times 10^{-7}(T - T_s)^2]} \tag{3.76}$$

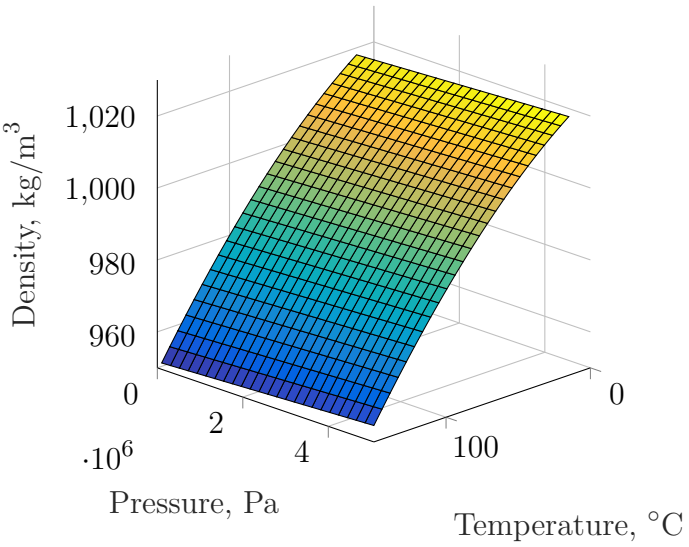

Fig. 3.12. Equation of state for NaCl brine

3.3.3 Properties of produced fluid in the tubing

The produced fluid is assumed to be single phase, Newtonian, and its properties may be approximated by dead oil temperature correlations. Unfortunately, as for the brine correlations, some of the dead oil correlations are also presented in other units than SI.

The thermal conductivity of crude oil may be estimated by Cragoe's equation (Mansure, 1996). It is given as:

$$k_{\mathrm{o}} = \frac{1.62(1 - 0.0003[T - 32])}{\gamma_{\mathrm{o}}} \tag{3.77}$$

where: k_{o} : Thermal conductivity of crude oil $[\mathrm{W\,m^{-1}\,K^{-1}}]$
γ_{o} : Oil gravity (°API)

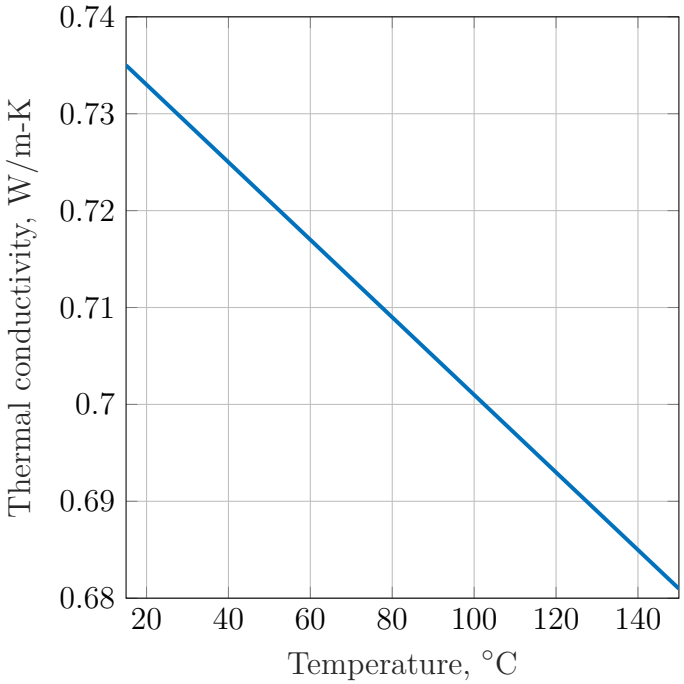

Fig. 3.13. Thermal conductivity of dead oil vs temperature

The dead oil specific heat capacity as a function of temperature can be calculated by the following correlation equation obtained by Wright (2014):

$$c_{\text{od}} = \left[(2\times10^{-3}T - 1.429)sg + 2.67\times10^{-3}T + 3.049\right]\times10^{3} \tag{3.78}$$

where: c_{od} : Specific heat capacity of dead oil at T $[\text{J}\,\text{kg}^{-1}\,\text{K}^{-1}]$
sg : Specific gravity of dead oil

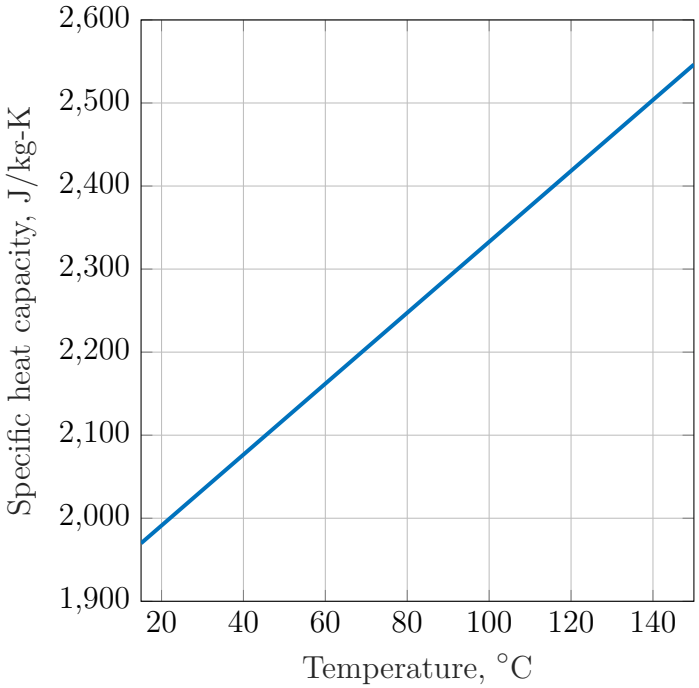

Fig. 3.14. Specific heat capacity of dead oil vs temperature (sg = 0.8)

The dead oil viscosity as a function of temperature is given by the Beggs-Robinson correlation (Beggs and Robinson, 1975):

$$\mu_{\text{od}} = 10^X - 1 \tag{3.79}$$

where the model coefficients:

$$\begin{aligned} X &= yT^{-1.163} \\ y &= 10^Z \\ Z &= 3.0324 - 0.02023\gamma_{\text{o}} \end{aligned}$$

where: μ_{od} : Dead oil viscosity at T (cP)
γ_{o} : Dead oil density (°API)
T : Temperature (°F)

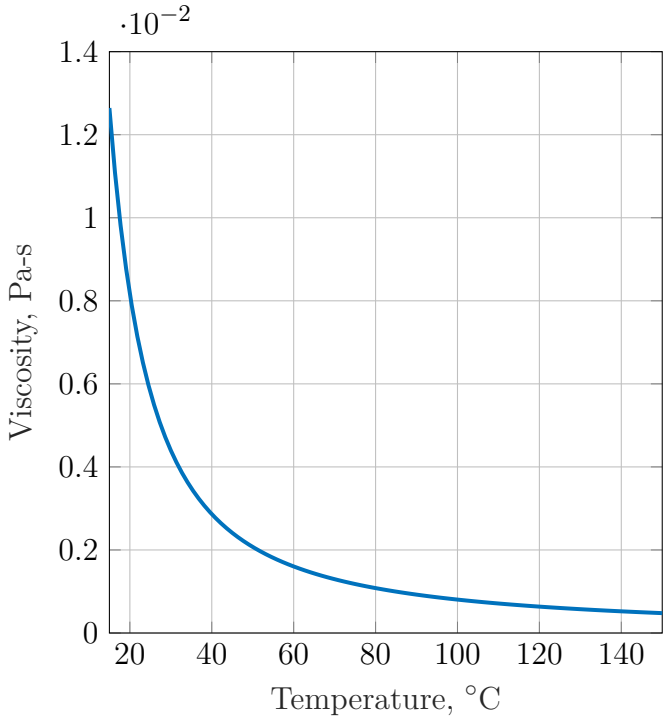

Fig. 3.15. Viscosity of dead oil vs temperature (sg = 0.8)

The density as a function of temperature and pressure may be described by the following equation of state (Standing's relationship, found in Sattarin, Modarresi, Bayat, and Teymori (2007)):

$$\rho = \rho_{\text{sc}} + \Delta\rho_P - \Delta\rho_T \tag{3.80}$$

where:

$$\begin{aligned}
\Delta\rho_P =& [0.167 + 16.181 \times 10^{-0.0425\rho_{\text{sc}}}] \left(\frac{P}{1000}\right) \\
\Delta\rho_T =& [0.0133 + 152.4(\rho_{\text{sc}} + \Delta\rho_P)^{-2.45}](T - 520) \\
& - [(8.1 \times 10^{-6} - 90.0622) \times 10^{-0.764(\rho_{\text{sc}} + \Delta\rho_P)}](T - 520)^2
\end{aligned}$$

where: ρ : Density of oil at pressure and temperature (lbm/ft^3)
ρ_{sc} : Density at standard conditions (lbm/ft^3)
$\Delta\rho_P$: Density correction for compression (lbm/ft^3)
$\Delta\rho_T$: Density correction for thermal expansion (lbm/ft^3)
T : Temperature (°R)
P : Pressure (psi)

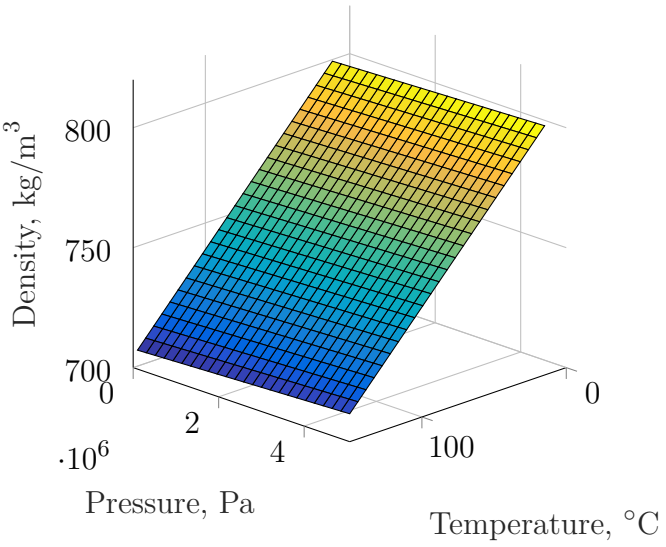

Fig. 3.16. Equation of state for dead oil

3.3.4 Thermal conductivity of tubing, casing and cement

Assuming the tubing and casing is made of Alloy 316, the thermal conduction temperature behavior can be described by the following correlation from Furrer and Semiatin (2010):

$$k_{\mathrm{A316}} = 6.31 + 27.2 \times 10^{-3} T - 7.0 \times 10^{-6} T^2 \tag{3.81}$$

where: k_{A316} : Thermal conductivity of Alloy 316 as function of T [$\mathrm{W\,m^{-1}\,K^{-1}}$]
T : Temperature [K]

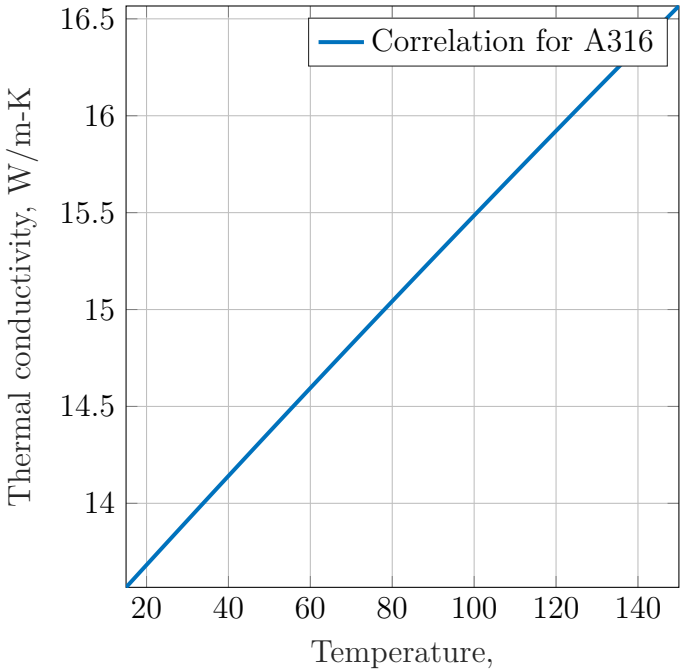

Fig. 3.17. Thermal conductivity of Alloy 316 vs temperature

For the cement between casing and wellbore wall a thermal conductivity correlation for set cement is used, taken from Santoyo, García, Morales, Contreras, and Espinosa-Paredes (2001). The reference provides correlations for six different cementing systems in the temperature range of 20-280°C, where system "D" in the reference is chosen. System "D" is an API Cement G with some additional components. The thermal conductivity is given as:

$$k_{\text{cement}} = 0.50442 + 0.0003125T \tag{3.82}$$

where: k_{cement} : Thermal conductivity of set cement $[\mathrm{W\,m^{-1}\,K^{-1}}]$
T : Temperature (°C)

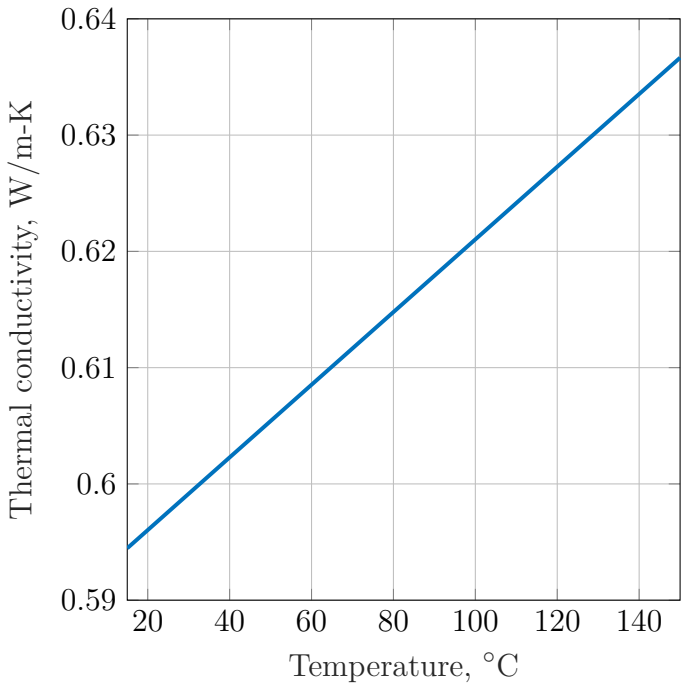

Fig. 3.18. Thermal conductivity of set cement vs temperature

3.4 Well temperature profile calculation procedure

	Parameter for cell (i)		**Given in:**
Produced fluid:	Density	$\rho_{\mathrm{o}}(i)$	Eq. (3.80)
	Specific heat capacity	$c_{\mathrm{po}}(i)$	Eq. (3.78)
	Thermal conductivity	$k_{\mathrm{o}}(i)$	Eq. (3.77)
	Viscosity	$\mu_{\mathrm{o}}(i)$	Eq. (3.79)
Fluid in annulus:	Density	$\rho_{\mathrm{a}(1,2,3)}(i)$	Eq. (3.76)
	Specific heat capacity	$c_{\mathrm{pa}(1,2,3)}(i)$	Eq. (3.70)
	Thermal conductivity	$k_{\mathrm{a}(1,2,3)}(i)$	Eq. (3.69)
	Viscosity	$\mu_{\mathrm{a}(1,2,3)}(i)$	Eq. (3.74)
Tubing:	Thermal conductivity	$k_{\mathrm{tbg}}(i)$	Eq. (3.81)
Casing:	Thermal conductivity	$k_{\mathrm{csg}(1,2,3,4,5)}(i)$	Eq. (3.81)
Cement:	Thermal conductivity	$k_{\mathrm{cem}(1,2,3,4,5)}(i)$	Eq. (3.82)

Table 3.1. Model input parameters for cell (i)

The simplified calculation procedure:

1. Set starting parameters:

   - Volume flow rate and produced oil density at standard conditions to calculate the mass flow rate.
   - Constant formation properties: ρ_{e}, k_{e}, and c_{pe} (see Subsection 3.3.1).
   - Production time to calculate the transient wellbore temperature (see Equation 3.17).
   - Well configurations (Setting depths and casing dimensions).
   - Wellbore trajectory (DL and the vertical, bending, and sail section lengths).
   - Surface earth temperature, T_e(surface).
   - Geothermal gradient, g_G (see Subsection 3.3.1).

2. For each cell, starting from the bottom cell at the bottom of the well:

   - Calculate thermophysical properties of produced and annular fluids, casings and cement (see Table 3.1), according to the configuration of the well section (see Subsection 3.2.2), at previous cell $(i-1)$ conditions (approximation). The first cell assumes all temperatures equal to the undisturbed bottomhole formation temperature, T_{ei}(bh).

- Estimate $U_{\mathrm{ti}}(i)$ for the current well section (1, 2, 3, 4 or 5) by iteration:
  - For the first iteration assume produced fluid temperature equal to its previous cell value, $T_{\mathrm{f}}(i) = T_{\mathrm{f}}(i-1)$ (see Equation 3.37), and overall heat transfer coefficient for the current well section equal to its previous cell value, $U_{\mathrm{ti}}(i) = U_{\mathrm{ti}}(i-1)$ (see Subsection 3.2.2).
  - Estimate the individual $h_{\mathrm{ca}}(i)$ (see Eq. (3.2.4)) for each separate annulus in the current section based on $U_{\mathrm{ti}}(i)$.
  - Calculate $h_{\mathrm{ti}}(i)$ (see Subsection 3.2.3).
  - Estimate new $U_{\mathrm{ti}}(i)$.
  - Check for $U_{\mathrm{ti}}(i)$ convergence. As long as error is larger than a specified tolerance, the calculated $U_{\mathrm{ti}}(i)$ is fed in to the start of the loop as a new starting value for the following iterative step, and we get new $h_{\mathrm{ti}}(i)$ and $h_{\mathrm{ca}}(i)$ values for the next iteration of $U_{\mathrm{ti}}(i)$ and so on.
- Calculate the current cell produced fluid temperature $T_{\mathrm{f}}(i)$ by Equation 3.37 based on the estimated $U_{\mathrm{ti}}(i)$.
- Calculate the current cell temperatures of the different interfaces (tubing and casing inside and outside walls, and the wellbore/formation interface) based on the correct $U_{\mathrm{ti}}(i)$ found by iteration (see Section 3.5 for the definition of U_{ti})

3.5 Example calculation of temperatures at the different tubing, casing and wellbore interfaces for Section 1

As the heat transfer is considered to be steady state in the wellbore for each cell, the heat transferred through each resistance term is equal to the total heat transferred laterally across the well configuration between the tubing fluid and the wellbore for each section, given by Eq. (3.13). After the value of U_{ti} for the current well section is found, the respective resistance terms of the cell in the section of interest is set equal to the total heat transferred through the wellbore Eq. (3.85).

To show how the temperatures are calculated, the following example shows the calculations for section 1.

After finding the U_{ti1} for the cell in question in section 1, the total heat transfer across the wellbore is known. This must equal the heat transferred through the individual thermal resistances such as casing wall, cement etc.

Working our way through the wellbore, from either side, the temperature at the interfaces can be found, one by one. Starting by calculating the production fluid temperature, $T_{\mathrm{f}}(\mathrm{i})$, given by Eq. (3.37). The temperature of the wellbore wall is found:

$$T_{\mathrm{wb}}(i) = \frac{k_{\mathrm{e}}(i)T_{\mathrm{ei}}(i) + r_{\mathrm{ti}}U_{\mathrm{ti}}(i)T_{\mathrm{D}}(i)T_{\mathrm{f}}(i)}{k_{\mathrm{e}}(i) + r_{\mathrm{ti}}U_{\mathrm{ti}}(i)T_{\mathrm{D}}(i)} \tag{3.83}$$

Calculating from the wellbore wall inwards towards the tubing, the temperature at the casing outside, $T_{\mathrm{co1}}(i)$ is found by setting the heat transferred between wellbore and casing outside through the cement equal to the total heat transferred, given that $U_{\mathrm{ti1}}(i)$ and $h_{\mathrm{ti}}(i)$ already have been calculated:

$$Q_{(r_{\mathrm{co1}} \to r_{\mathrm{wb1}})}(i) = Q_{\mathrm{total}}(i) \tag{3.84}$$

$$\frac{2\pi L k_{\mathrm{cem1}}(i)}{\ln\left(\frac{r_{\mathrm{wb1}}}{r_{\mathrm{co1}}}\right)}(T_{\mathrm{co1}}(i) - T_{\mathrm{wb1}}(i)) = 2\pi L r_{\mathrm{ti}}U_{\mathrm{ti}}(T_{\mathrm{f}}(i) - T_{\mathrm{wb1}}(i)) \tag{3.85}$$

$$T_{\mathrm{co1}}(i) = T_{\mathrm{wb1}}(i) + \frac{r_{\mathrm{ti}}U_{\mathrm{ti1}}(i)}{k_{\mathrm{cem1}}(i)} \ln\left(\frac{r_{\mathrm{wb1}}}{r_{\mathrm{co1}}}\right)(T_{\mathrm{f}}(i) - T_{\mathrm{wb1}}(i)) \tag{3.86}$$

To find the casing inside temperature, $T_{\mathrm{ci1}}(i)$, the term for heat transfer through the casing wall is set equal to the total heat transferred through the wellbore, and solved

for $T_{\mathrm{ci1}}(i)$:

$$Q_{(r_{\mathrm{ci1}} \to r_{\mathrm{co1}})}(i) = Q_{\mathrm{total}}(i) \tag{3.87}$$

$$\frac{2\pi L k_{\mathrm{csg1}}(i)}{\ln\left(\frac{r_{\mathrm{co1}}}{r_{\mathrm{ci1}}}\right)}(T_{\mathrm{ci1}}(i) - T_{\mathrm{co1}}(i)) = 2\pi L r_{\mathrm{ti}} U_{\mathrm{ti1}}(i)(T_{\mathrm{f}}(i) - T_{\mathrm{wb1}}(i)) \tag{3.88}$$

$$T_{\mathrm{ci1}}(i) = T_{\mathrm{wb1}}(i) + \frac{r_{\mathrm{ti}} U_{\mathrm{ti1}}(i)}{k_{\mathrm{csg1}}(i)} \ln\left(\frac{r_{\mathrm{co1}}}{r_{\mathrm{ci1}}}\right)(T_{\mathrm{f}}(i) - T_{\mathrm{wb1}}(i)) \tag{3.89}$$

We end up with the following expressions:

$$T_{\mathrm{wb1}}(i) = \frac{k_{\mathrm{e}}(i) T_{\mathrm{ei}}(i) + r_{\mathrm{ti}} U_{\mathrm{ti}}(i) T_{\mathrm{D}}(i) T_{\mathrm{f}}(i)}{k_{\mathrm{e}}(i) + r_{\mathrm{ti}} U_{\mathrm{ti1}}(i) T_{\mathrm{D}}(i)} \tag{3.90}$$

$$T_{\mathrm{co1}}(i) = T_{\mathrm{wb1}}(i) + \frac{r_{\mathrm{ti}} U_{\mathrm{ti1}}(i)}{k_{\mathrm{cem1}}(i)} \ln\left(\frac{r_{\mathrm{wb1}}}{r_{\mathrm{co1}}}\right)(T_{\mathrm{f}}(i) - T_{\mathrm{wb1}}(i)) \tag{3.91}$$

$$T_{\mathrm{ci1}}(i) = T_{\mathrm{co1}}(i) + \frac{r_{\mathrm{ti}} U_{\mathrm{ti1}}(i)}{k_{\mathrm{csg1}}(i)} \ln\left(\frac{r_{\mathrm{co1}}}{r_{\mathrm{ci1}}}\right)(T_{\mathrm{f}}(i) - T_{\mathrm{wb1}}(i)) \tag{3.92}$$

$$T_{\mathrm{to}}(i) = T_{\mathrm{ci1}}(i) + \frac{r_{\mathrm{ti}} U_{\mathrm{ti1}}(i)}{r_{\mathrm{to}} h_{\mathrm{ca}}(i)}(T_{\mathrm{f}}(i) - T_{\mathrm{wb1}}(i)) \tag{3.93}$$

$$T_{\mathrm{ti}}(i) = T_{\mathrm{to}}(i) + \frac{U_{\mathrm{ti1}}(i)}{k_{\mathrm{tbg}}(i)} \ln\left(\frac{r_{\mathrm{to}}}{r_{\mathrm{ti}}}\right)(T_{\mathrm{f}}(i) - T_{\mathrm{wb1}}(i)) \tag{3.94}$$

The direction of the calculations does not matter. Calculations may as well be performed from the tubing inside wall towards the wellbore wall.

Chapter 4

Sensitivity analysis

4.1 Wellbore configuration for sensitivity analysis

The casing/tubing and wellbore dimensions, and the setting depths of casings are shown in Table 4.1.

Section	Hole size	Casing	Depth
5	0.9144 m (36 in)	OD: 0.7620 m (30 in) ID: 0.7112 m (28 in)	200 m
4	0.6604 m (30 in)	OD: 0.5080 m (20 in) ID: 0.4826 m (19 in)	800 m
3	0.4445 m (17 1/2 in)	OD: 0.3397 m (13.375 in) ID: 0.3093 m (12.175 in)	1400 m
2	0.3111 m (12 1/4 in)	OD: 0.2445 m (9.625 in) ID: 0.2168 m (8.545 in)	2600 m
1	0.2168 m (8 1/2 in)	OD: 0.1937 m (7.625 in) ID: 0.1619 m (6.375 in) Tubing: OD: 0.1397 m (5.500 in) ID: 0.1186 m (4.670 in)	3000 m

Table 4.1. Wellbore and casing/tubing dimensions for the well

4.2 The base case

The thermophysical correlations used for the base case are listed in Section 3.3. Table 4.2 list constant model parameters used in the base case. Fig. 4.1 shows the temperature profiles plot resulting from the base case properties. The overall heat transfer coefficient profile for the base case is shown in Fig. 4.2. From Fig. 4.2 it is evident that the heat transfer is largest in the deeper parts of the well.

	Parameter:	**Value:**	
Formation (Clay):	ρ_e	2080	$[\mathrm{kg\,m^{-3}}]$
	k_e	1.42	$[\mathrm{W\,m^{-1}\,K^{-1}}]$
	c_{pe}	2127	$[\mathrm{J\,kg^{-1}\,K^{-1}}]$
Geothermal gradient:	g_G	0.0455	(deg/m)
Surface formation temperature	T_e	15	(°C)
Produced fluid:	ρ_o, sc	800	$[\mathrm{kg\,m^{-3}}]$
	Flow rate, sc	0.01736 (1500)	$[\mathrm{m^3\,s^{-1}}]$ $(\mathrm{m^3\,d^{-1}})$
Production time:	t	48	hours (172800 s)
Inclination	θ	0	(deg)

Table 4.2. Base case constant parameters

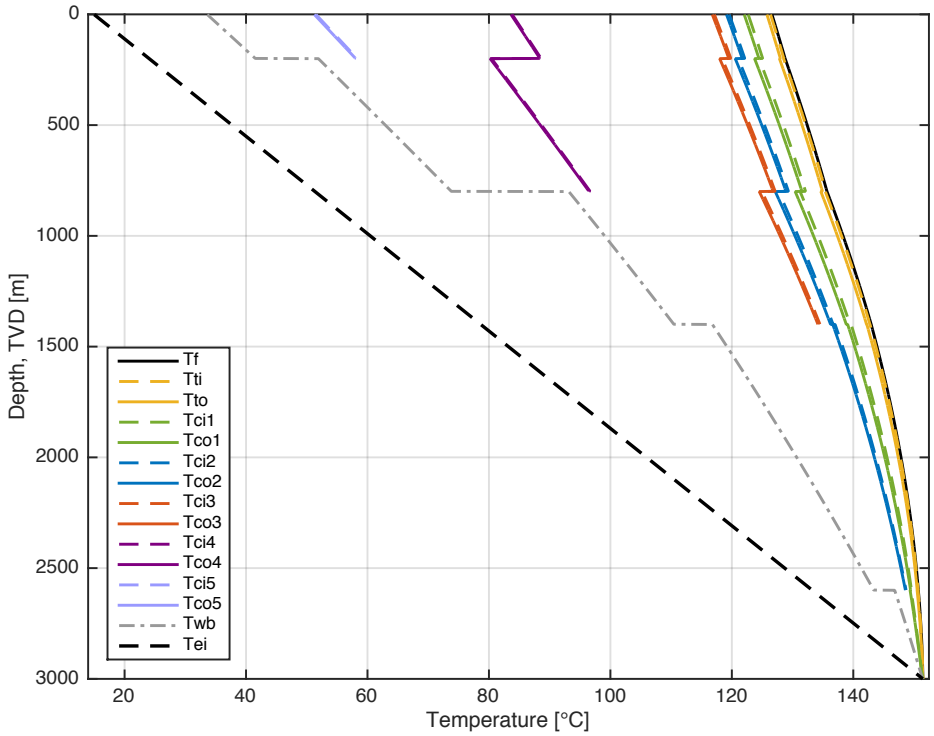

Fig. 4.1. Base case: Temperature profile of the wellbore

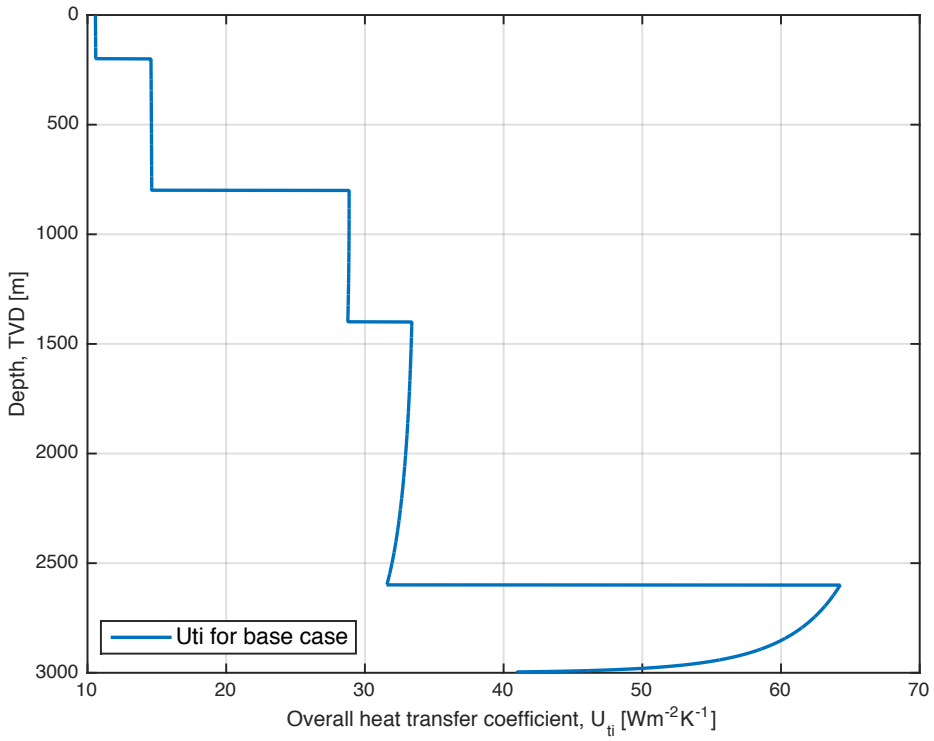

Fig. 4.2. Base case: Overall heat transfer coefficient profile of the wellbore

4.3 Flow rate

The production flow rate (at standard conditions) was varied in the following steps: 50, 100, 200, 500, 1500 and 4500 $m^3 d^{-1}$. As seen from the figures, the significance of the flow rate is large. A large flow rate, implying a large mass and energy transport, heats up the well, opposed to a small flow rate which in comparison has a significantly smaller impact on the well temperatures.

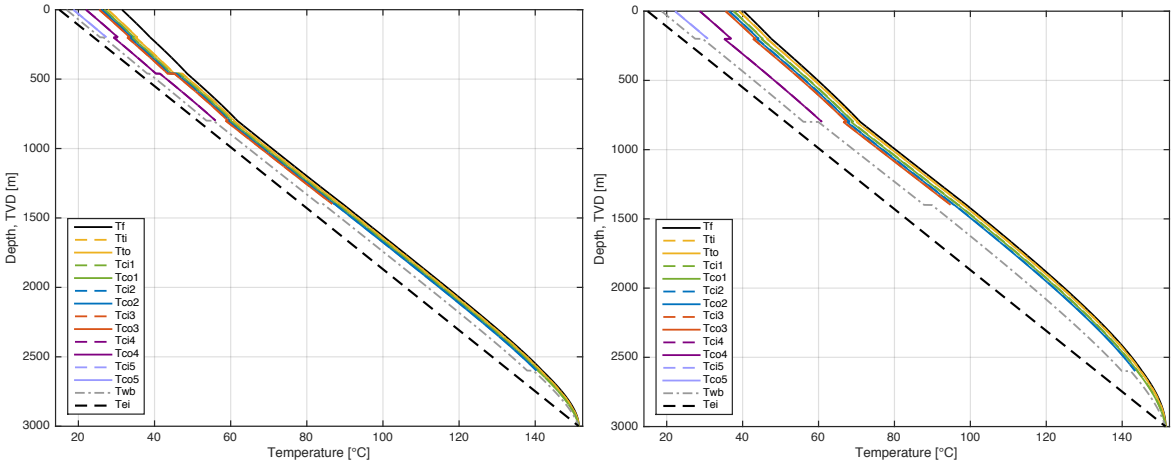

(a) 50 $[m^3 d^{-1}]$ **(b)** 100 $[m^3 d^{-1}]$

Fig. 4.3. Flow rate vs temperature for 50 and 100 $[m^3 d^{-1}]$

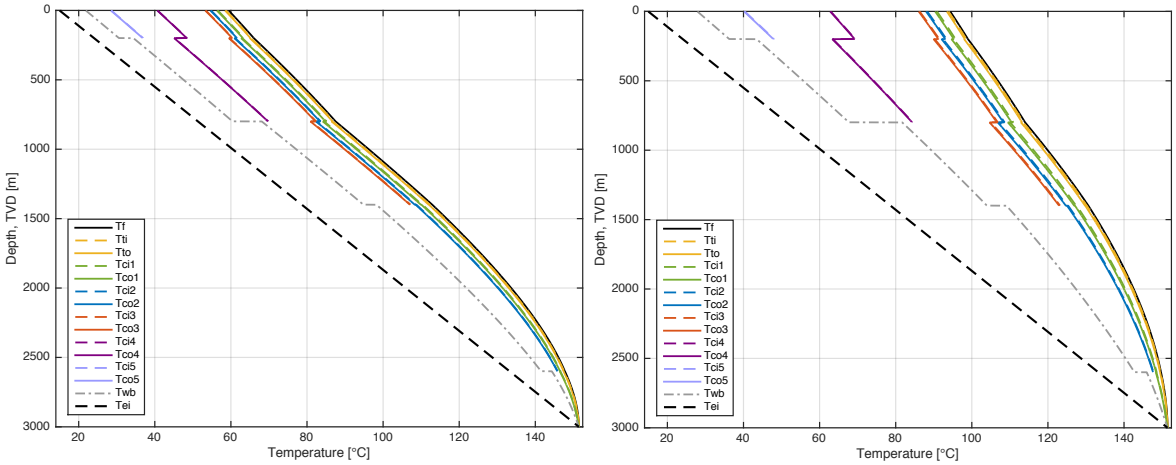

(a) 200 $[m^3 d^{-1}]$ **(b)** 500 $[m^3 d^{-1}]$

Fig. 4.4. Flow rate vs temperature for 200 and 500 $[m^3 d^{-1}]$

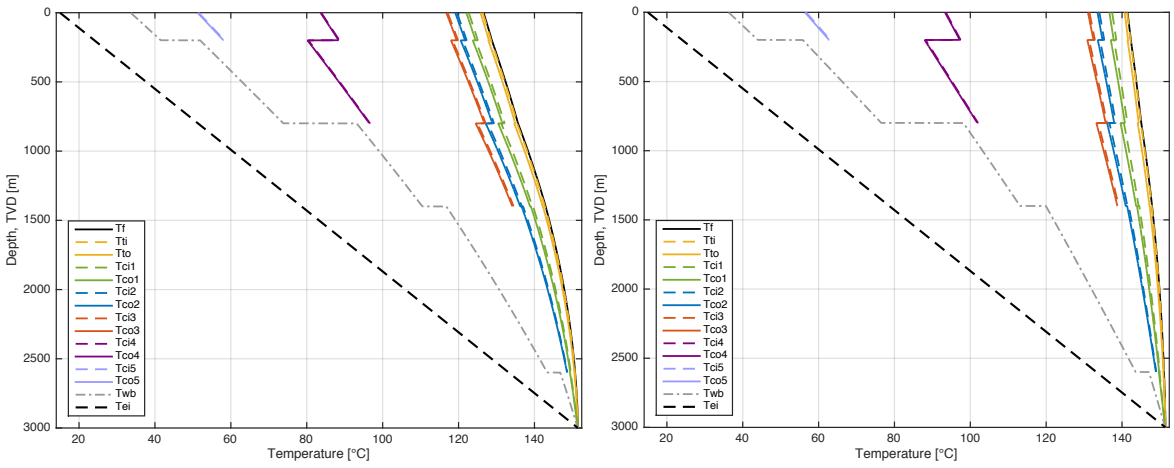

(a) 1500 $[\mathrm{m}^3\,\mathrm{d}^{-1}]$ **(b)** 4500 $[\mathrm{m}^3\,\mathrm{d}^{-1}]$

Fig. 4.5. Flow rate vs temperature for 1500 and 4500 $[\mathrm{m}^3\,\mathrm{d}^{-1}]$

4.4 Production time

The production time was varied in the following steps (hours): 1, 2, 5, 10, 24, 48, 100, 1000, 2000, 10000. From the figures it is clear that as the production time goes, the well is getting hotter and hotter. For increasing production time, the well temperatures are growing towards a steady state, as seen in Fig. 4.8.

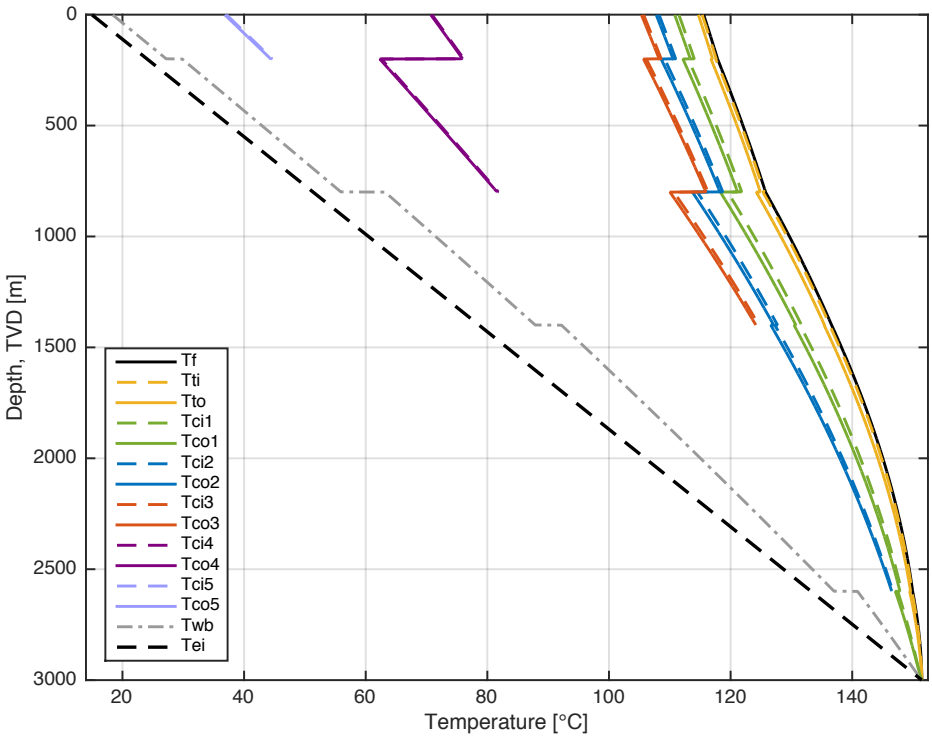

Fig. 4.6. Temperature profiles for $t = 1$ hour production time

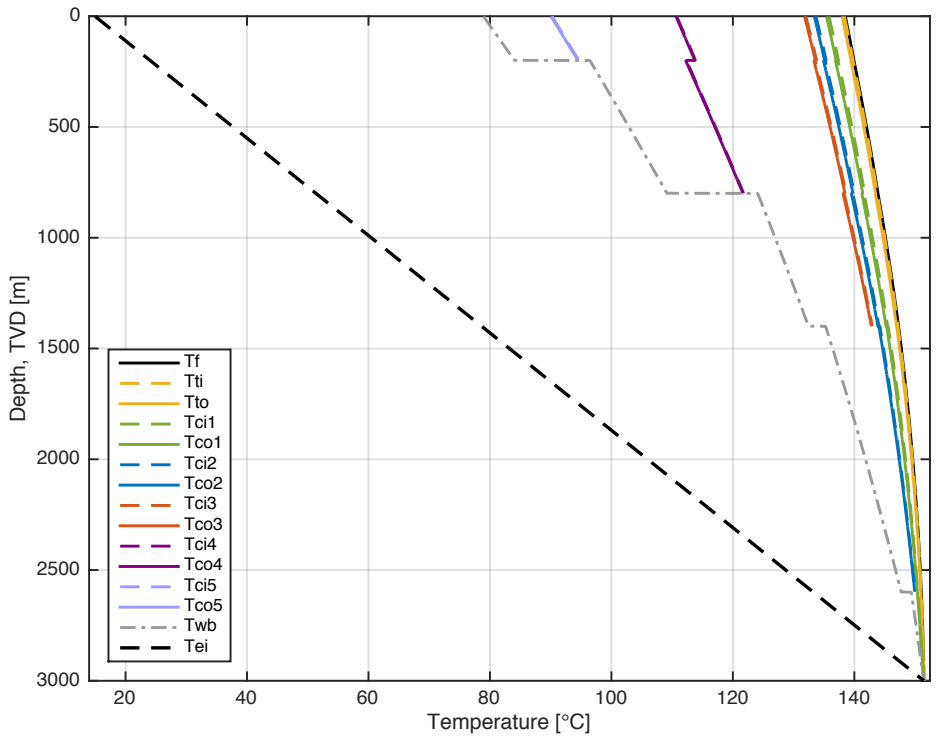

Fig. 4.7. Temperature profiles for $t = 10000$ hours production time

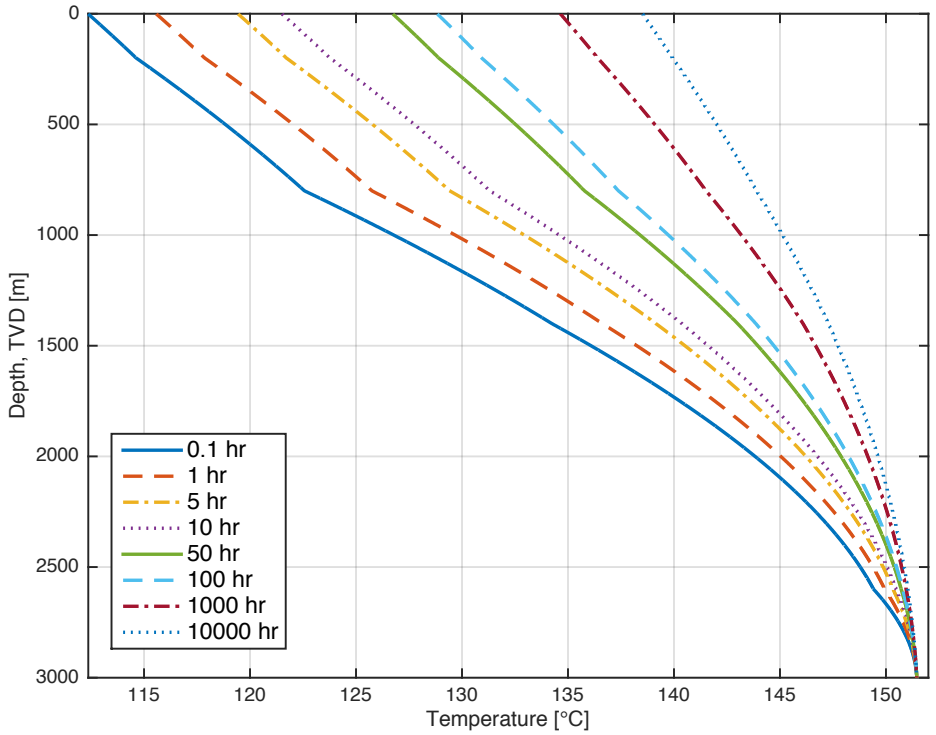

Fig. 4.8. Temperature profiles of produced fluid at different production times, t

4.5 Wellbore inclination

The wellbore inclination was varied in the following steps (deg): 0, 15, 30, 45, 60, 75, 90. Fig. 4.9 shows the wellbore trajectory plotted vs TVD and MD. Fig. 4.10 shows the produced fluid temperature profiles for different inclinations plotted vs TVD and MD. Fig. 4.11 shows the wellbore wall temperature profiles for different inclinations plotted vs TVD and MD.

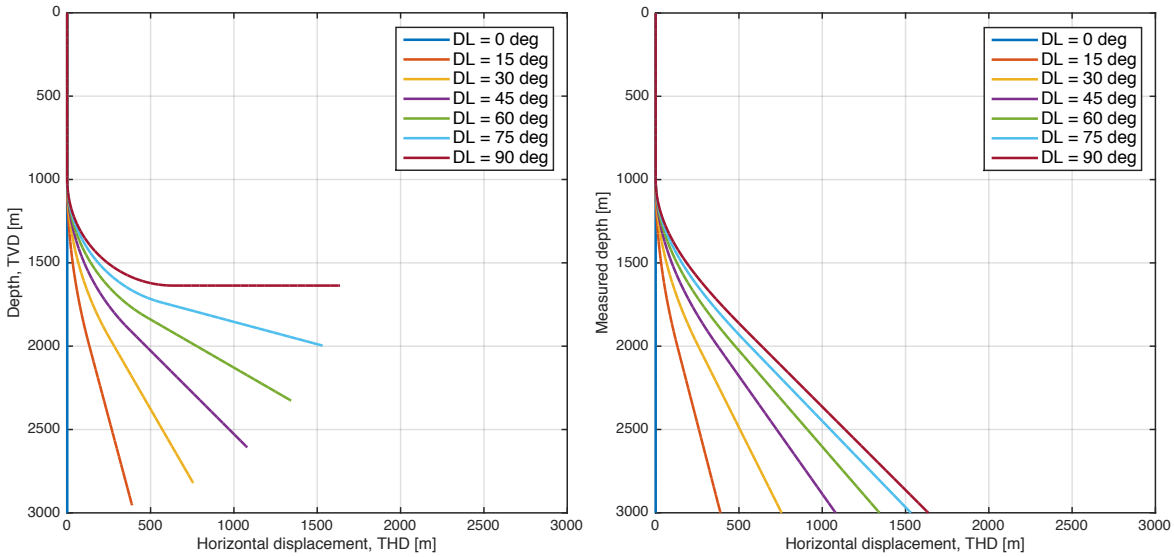

(a) WB trajectory vs TVD **(b)** WB trajectory vs MD

Fig. 4.9. Wellbore trajectory vs TVD and MD for various inclinations

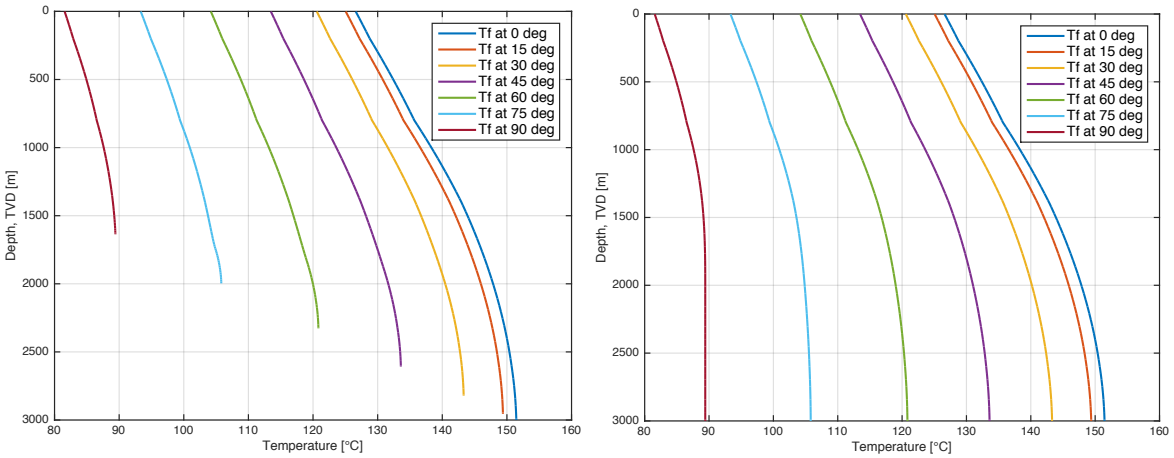

(a) Produced fluid temperature vs TVD **(b)** Produced fluid temperature vs MD

Fig. 4.10. Produced fluid temperature vs TVD and MD for various inclinations

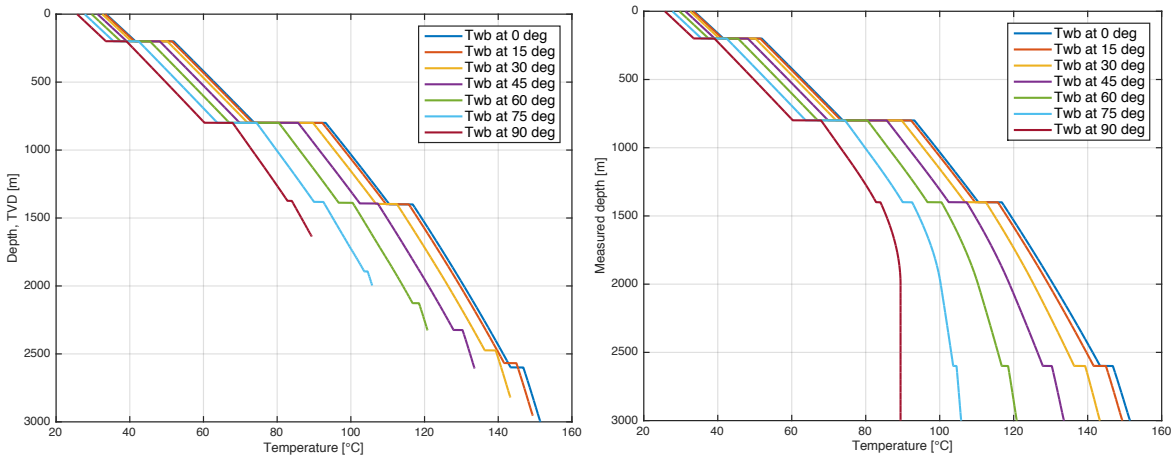

(a) Wellbore temperature vs TVD **(b)** Wellbore temperature vs MD

Fig. 4.11. Wellbore temperatures vs TVD and MD for various inclinations

4.6 Density of produced fluid

As the density of the produced oil at standard conditions are used as an input in the equation of state for the produced oil (Eq. (3.80)), the density of the produced fluid at standard conditions (as an input to the EOS) was varied in the following steps: 780, 800, 850, 900, 950 [$\mathrm{kg\,m^{-3}}$]. Increasing the density also increases the mass flow rate, if the production flow rate remains the same. Fig. 4.12 and Fig. 4.13 shows the resulting plots from 780 and 950 $\mathrm{kg\,m^{-3}}$, and a comparison of the different density steps are shown in Fig. 4.14. An increased temperature along the tubing length is observed with increasing oil density.

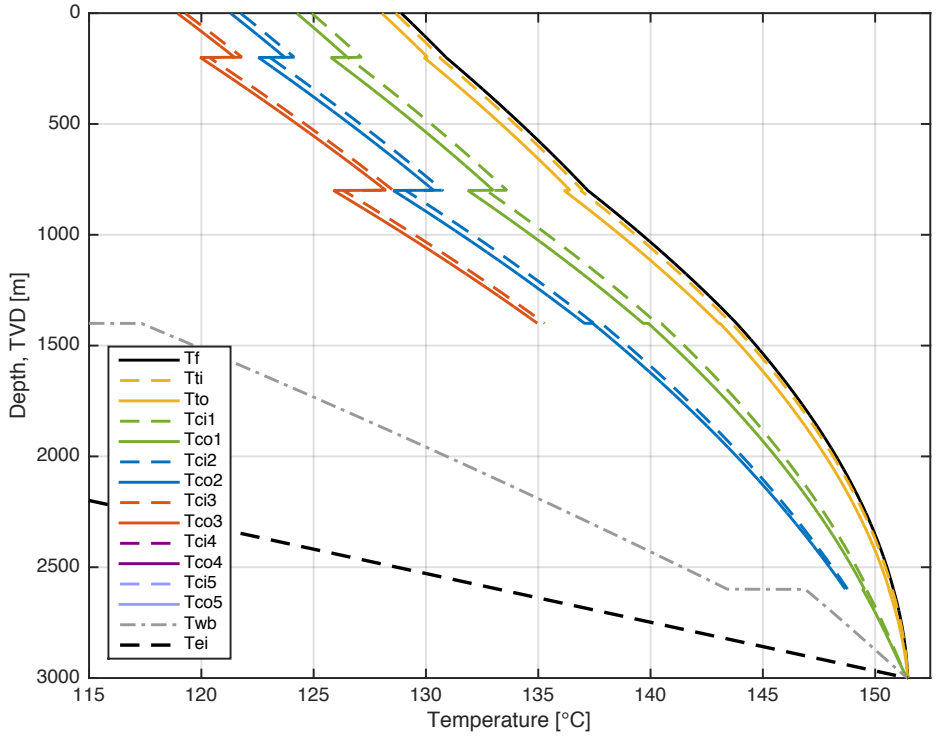

Fig. 4.12. Zoomed view of temperature profiles for $\rho_{\mathrm{o}} = 780$ [$\mathrm{kg\,m^{-3}}$]

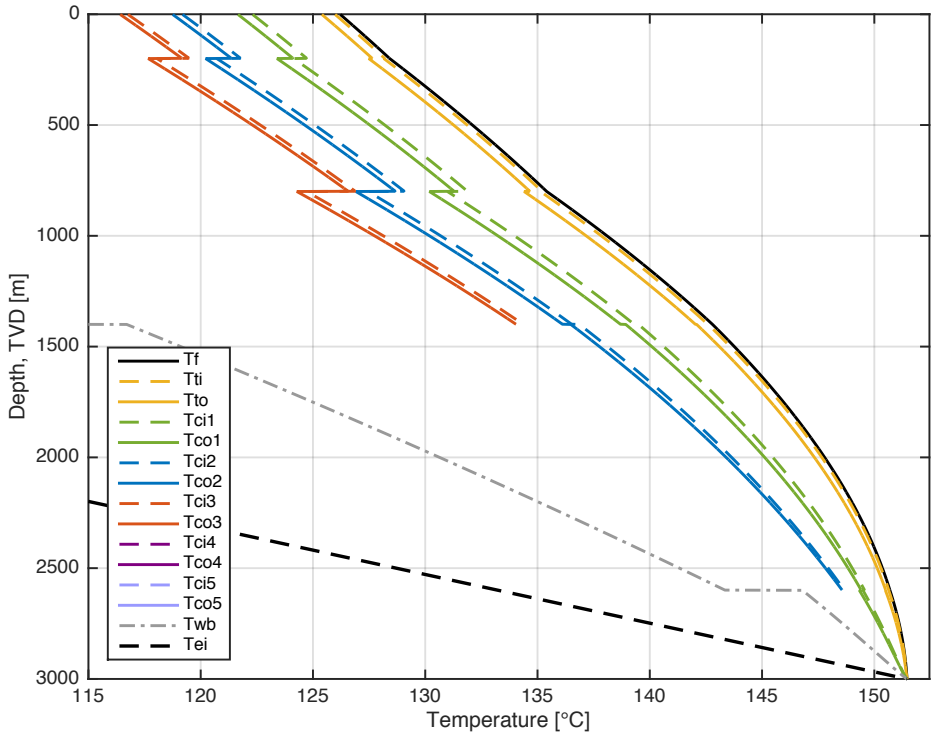

Fig. 4.13. Zoomed view of temperature profiles for $\rho_o = 950$ [kg m^{-3}]

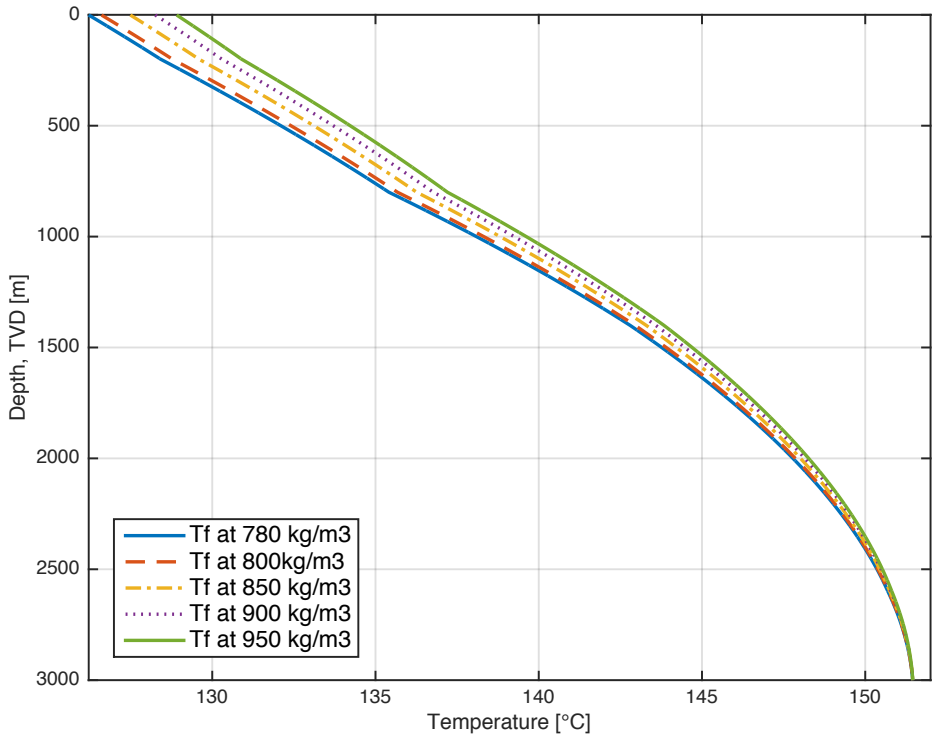

Fig. 4.14. Temperature profiles of produced fluid at different ρ_o

4.7 Joule-Thomson coefficient of the produced fluid

The Joule-Thomson coefficient is plotted versus the tubing pressure in Fig. 4.15. From the plot it is clear that it decreases with increasing pressure, as one would expect.

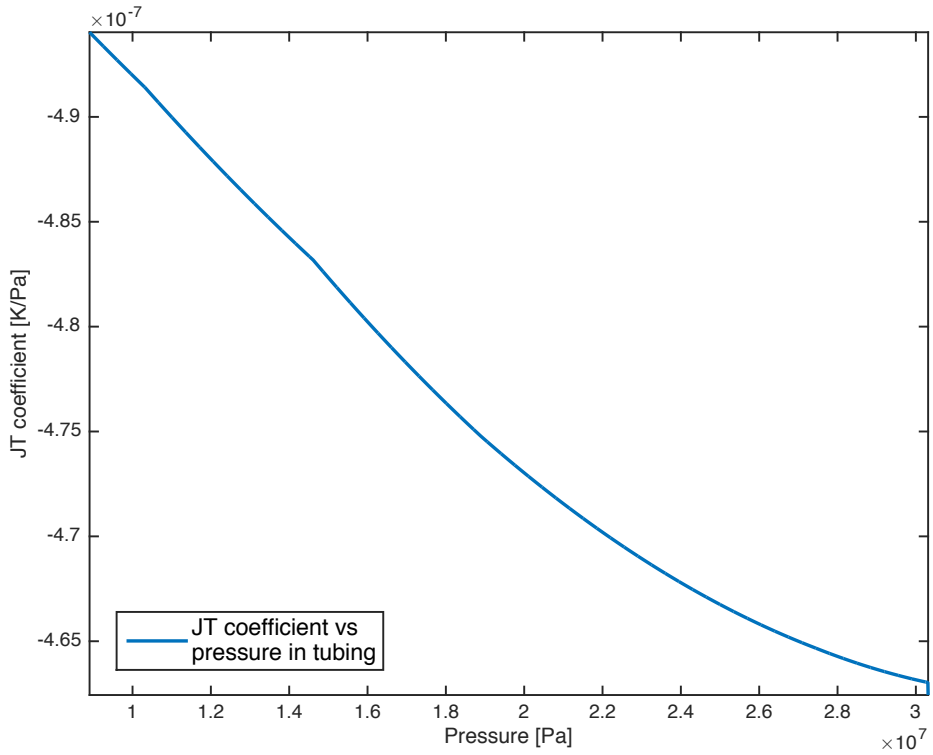

Fig. 4.15. The Joule-Thomson coefficient vs pressure for the produced fluid in tubing

In Fig. 4.16 the the produced fluid temperature of the base case is compared to the produced fluid of the base case when neglecting the Joule-Thomson effect. The figure also shows the Joule-Thomson temperature contribution resulting from the pressure decrease. The Joule-Thomson coefficient, μ_{JT}, and its approximation ($\mu_{\mathrm{JT}} = -1/(\rho_{\mathrm{o}} c_{\mathrm{po}})$, see Eq. (3.29)) was plotted vs depth for the different oil densities at standard conditions as presented in Section 4.6 (780, 800, 850, 900, 950 [$\mathrm{kg\,m^{-3}}$]).

From the plot in Fig. 4.17 it is observed that μ_{JT} decreases with increasing oil density (see Section 4.6 for details of the densities), meaning decreased Joule-Thomson heating effect within the fluid. The approximated μ_{JT} are fairly close to the real values.

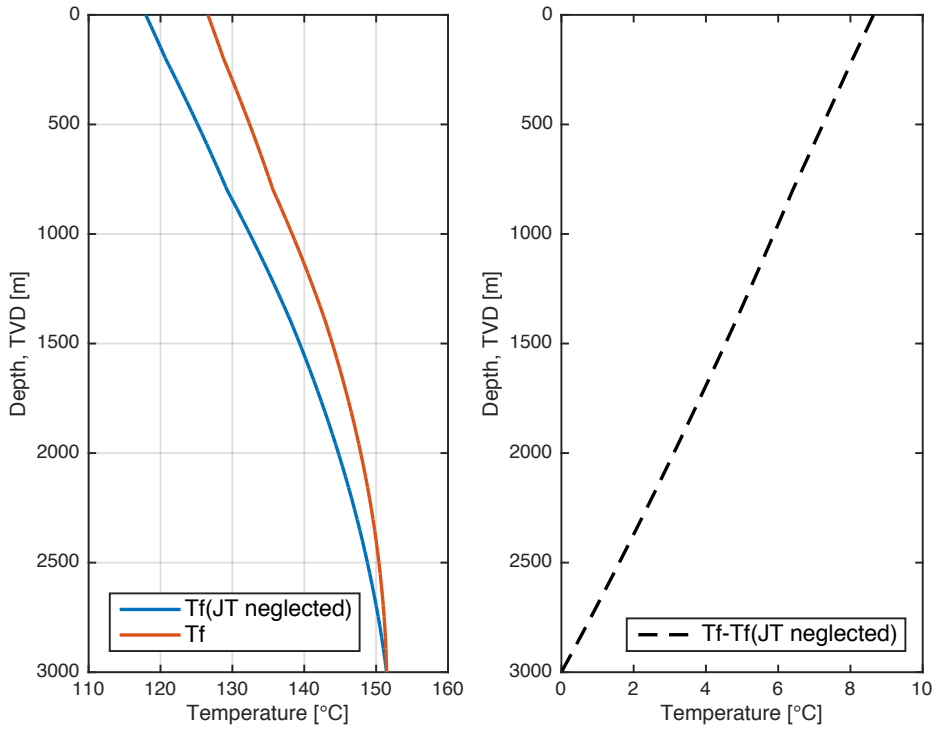

Fig. 4.16. The Joule-Thomson heating effect on the produced fluid temperature

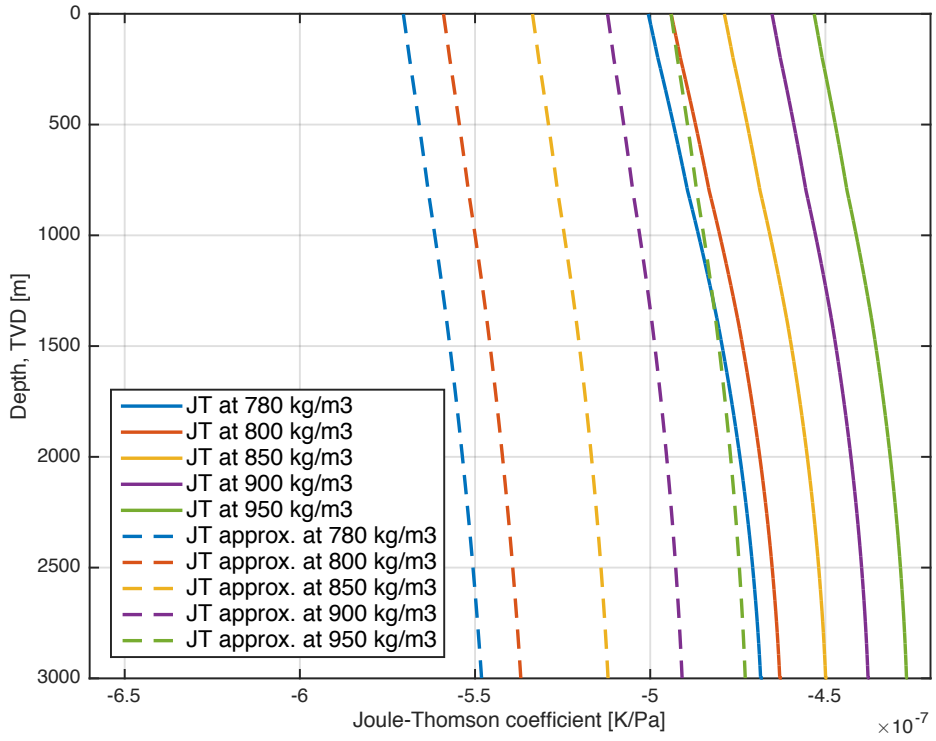

Fig. 4.17. μ_{JT} and its approximation vs depth

4.8 Specific heat capacity of produced fluid

The specific heat of the produced fluid was assumed constant and the resulting temperature profiles plotted for two values: 1000 and 4000 $\mathrm{J\,kg^{-1}\,K}$. It is observed a significant change in temperature between the two cases, as seen when comparing Fig. 4.18 and Fig. 4.19, implying that the specific heat of the produced fluid as a important parameter.

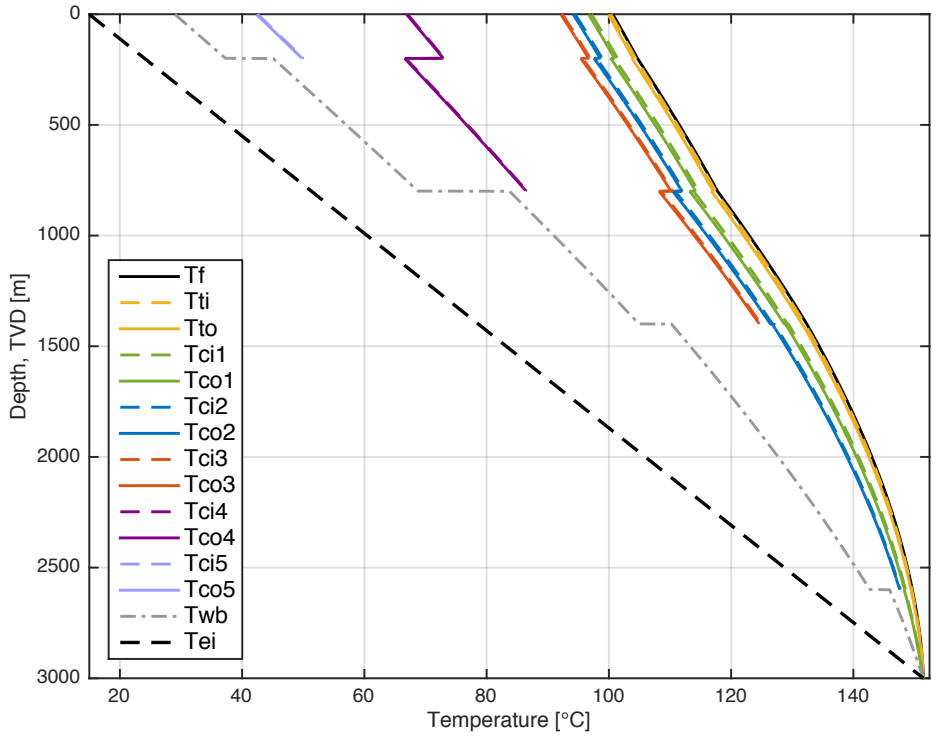

Fig. 4.18. Temperature profiles for a constant $c_{\mathrm{po}} = 1000$ $[\mathrm{J\,kg^{-1}\,K}]$

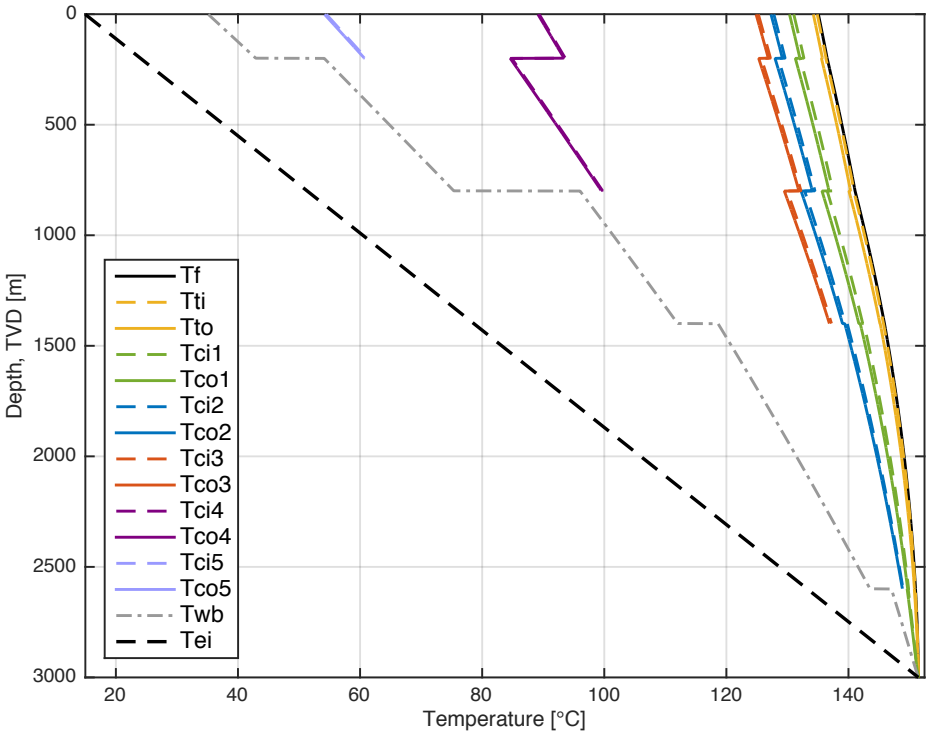

Fig. 4.19. Temperature profiles for a constant $c_{\mathrm{po}} = 4000$ [$\mathrm{J\,kg^{-1}\,K}$]

4.9 Thermal conductivity of produced fluid

The thermal conductivity was assumed constant and the resulting temperature profiles plotted for two values of k_o, 0.01 and 2 $\mathrm{W\,m^{-1}\,K^{-1}}$. The difference in temperatures are very small, as shown in Fig. 4.20. The temperature difference at the top was only 0.62 °C. As the base case is producing at a flow rate of 1500 $\mathrm{m^3\,d^{-1}}$, the heat transfer is mostly by forced convection in the tubing, thus minimizing the effect of reducing the thermal conductivity of the fluid. Now plotting the temperature profiles assuming a production flow rate of 200 $\mathrm{m^3\,d^{-1}}$ and the same thermal conductivities, the temperature difference is significantly larger as observed from comparing Fig. 4.21 to Fig. 4.22.

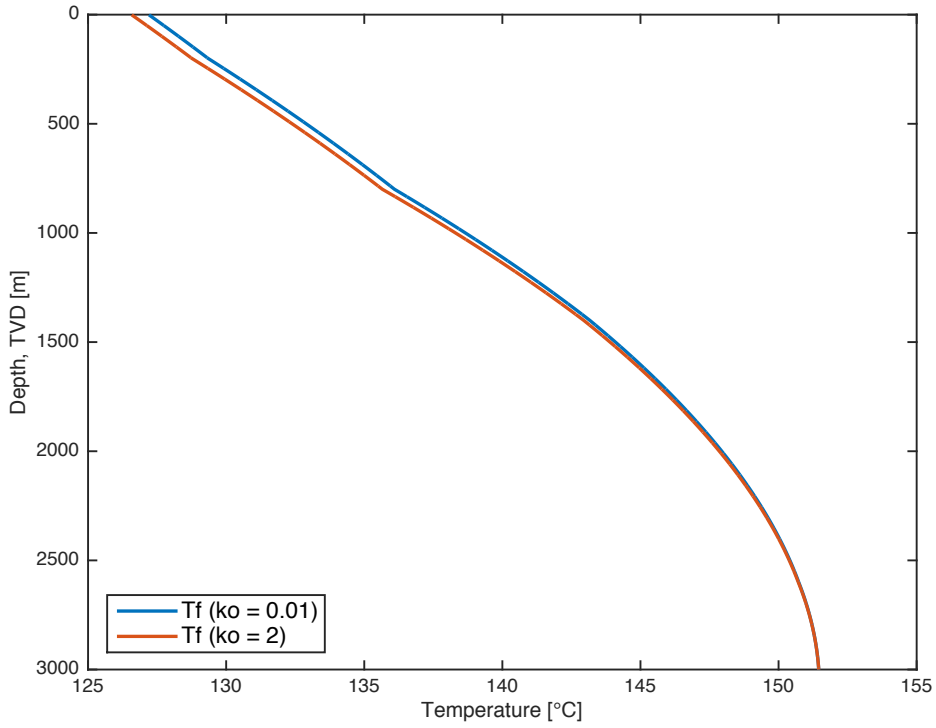

Fig. 4.20. Temperature profiles for a constant $k_o = 0.01$ vs 2 $[\mathrm{J\,kg^{-1}\,K^{-1}}]$ for a flow rate of 1500 $[\mathrm{m^3\,d^{-1}}]$

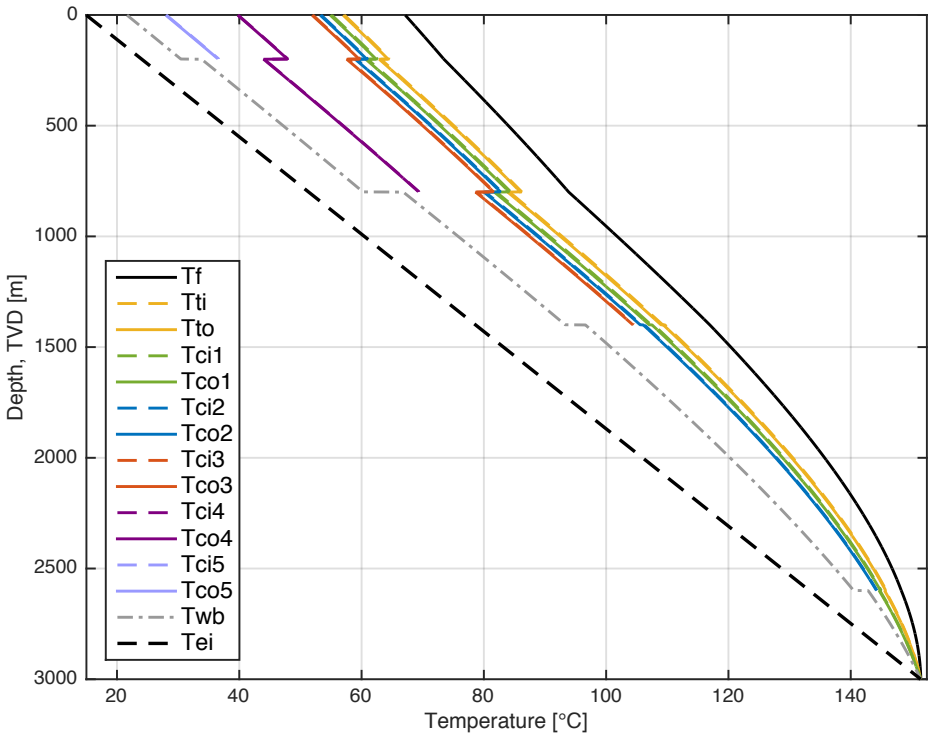

Fig. 4.21. Temperature profiles for a constant $k_o = 0.01$ $[\mathrm{J\,kg^{-1}\,K^{-1}}]$ for a production flow rate of 200 $[\mathrm{m^3\,d^{-1}}]$

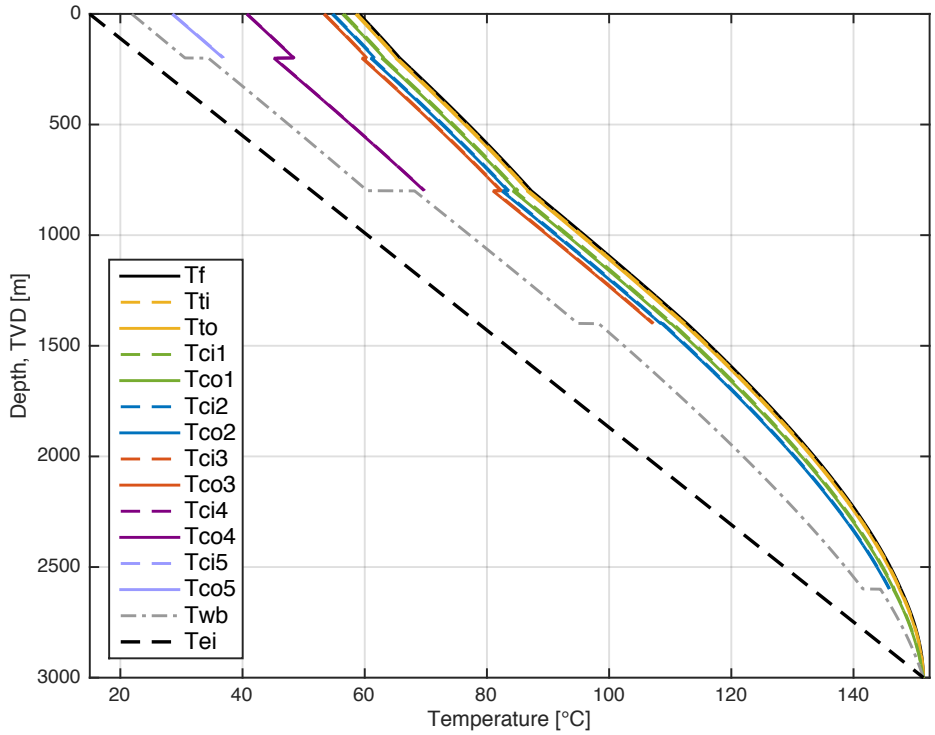

Fig. 4.22. Temperature profiles for a constant $k_o = 2$ $[\mathrm{J\,kg^{-1}\,K^{-1}}]$ for a production flow rate of 200 $[\mathrm{m^3\,d^{-1}}]$

4.10 Water as the produced fluid

Assuming 100 % of the produced fluid is water, the annular fluid properties (for 3.5%wt NaCl brine) is used to represent the produced fluid. Fig. 4.23 shows that the temperature profiles have shifted right relative to the base case, indicating higher produced fluid and well temperatures, as one would expect due mainly due to a much larger specific heat capacity of water compared to oil. The large difference is easily observed in the simplified temperature profile comparison in Fig. 4.24. The produced fluid temperatures at the top of the well for oil and water was, respectively, 126.6 and 135.7 °C. The temperatures for various water cuts for this case could be expected to be within this temperature interval.

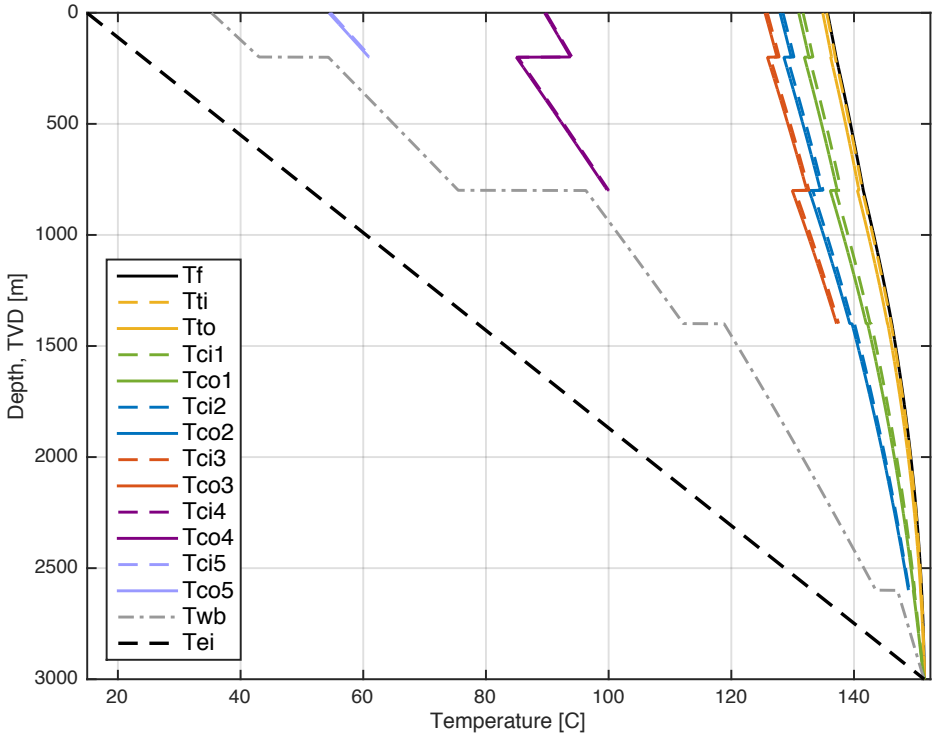

Fig. 4.23. Temperature profiles for water as the produced fluid

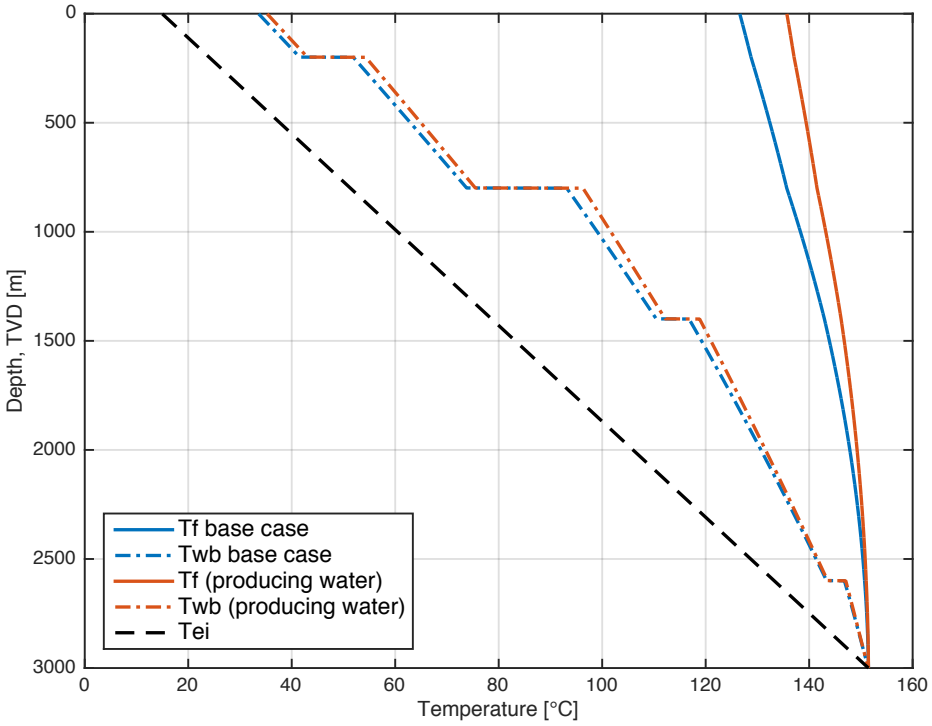

Fig. 4.24. Simplified temperature profile comparison for the change in temperature when producing water vs oil

4.11 Specific heat capacity of annular fluid

Instead of the temperature correlation used for c_{pa} in all three annulus, a constant value of c_{pa} obtained by evaluating the specific heat capacity temperature correlation (Eq. (3.70)) at 15 °C (3997 $\mathrm{J\,kg^{-1}\,K^{-1}}$), is used. Fig. 4.25 shows the temperature change. A resulting temperature increase in the produced fluid, and a temperature decrease in the three annulus, is observed. The difference in temperatures are relatively small.

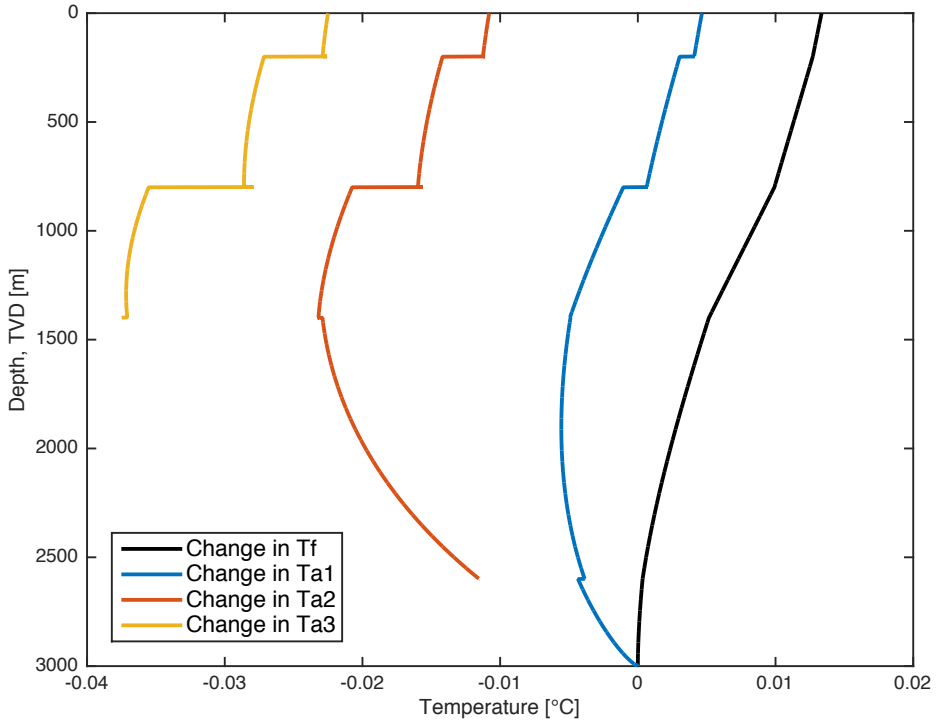

Fig. 4.25. Resulting temperature change when assuming a constant c_{pa} vs base case c_{pa} correlation

The temperature profiles was also plotted for the cases of constant $c_{pa} = 1000$ and 4000 $\mathrm{J\,kg^{-1}\,K}$, shown in Fig. 4.26 and Fig. 4.27. It is seen that specific heat capacity on its own has a small influence on the temperature profiles:

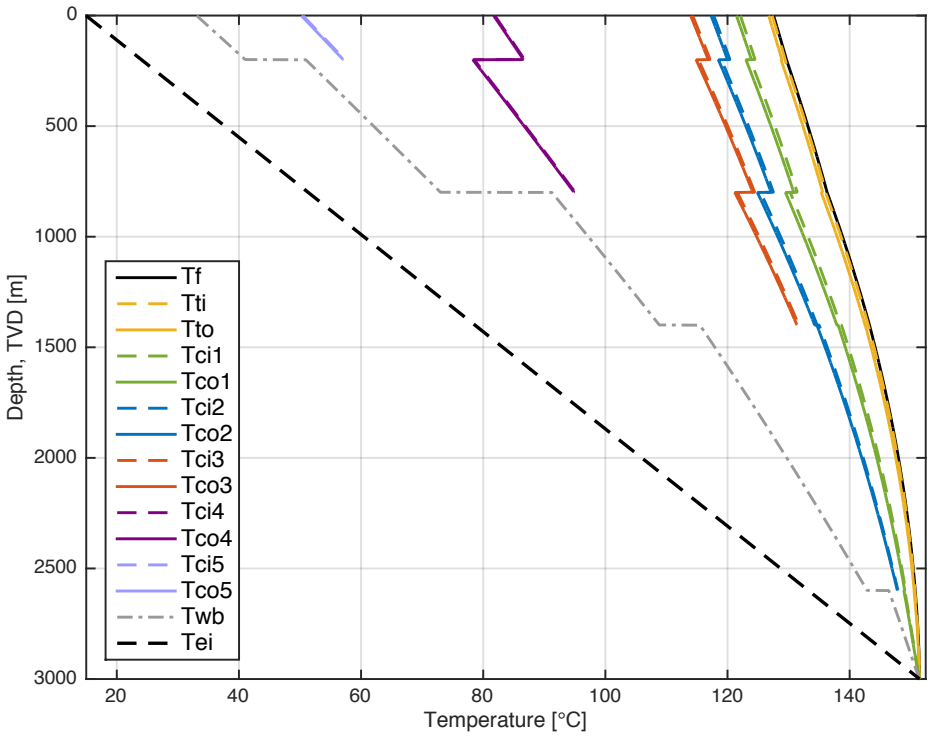

Fig. 4.26. Temperature profiles for a constant $c_{\mathrm{pa}} = 1000$ $[\mathrm{J\,kg^{-1}\,K^{-1}}]$

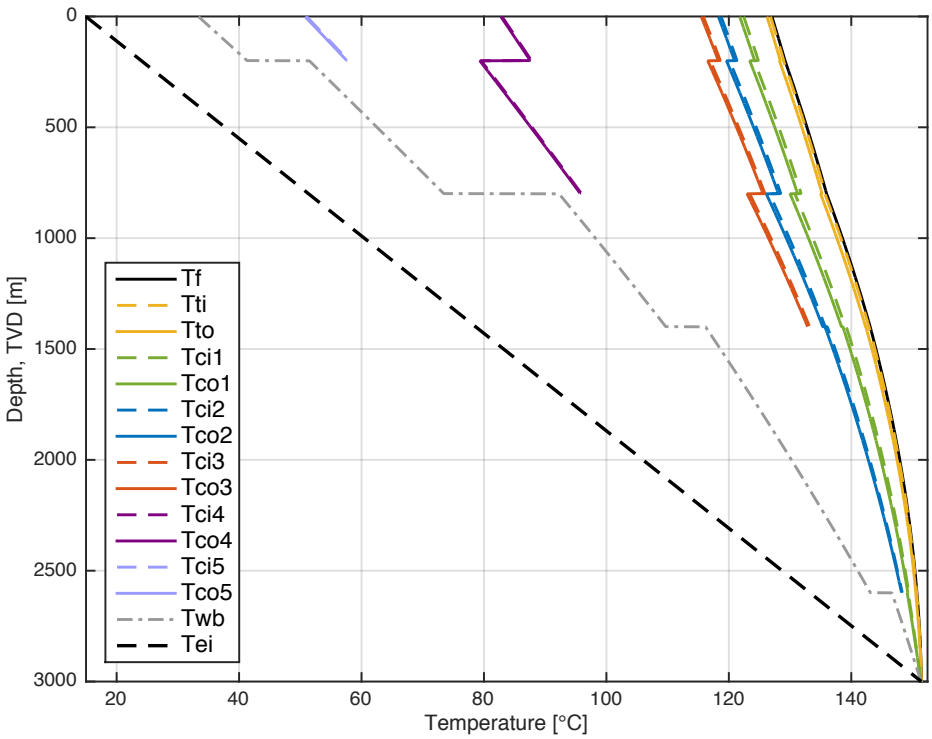

Fig. 4.27. Temperature profiles for a constant $c_{\mathrm{pa}} = 4000$ $[\mathrm{J\,kg^{-1}\,K^{-1}}]$

4.12 Thermal conductivity of annular fluid

Instead of the temperature correlation used for k_a in all three annulus, a constant value of k_a obtained by evaluating the thermal conductivity temperature correlation at 15 °C (0.59 $\mathrm{W\,m^{-1}K^{-1}}$), is used. Fig. 4.28 shows the temperature change. A resulting temperature increase in the produced fluid, and a temperature decrease in the three annulus, is observed. The difference in temperatures are relatively small, just as for the heat capacity, even though it is one order of magnitude larger than the difference in the specific heat capacity case (Fig. 4.25). The temperature profiles for constant

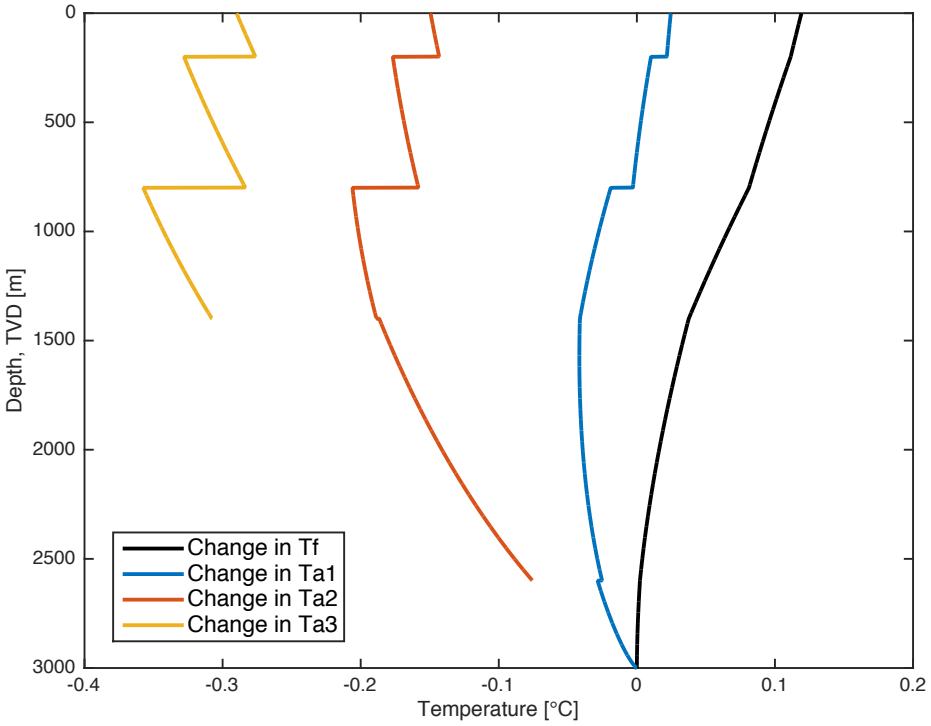

Fig. 4.28. Resulting temperature change when assuming a constant k_a vs base case k_a correlation

thermal conductivity of the annulus fluid for k_a = 1, 0.1 and 0.01 $\mathrm{W\,m^{-1}K^{-1}}$ are shown in Fig. 4.29, Fig. 4.30 and Fig. 4.31 respectively. From the plots it can be observed that the thermal conductivity of the fluids plays a central role in dictating the well temperatures.

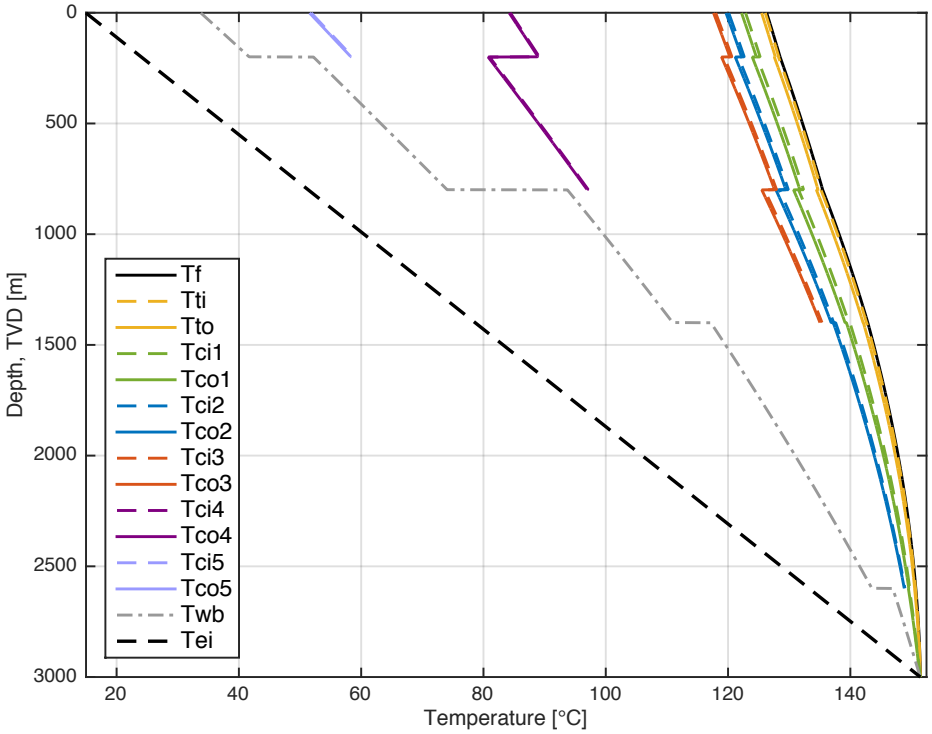

Fig. 4.29. Temperature profiles for a constant $k_a = 1$ [$\mathrm{W\,m^{-1}\,K^{-1}}$]

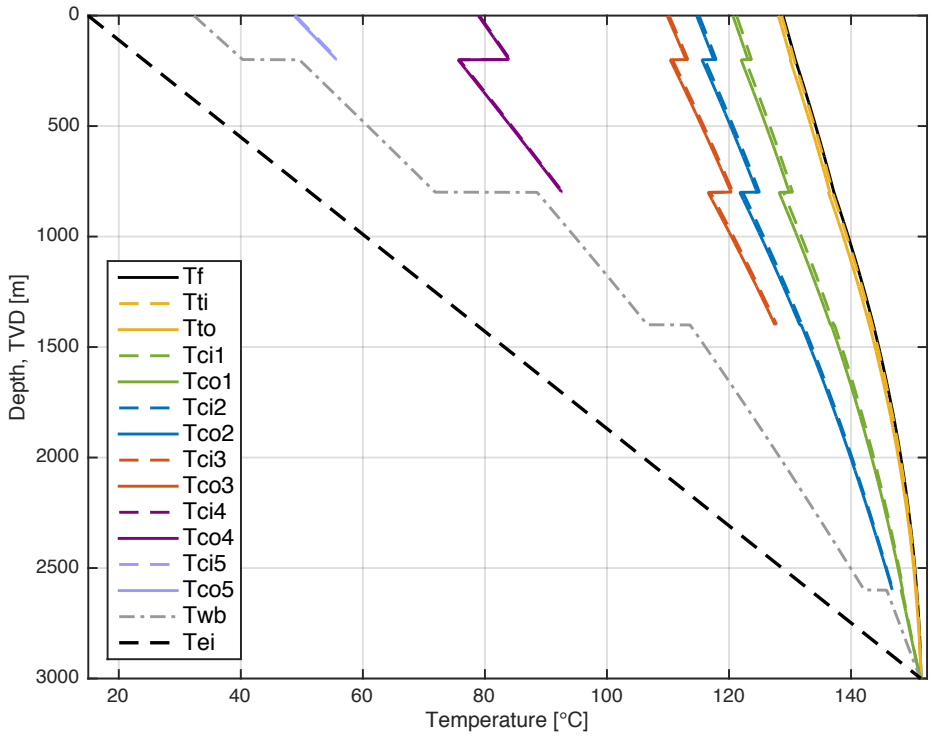

Fig. 4.30. Temperature profiles for a constant $k_a = 0.1$ [$\mathrm{W\,m^{-1}\,K^{-1}}$]

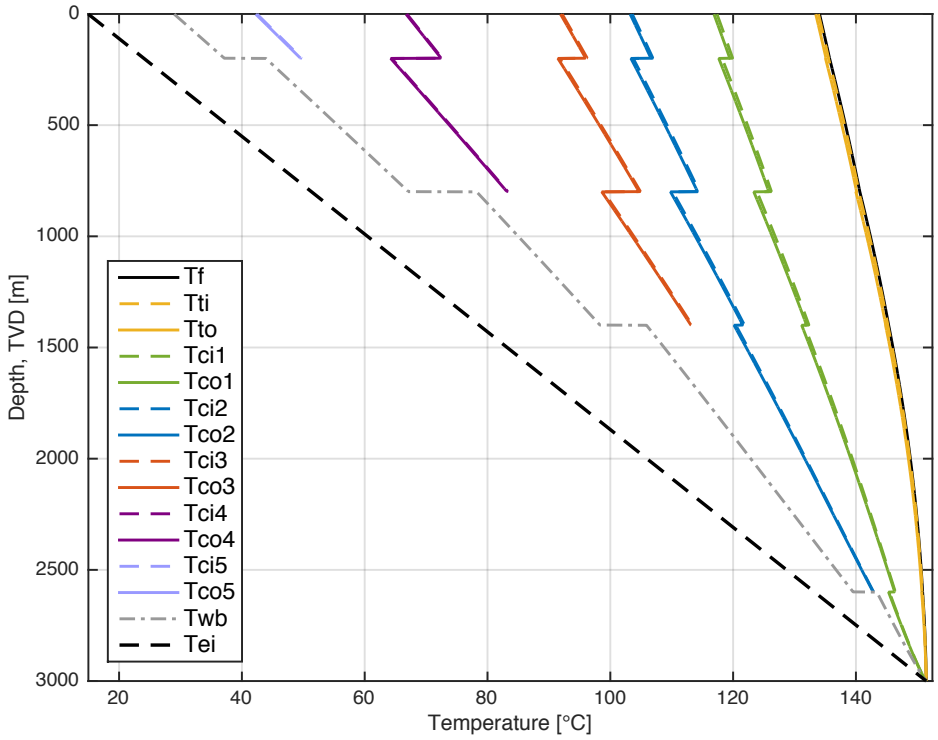

Fig. 4.31. Temperature profiles for a constant $k_{\mathrm{a}} = 0.01$ [$\mathrm{W\,m^{-1}\,K^{-1}}$]

4.13 Free/natural convection vs pure conduction in annulus

As internal movement in the fluid column of the annulus improves heat transfer, it makes the effect of fluid thermal conductivity less impactful on the heat transfer. Therefore, free convection was neglected, leaving pure conduction as the only means of heat transfer. Fig. 4.32 shows the temperature profiles when neglecting the free convection. By superimposing the overall heat transfer coefficient for the case of neglecting the free convection, onto the overall heat transfer coefficient of the base case (Fig. 4.2), presented in Fig. 4.33, the difference in heat transfer can be compared. Fig. 4.33 shows a very large difference in heat transfer for the two cases, with around 50 % or larger heat transfer for the free convection case.

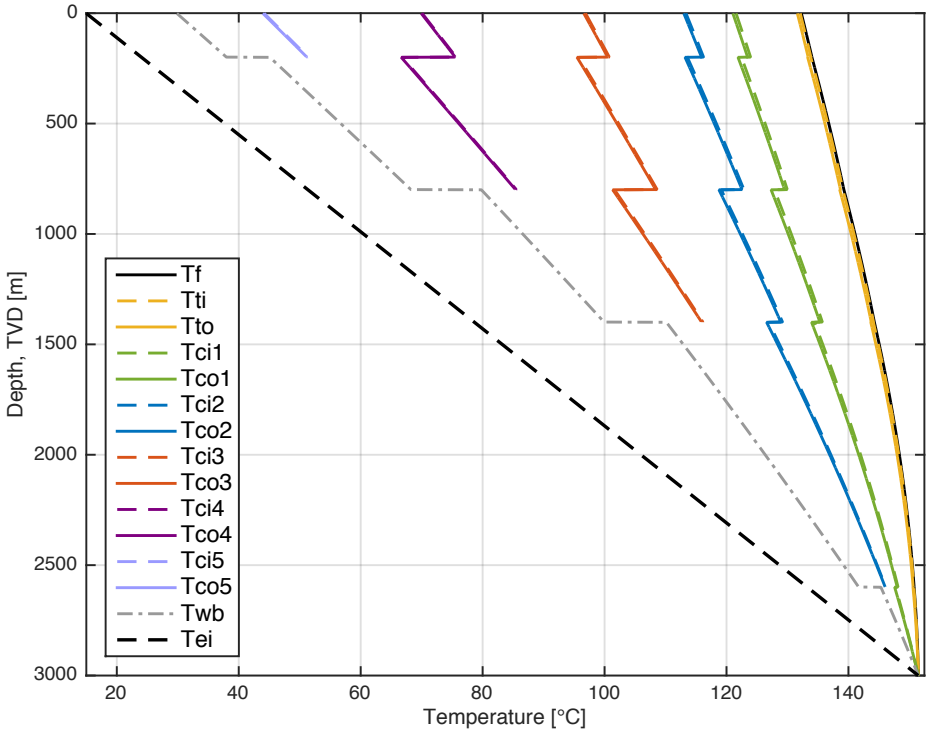

Fig. 4.32. Temperature profiles when neglecting free/natural convection in the three annulus

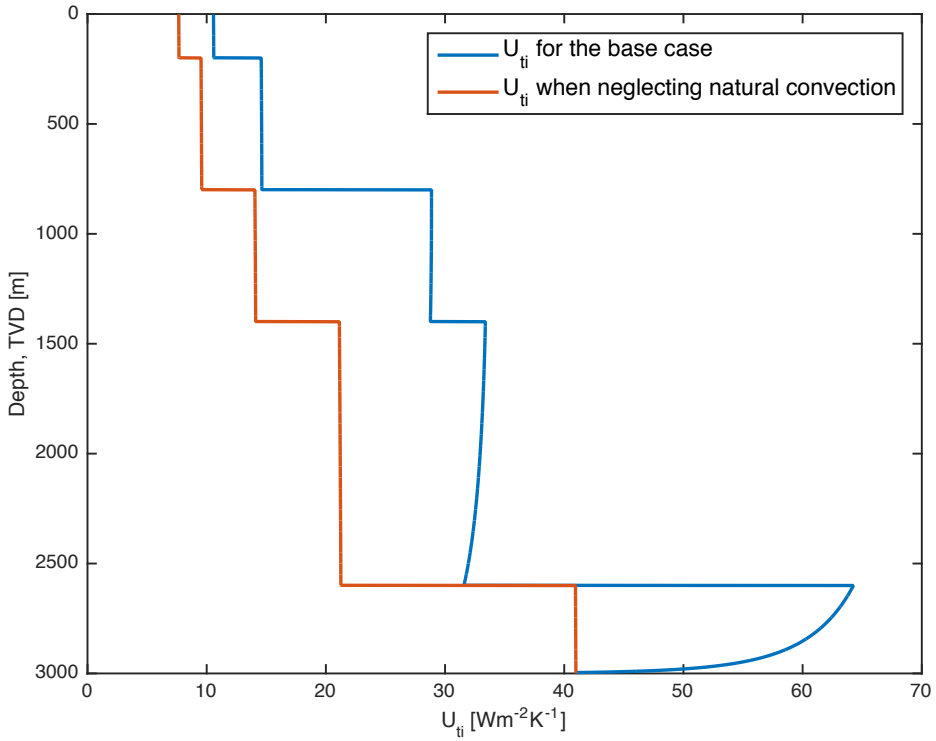

Fig. 4.33. Overall heat transfer coefficient profiles for the cases of free convection vs neglecting free convection

4.14 Viscosity of annular fluid

The viscosity of the annular fluid was varied in two steps, $\mu_a = 0.001$ (1) and 0.00001 (0.01) Pas (cP), and plotted in Fig. 4.34 and Fig. 4.35. By comparing the plots, it is observed that a higher viscosity will slow down the heat transfer, while a lower viscosity increases the heat transfer due to increased mobility of the fluid.

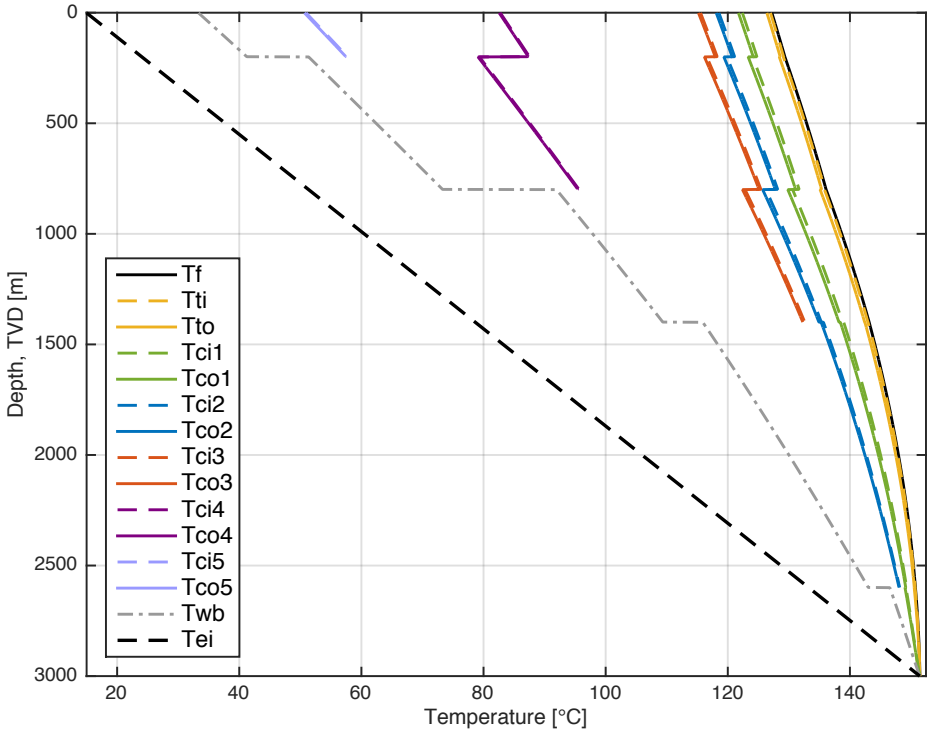

Fig. 4.34. Temperature profiles for a constant $\mu_a = 0.001$ [Pas]

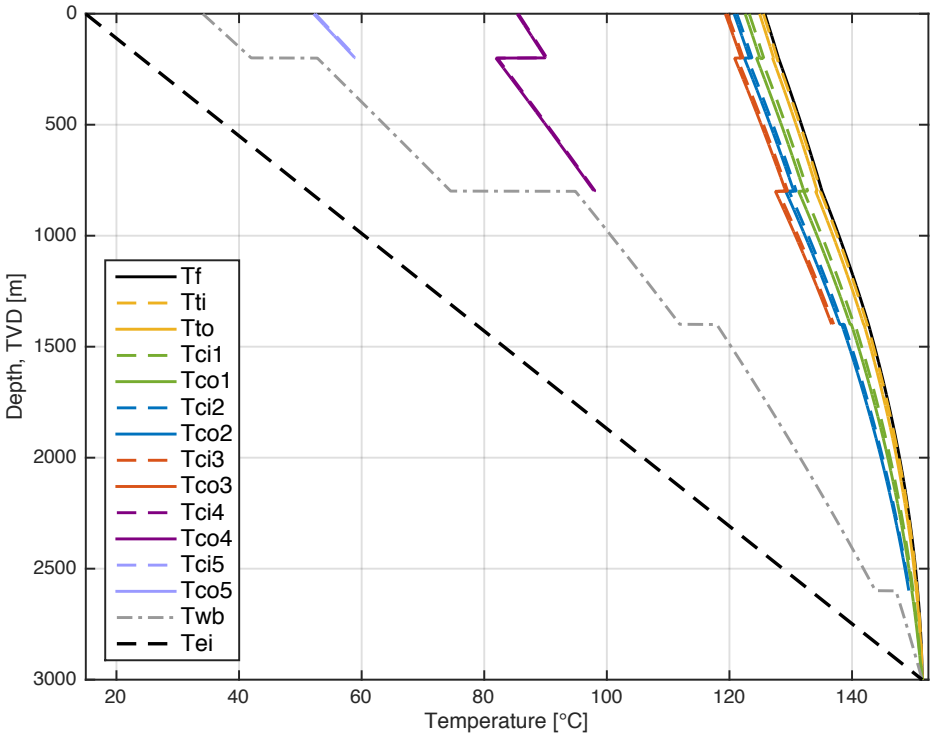

Fig. 4.35. Temperature profiles for a constant $\mu_a = 0.00001$ [Pas]

4.15 Annular clearance

The effect of annular clearance was tested by reconfiguring the casing sizes such that the annular clearance was the same for all three annulus spaces, and equal to 0.0111 m and 0.0211 m. The wall thickness of the tubing and casings was preserved. The base case Nu profiles (Fig. 4.36) are shown first as a reference point. The reason for the large Nu for annulus 3 is due to its large annular clearance being the controlling factor. Fig. 4.37 shows the comparison of the two annular clearance values. It is clear that

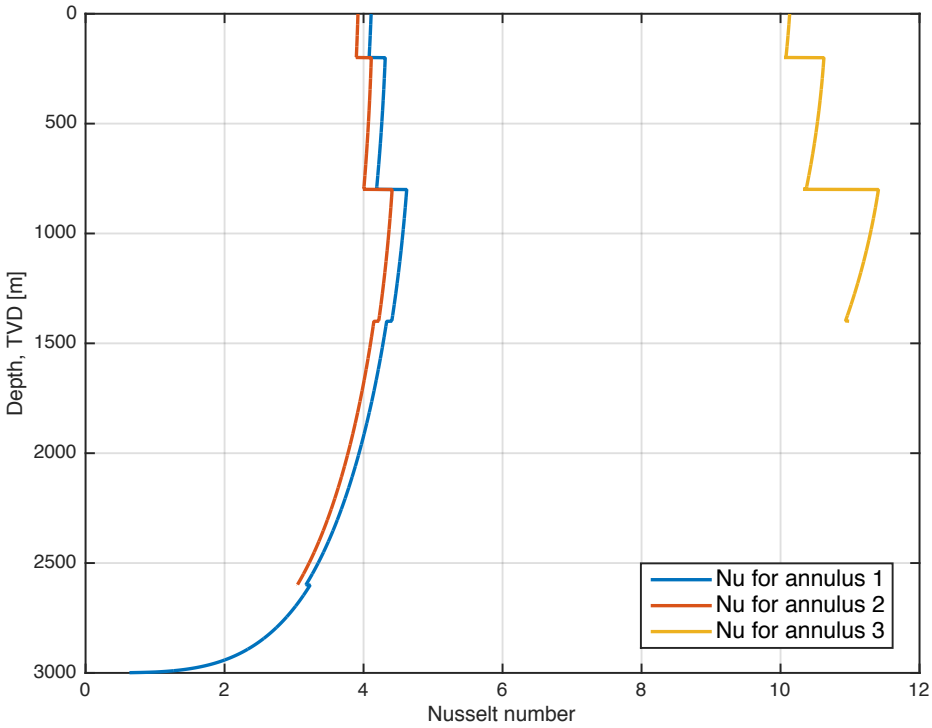

Fig. 4.36. Nusselt number for the three separate annulus spaces for the base case

increasing the clearance will increase the heat transfer through annulus, thus heating the wellbore and cooling the produced fluid. This can be seen by comparing Fig. 4.39 to Fig. 4.40. The overall heat transfer coefficient for all sections, U_{ti}, for the two cases are represented in Fig. 4.38. A much larger U_{ti} is observed for the 0.0211 m clearance at the bottom. The effect of increased clearance tapers off towards the top of the well.

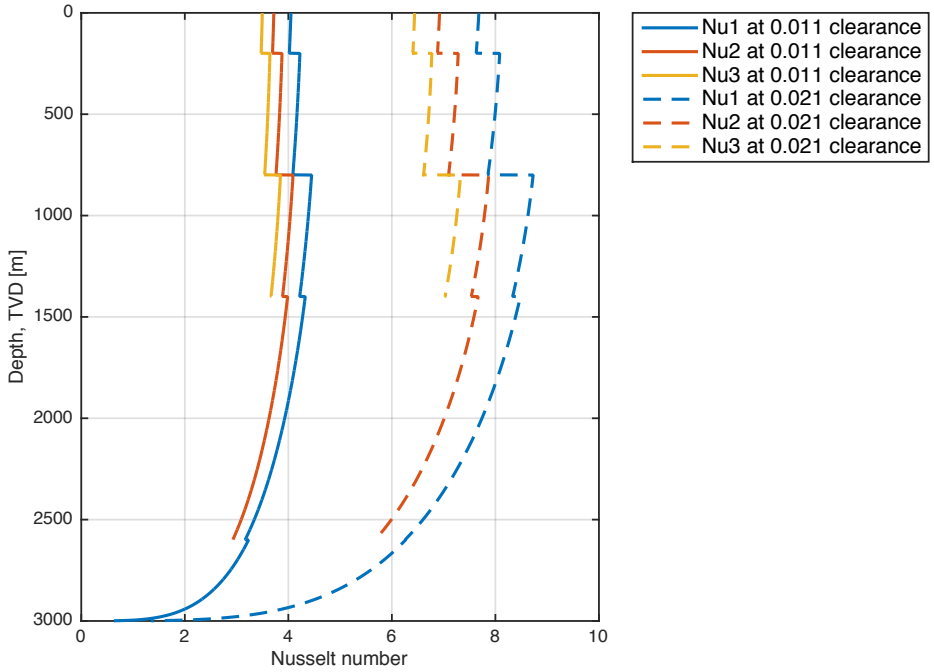

Fig. 4.37. The effect of annular clearance on the Nusselt number of the three separate annular spaces

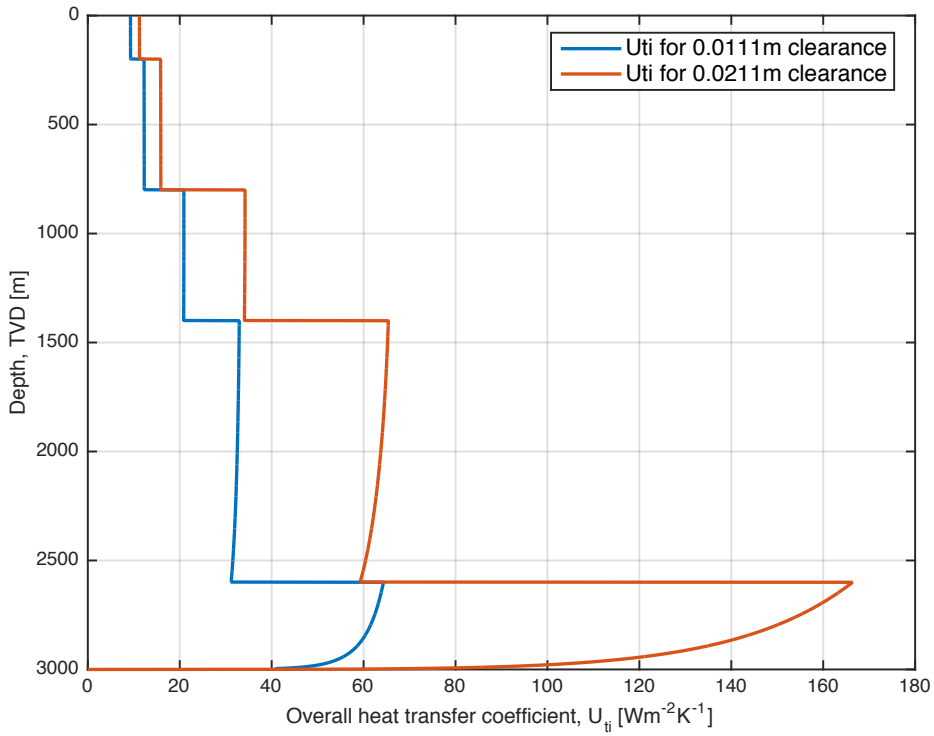

Fig. 4.38. The effect of annular clearance on the overall heat transfer coefficient when setting equal clearance in all three separate annular spaces

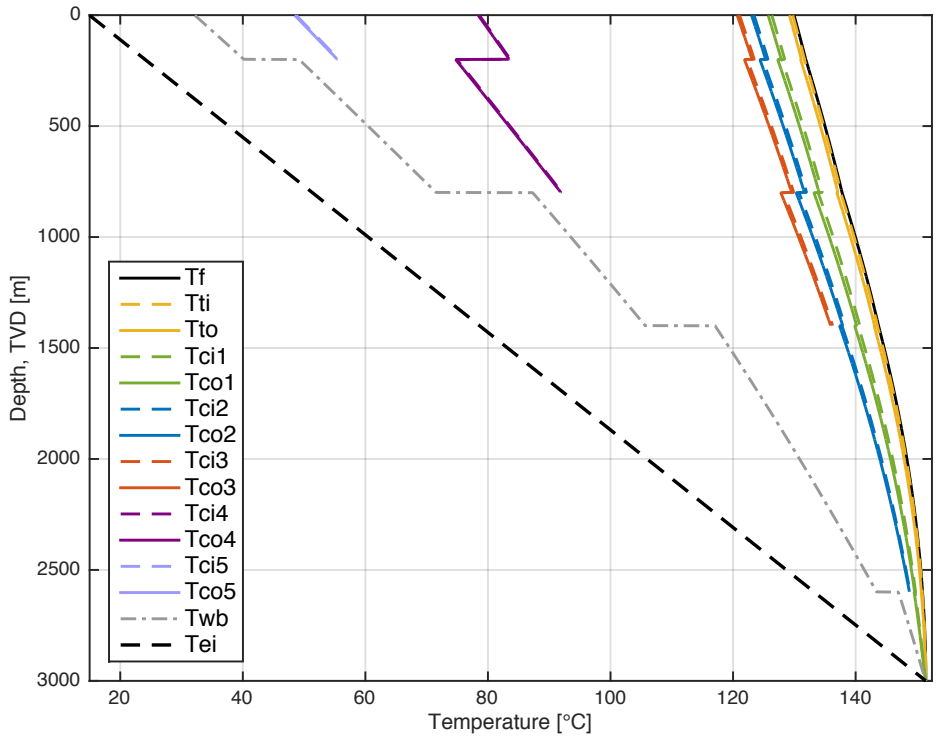

Fig. 4.39. Temperature profile resulting from annular clearance equal to 0.0111 m for all annulus

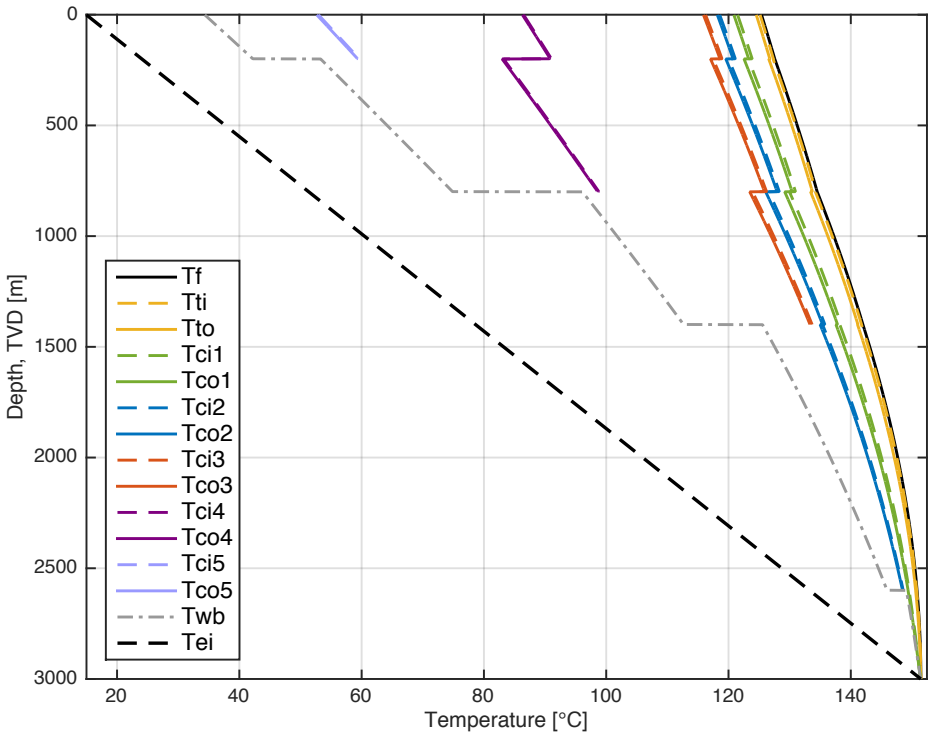

Fig. 4.40. Temperature profile resulting from annular clearance equal to 0.0211 m for all annulus

4.16 Formation parameters

The properties of four different formation rocks (Table 4.3) are implemented and the resulting temperature profiles are plotted. The base case (Fig. 4.41) is added as a reference for comparison. While the changes are generally small from clay to the water saturated sandstone (Fig. 4.42) or the limestone (Fig. 4.43), it is seen that compacted chalk (Fig. 4.44) has a fairly large impact on the wellbore and well temperatures.

Formation rock	$\rho_\mathbf{e}$ $[\mathrm{kg\,m^{-3}}]$	$\mathbf{c_{pe}}$ $[\mathrm{J\,kg^{-1}\,K^{-1}}]$	$\mathbf{k_e}$ $[\mathrm{W\,m^{-1}\,K^{-1}}]$	$\alpha_\mathbf{e} \times 10^{-7}$ $[\mathrm{m^2\,s^{-1}}]$
Clay (Base case)	2080	2127	1.42	3.210
Sandstone, water saturated	2300	840	2.46	0.127
Limestone	2700	851	2.20	9.575
Chalk, compacted	1920	922	1.02	5.762

Table 4.3. Formation properties (Kutasov and Eppelbaum, 2015)

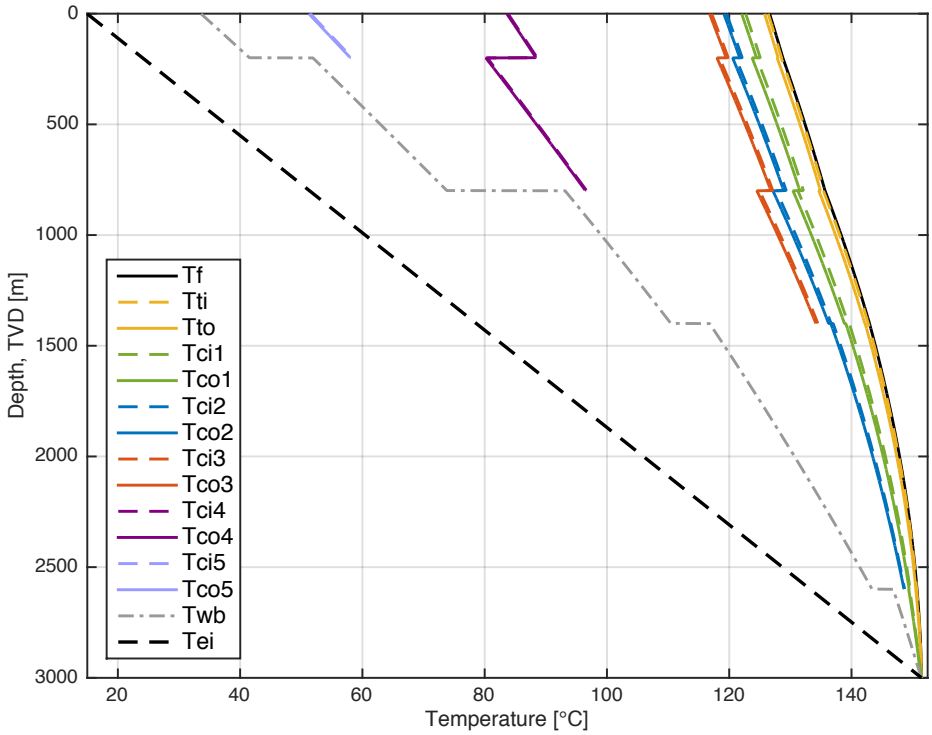

Fig. 4.41. Temperature profiles for clay rock formation properties (base case)

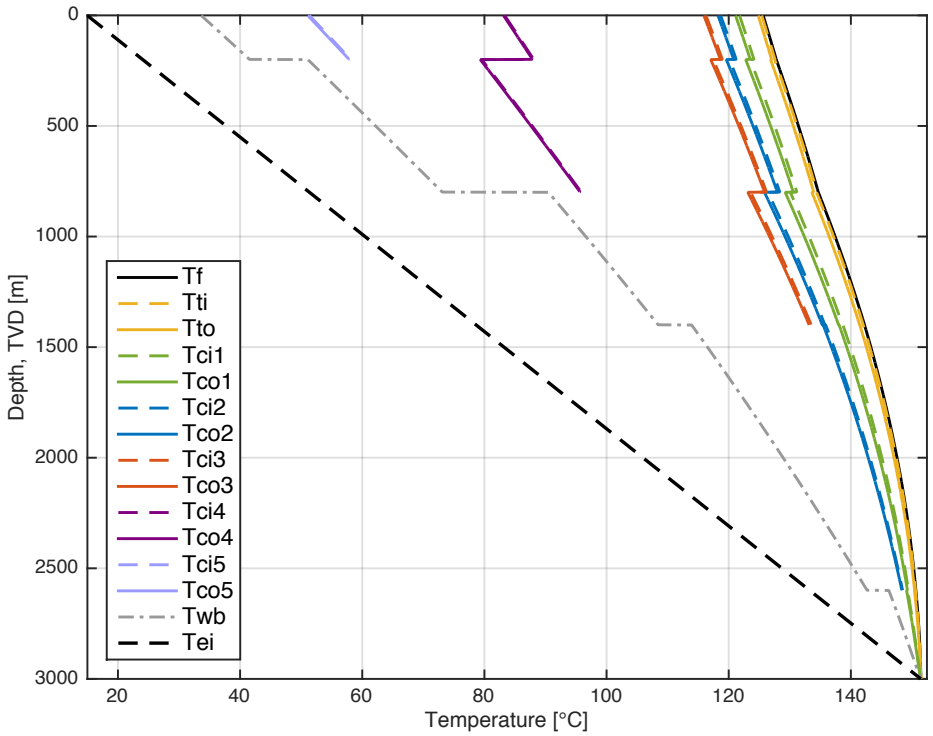

Fig. 4.42. Temperature profiles for water saturated sandstone formation properties

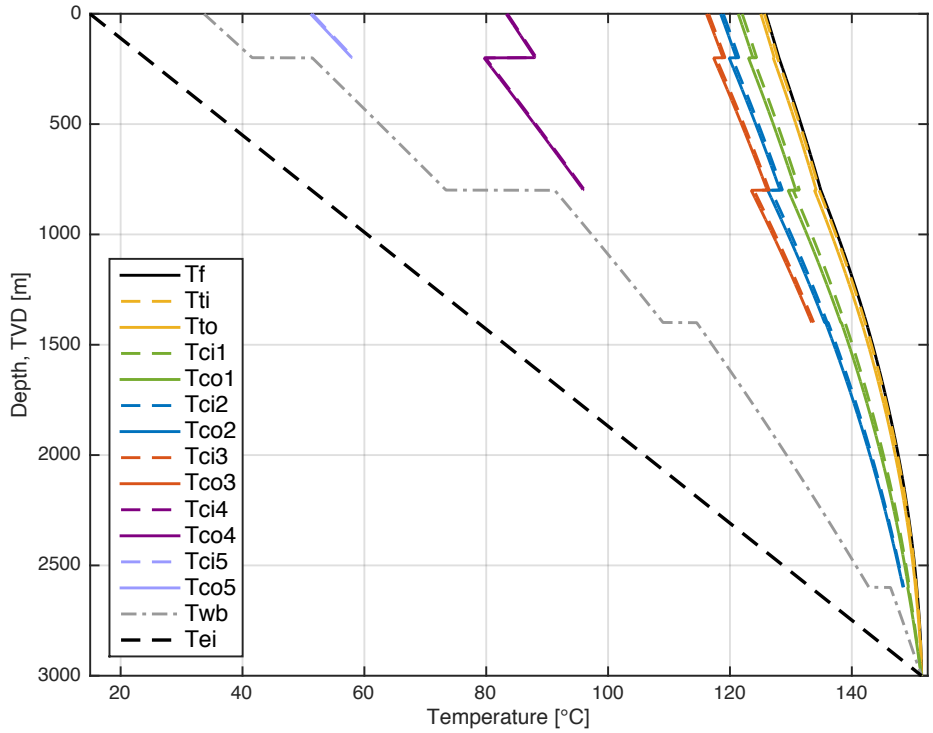

Fig. 4.43. Temperature profiles for limestone formation properties

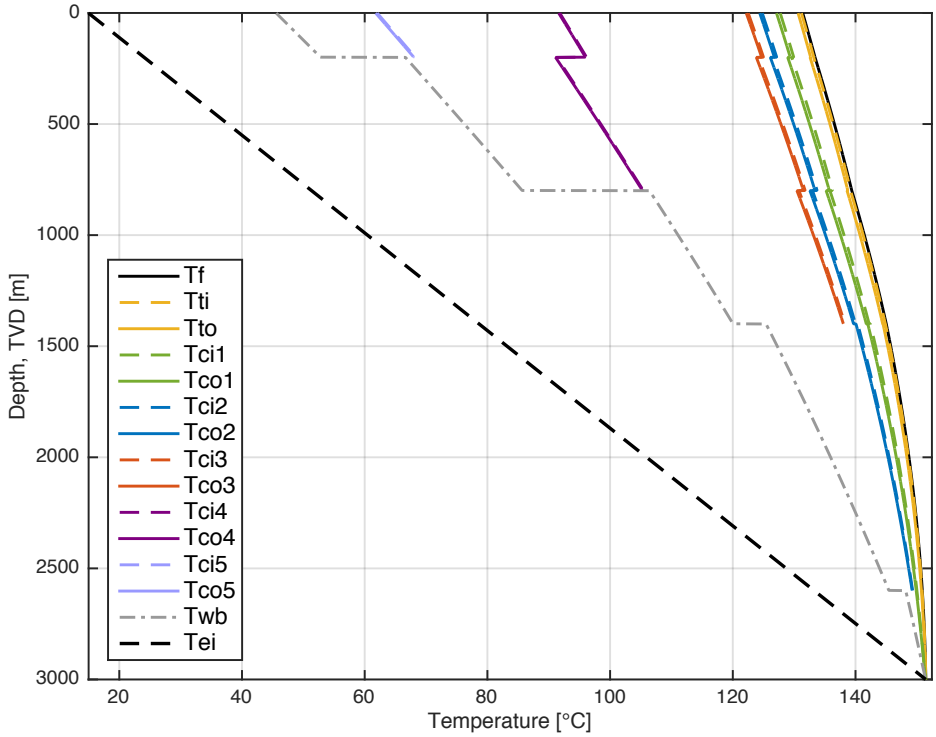

Fig. 4.44. Temperature profiles for compacted chalk formation properties

4.17 Geothermal gradient

The effect of geothermal gradient on the undisturbed earth temperature, T_{ei}, the wellbore temperature, T_{wb}, and the produced fluid temperature, T_f, was plotted for three different geothermal gradients: 0.03 °C/m, 0.04 °C/m, and 0.05 °C/m. An expected increase in temperatures when increasing the geothermal gradient is observed in Fig. 4.45

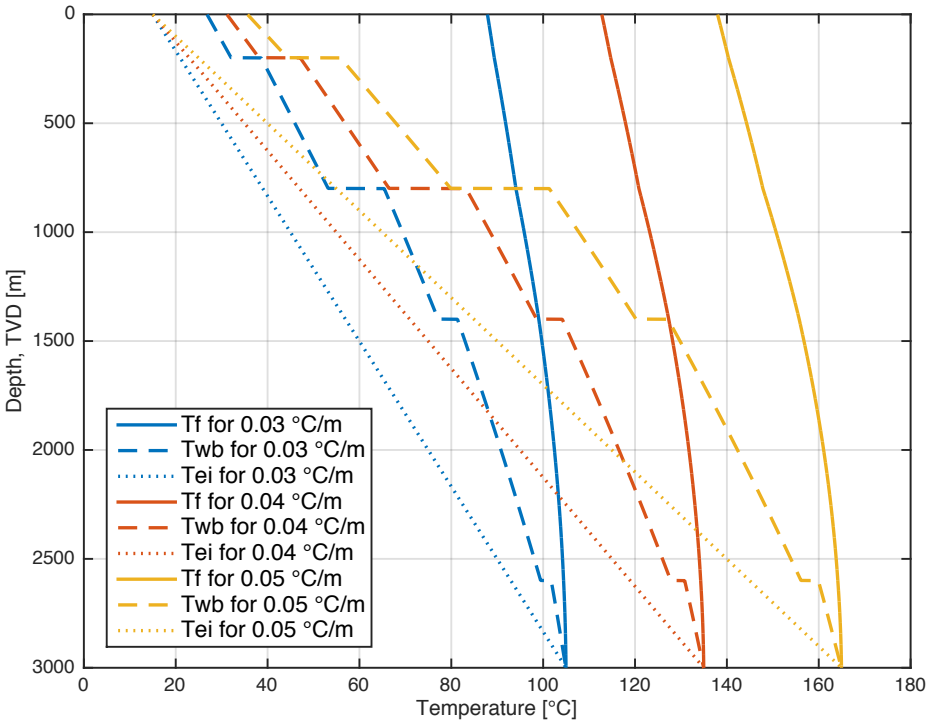

Fig. 4.45. Temperature profiles for different geothermal gradients

Chapter 5

Result and Conclusion

A temperature model for a single phase production scenario has been implemented in MATLAB, carrying out a cell-by-cell piecewise calculation procedure, able to consider consider complex well configurations, a simple inclined wellbore trajectory, varying properties of annular and produced fluids, temperature and pressure dependence of thermophysical parameters, and natural convection in multiple annulus. Given that the overall heat transfer coefficient is found, the model is able to estimate the temperature of the produced fluid and the temperatures at all interfaces in the well configuration, also taking into consideration the Joule-Thomson heating effect on the produced fluid temperature.

The heat transfer to the formation is largest in the deeper parts of the well. The effect of production flow rate was found to have a large impact on the well temperatures, increasing with increasing production rate. As the well is produced, and as time goes, the temperature increases in the formation around the wellbore, growing towards a steady state. The composition of the fluid being produced had a large impact on the well temperatures, with the thermal conductivity of the produced fluid being only important at low flow rates, and the specific heat capacity of the fluid as the most influential parameter all over. Density variations within the available fluid definition range of the dead oil density equation of state was found to have a significant impact on the temperatures. For the annular fluid, specific heat capacity had a minor impact on the temperatures, while thermal conductivity and viscosity had a larger impact. When neglecting the free convection in annulus, the heat transfer through annulus becomes purely conductive, leading to an underestimation of the casing and annular temperatures. When assuming the same brine properties for the produced fluid as used in the annulus, the temperatures for the whole well increased significantly,

underlining the importance of knowing the composition of the produced fluid. Annular clearance was investigated, revealing a larger heat transfer with increasing annular clearance. Temperatures was found to vary significantly with varying formation properties, underlining the importance of correct input parameters.

One possible pitfall for the calculation of heat transfer in the annulus is the adaption of the free convection Nu correlation, developed by Dropkin et al. (1965). By adapting this correlation one must neglect the effect of the curved annulus, seeing as the correlation was originally developed for two parallel plates. The correlation is adapted by other studies concerning free convection in annulus, and there is no, to the authors knowledge, available correlations specifically developed for long concentric annulus of various inclination.

An other limitation of this model is the range of validity for many of the thermophysical properties. By simulating even deeper wells, one may end up with temperatures outside the confirmed validity range of the properties, yielding uncertainties in the temperature estimates. By replacing the current correlations for thermophysical properties with ones developed for a broader range of temperatures and pressures, this problem can be bypassed.

The simulator has yet to be verified against any real well data.

References

Ramey, H.J. 1962. "Wellbore Heat Transmission." *Journal of Petroleum Technology* 14, no. 04 (April): 427–435. https://doi.org/10.2118%2F96-pa. (Cited on page 2).

Dropkin, D., and E. Somerscales. 1965. "Heat Transfer by Natural Convection in Liquids Confined by Two Parallel Plates Which Are Inclined at Various Angles With Respect to the Horizontal." *Journal of Heat Transfer* 87 (1): 77. https://doi.org/10.1115%2F1.3689057. (Cited on pages 42, 43, 124).

Willhite, G.P. 1967. "Over-all Heat Transfer Coefficients in Steam And Hot Water Injection Wells." *Journal of Petroleum Technology* 19, no. 05 (May): 607–615. https://doi.org/10.2118%2F1449-pa. (Cited on pages 2, 10, 42, 64).

Jamieson, D.T., J.S. Tudhope, R. Morris, and G. Cartwright. 1969. "Physical properties of sea water solutions: heat capacity." *Desalination* 7, no. 1 (January): 23–30. https://doi.org/10.1016%2Fs0011-9164%2800%2980271-4. (Cited on page 70).

Beggs, H.D., and J.R. Robinson. 1975. "Estimating the Viscosity of Crude Oil Systems." *Journal of Petroleum Technology* 27, no. 09 (September): 1140–1141. https://doi.org/10.2118%2F5434-pa. (Cited on page 76).

Evans, Tom R. 1977. "Thermal properties of North Sea rocks." *The Log Analyst* 18 (02). (Cited on pages 31, 32).

Numbere, D, W Brigham, and M Standing. 1977. *Correlations for physical properties of petroleum reservoir brines.* Technical report. November. https://doi.org/10.2172%2F6733264. (Cited on page 71).

Ozbek, H, and S L Phillips. 1979. *Thermal conductivity of aqueous NaCl solutions from 20 C to 330 C.* Technical report. May. https://doi.org/10.2172%2F6269880. (Cited on page 69).

Reed, R. P. 1983. *Materials at low temperatures.* Metals Park, Ohio: American Society for Metals. ISBN: 9781615039852. (Cited on page 20).

Skjeggestad, O. 1989. *Boreslamteknologi.* Bergen: Alma Mater Forlag AS. ISBN: 82-419-0010-4. (Cited on page 24).

Hasan, A.R., and C.S. Kabir. 1991. "Heat Transfer During Two-Phase Flow in Wellbores: Part I–Formation Temperature." In *Proceedings of SPE Annual Technical Conference and Exhibition.* Society of Petroleum Engineers, October. https://doi.org/10.2523%2F22866-ms. (Cited on page 33).

Alves, I.N., F.J.S. Alhanati, and Ovadia Shoham. 1992. "A Unified Model for Predicting Flowing Temperature Distribution in Wellbores and Pipelines." *SPE Production Engineering* 7, no. 04 (November): 363–367. https://doi.org/10.2118%2F20632-pa. (Cited on page 2).

Hasan and Kabir. 1994. "Aspects of Wellbore Heat Transfer During Two-Phase Flow (includes associated papers 30226 and 30970)." *SPE Production & Facilities* 9, no. 03 (August): 211–216. https://doi.org/10.2118%2F22948-pa. (Cited on pages 2, 42, 47, 51, 64).

Mansure, A.J. 1996. *Hot oiling spreadsheet.* Technical report. September. https://doi.org/10.2172%2F446318. (Cited on page 74).

Santoyo-Gutierrez, Edgar Rolando. 1997. "Transient numerical simulation of heat transfer processes during drilling of geothermal wells." PhD diss., University of Salford. (Cited on page 38).

Santoyo, E, A García, J.M Morales, E Contreras, and G Espinosa-Paredes. 2001. "Effective thermal conductivity of Mexican geothermal cementing systems in the temperature range from 28°C to 200°C." *Applied Thermal Engineering* 21, no. 17 (December): 1799–1812. https://doi.org/10.1016%2Fs1359-4311%2801%2900048-5. (Cited on page 79).

Ipek, G., J.R. Smith, and Z. Bassiouni. 2002. "Estimation of Underground Blowout Magnitude Using Temperature Logs." In *SPE Annual Technical Conference and Exhibition.* Society of Petroleum Engineers. https://doi.org/10.2118%2F77476-ms. (Cited on page 37).

Cengel, Yunus A., and Michael A. Boles. 2006. *Thermodynamics: An engineering approach.* 5th ed. Boston: McGraw-Hill Higher Education. (Cited on pages 29, 30, 46).

García, A., E. Santoyo, and G. Espinosa. 2006. "Convective Heat Transfer Coefficients of Non-Newtonian Geothermal Drilling Fluids." *Journal of Geochemical Exploration* 30:259–264. (Cited on page 39).

Sattarin, M., H. Modarresi, M. Bayat, and M. Teymori. 2007. "NEW VISCOSITY CORRELATIONS FOR DEAD CRUDE OILS." *Petroleum and Coal* 49 (2): 33–39. (Cited on page 77).

Hasan, Kabir, and Wang. 2009. "A Robust Steady-State Model for Flowing-Fluid Temperature in Complex Wells." *SPE Production & Operations* 24, no. 02 (May): 269–276. https://doi.org/10.2118/2F109765-pa. (Cited on pages vii, 2, 29, 38, 50, 51).

Furrer, DU, and SL Semiatin. 2010. *ASM Handbook, Volume 22B, Metals Process Simulation.* 405:18–32. Materials Park, OH: ASM International. (Cited on pages 20, 78).

Holman, JP. 2010. *Heat transfer, 10th edition.* 10th ed. Boston: McGraw-Hill Higher Education. ISBN: 978–0–07–352936–3. (Cited on pages 11–13, 43, 64).

Izgec, Bulent, A. Rashid Hasan, Dongqing Lin, and C. Shah Kabir. 2010. "Flow-Rate Estimation From Wellhead-Pressure and -Temperature Data." *SPE Production & Operations* 25, no. 01 (February): 31–39. https://doi.org/10.2118%2F115790-pa. (Cited on page 35).

Bergman, Theodore L, Frank P Incropera, David P DeWitt, and Adrienne S Lavine. 2011. *Fundamentals of heat and mass transfer.* Hoboken, NJ: John Wiley & Sons. ISBN: 978-0470-50197-9. (Cited on pages 5, 7–9, 15, 17, 19–21, 23, 38–42, 63).

Shoushtari, Mohd Amin, Hussain H Al-Kayiem, and Ogboo Chikere Aja. 2011. "On the natural convection heat transfer in the casing annulus of oil wells." In *Proceedinds of the Asian Conference on Scientific and Social Science Research, ACSSSR2011.* (Cited on page 11).

Bolmatov, D., V. V. Brazhkin, and K. Trachenko. 2012. "The phonon theory of liquid thermodynamics." *Scientific Reports* 2 (May). doi:10.1038/srep00421. https://doi.org/10.1038%2Fsrep00421. (Cited on page 21).

Wright, Wes. 2014. "Simple Equations to Approximate Changes to the Properties of Crude Oil with Changing Temperature." May 1. Accessed May 10, 2017. http://www.jmcampbell.com/tip-of-the-month/2014/04/simple-equations-to-approximate-changes-to-the-properties-of-crude-oil-with-changing-temperature/. (Cited on page 75).

Kutasov, Izzy, and Lev Eppelbaum. 2015. *Pressure and Temperature Well Testing.* CRC Press, October. https://doi.org/10.1201%2Fb19295. (Cited on pages 69, 73, 118).

MATLAB. 2015. *version 8.5.0.197613 (R2015a).* Natick, Massachusetts: The MathWorks Inc. (Cited on pages vii, 1, 3, 123).

Skalle, P. 2015. *Drilling Fluid Engineering.* 6th ed. bookboon.com. ISBN: 978-87-403-1139-6. (Cited on pages 24, 25).

Zhou, Fuzong, and Xiuhua Zheng. 2015. "Heat transfer in tubing-casing annulus during production process of geothermal systems." *Journal of Earth Science* 26, no. 1 (January): 116–123. https://doi.org/10.1007%2Fs12583-015-0511-5. (Cited on pages 38, 42).

Appendix A

MATLAB program codes

Some essential files have been left out, but the remaining code should be able to give an overview of the program. The files are presented in chronological order of appearance in the program.

```
clc
clear
close all

%%
%=========================================================================%
%-------------------Casing and tubing dimensions:---------------------%
%=========================================================================%

global r_ti1 r_to1 r_ci1 r_co1 r_wb1 r_ci2 r_co2 r_wb2 r_ci3 r_co3...
    r_wb3 r_ci4 r_co4 r_wb4 r_ci5 r_co5 r_wb5

% Dimensions given directly by component radius           % [m]

% Tubing int. radius:
r_ti1 = 0.11862/2;              % (d = 4.670 in)

% Tubing ext. radius:
r_to1 = 0.1397/2;               % (d = 5 1/2 in)

% Casing 1 int. radius:
r_ci1 = 0.16193/2;              % (d = 6.375 in)

```

```
24 % Casing 1 ext. radius:
25 r_co1 = 0.19368/2;                % (d = 7 5/8 in)
26
27 % Wellbore 1 radius:
28 r_wb1 = 0.2159/2;                 % (d = 8 1/2 in)
29
30 % Casing 2 int. radius:
31 r_ci2 = 0.21679/2;                % (d = 8.535 in)
32
33 % Casing 2 ext. radius:
34 r_co2 = 0.24448/2;                % (d = 9 5/8 in)
35
36 % Wellbore 2 radius:
37 r_wb2 = 0.3111/2;                 % (d = 12 1/4 in)
38
39 % Casing 3 int. radius:
40 r_ci3 = 0.30925/2;                % (d = 12.175 in)
41
42 % Casing 3 ext. radius:
43 r_co3 = 0.33973/2;                % (d = 13 3/8 in)
44
45 % Wellbore 3 radius:
46 r_wb3 = 0.4445/2;                 % (d = 17 1/2 in)
47
48 % Casing 4 int. radius:
49 r_ci4 = 0.4826/2;                 % (d = 19 in)
50
51 % Casing 4 ext. radius:
52 r_co4 = 0.508/2;                  % (d = 20 in)
53
54 % Wellbore 4 radius:
55 r_wb4 = 0.6604/2;                 % (d = 26 in)
56
57 % Casing 5 int. radius:
58 r_ci5 = 0.7112/2;                 % (d = 28 in)
59
60 % Casing 5 ext. radius:
61 r_co5 = 0.762/2;                  % (d = 30 in)
62
63 % Wellbore 5 radius:
64 r_wb5 = 0.9144/2;                 % (d = 36 in)
65
```

```
66
67 %=========================================================================%
68 %--------------------Production time/rate/density:--------------------%
69 %=========================================================================%
70
71 % Oil production flow rate through tubing:                 % [m^3/s]
72 flowrate_sc = 1500/(60*60*24);
73
74 % Density of produced fluid at standard conditions:        % [kg/m^3]
75 rho_o_sc = 800;
76
77 % Circulation hours:
78 t = 48;
79
80 % Circulation time:                                        % [s]
81 time = 3600*t;
82
83 %=========================================================================%
84 %-------------------------Wellbore Trajectory:----------------------%
85 %=========================================================================%
86
87 % Set the setting depth (MD) of casing shoes
88 % (1 is deepest set, 5 shallowest)                         % [m]
89 csg_shoe1 = 3000;
90 csg_shoe2 = 2600;
91 csg_shoe3 = 1400;
92 csg_shoe4 = 800;
93 csg_shoe5 = 200;
94
95 % Well measured depth at bottom:                           % [m]
96 MD_bh = csg_shoe1;
97
98 % Number of cells set equal to measured depth,
99 % yielding 1 m long cells along the wellbore.
100 number_cells = MD_bh;
101
102 % Set the dogleg angle:                                   % (Deg)
103 DL = 0;
104
105 % Set the length of the different well sections:          % [m]
106 vertical_section = 1000;
107 dogleg_section = 10*DL;
```

```
108 sail_section = csg_shoe1 - vertical_section...
109     - dogleg_section;
110 
111 % Inclination (deg), true horizontal and vertical
112 % displacement (THD,TVD):
113 [incl,TVD,THD] = well_trajectory(MD_bh,number_cells,...
114     DL,vertical_section,dogleg_section,sail_section);
115 %%
116 %=========================================================================%
117 %-------------------------Temperature model:------------------------------%
118 %=========================================================================%
119 
120 [Tf,Tti,Tto,Ta1,Ta2,Ta3,Tci1,Tco1,Twb1,Tci2,Tco2,Twb2,Tci3,Tco3,...
121     Twb3,Tci4,Tco4,Twb4,Tci5,Tco5,Twb5,Tei,Pressure_tubing,...
122     ploss_fric,ploss_stat,ploss_kin,rho_tub,rho_an1,rho_an2,...
123     rho_an3,h_ti,h_ca1,h_ca2,h_ca3,Nu1_plot,Nu2_plot,Nu3_plot,...
124     Ra1_plot,Ra2_plot,Ra3_plot,phi_plot,Cj_plot,U_ti]...
125     = temperature_tubing(flowrate_sc,rho_o_sc,TVD,number_cells,...
126     incl,time,csg_shoe1,csg_shoe2,csg_shoe3,csg_shoe4,csg_shoe5);
127 
128 %%
129 %=========================================================================%
130 %----------------------------Plotting:------------------------------------%
131 %=========================================================================%
132 
133 % Compiling WB vector
134 Twb1 = Twb1(~isnan(Twb1));
135 Twb2 = Twb2(~isnan(Twb2));
136 Twb3 = Twb3(~isnan(Twb3));
137 Twb4 = Twb4(~isnan(Twb4));
138 Twb5 = Twb5(~isnan(Twb5));
139 Twb = [Twb5;Twb4;Twb3;Twb2;Twb1];
140 
141 %Plotting wellbore trajectory
142 figure
143 plot(THD,TVD,'b','LineWidth',2)
144 xstring = num2str(THD(end) );
145 ystring = num2str(TVD(end) );
146 set(gca,'YDir','Reverse')
147 xlim([0,THD(end)+1])
148 axis equal
149 axis tight
```

```
150
151 % Plotting temperature profiles
152 plotcolors = [0,0,0;              % Tf
153     0.9290,0.6940,0.1250;         % Tti
154     0.9290,0.6940,0.1250;         % Tto
155     %0,0.447,0.7410;              % Ta1
156     0.4660,0.6740,0.1880;         % Tci1
157     0.4660,0.6740,0.1880;         % Tco1
158     %0,0.447,0.7410;              % Ta2
159     0,0.447,0.7410;               % Tci2
160     0,0.447,0.7410;               % Tco2
161     %0,0.447,0.7410;              % Ta3
162     0.85,0.325,0.098;             % Tci3
163     0.85,0.325,0.098;             % Tco3
164     0.5 0 0.5                     % Tci4
165     0.5 0 0.5                     % Tco4
166     0.6,0.6,1.0000                % Tci5
167     0.6,0.6,1.0000                % Tco5
168     0.6,0.6,0.6;                  % Twb
169     0,0,0];                       % Tei
170
171 figure
172 MyColorOrder = plotcolors;
173 axes('NextPlot','replacechildren','ColorOrder',MyColorOrder);
174 plot(Tf,TVD,Tti,TVD,'--',Tto,TVD,Tci1,TVD,'--',Tco1,TVD,Tci2,...
175     TVD,'--',Tco2,TVD,Tci3,TVD,'--',Tco3,TVD,Tci4,TVD,'--',Tco4,...
176     TVD,Tci5,TVD,'--',Tco5,TVD,Twb,TVD,'-.','LineWidth',1.5);
177 grid on
178 hold on
179 plot(Tei,TVD,'--','LineWidth',1.75)
180 set(gca,'YDir','Reverse')
181 legend('Tf','Tti','Tto','Tci1','Tco1','Tci2','Tco2','Tci3',...
182     'Tco3','Tci4','Tco4','Tci5','Tco5','Twb','Tei','location',...
183     'southwest');
184 xlabel('Temperature [C]')
185 ylabel('Depth, TVD [m]')
186 set(0,'DefaultLegendFontSize',22)
187 xlim([min(Tei), max(Tf)+1]);
```

```
1 function [Tf_vector,Tti_vector,Tto_vector,Ta1_vector,Ta2_vector,...
2     Ta3_vector,Tci1_vector,Tco1_vector,Twb1_vector,Tci2_vector,...
```

```
    Tco2_vector,Twb2_vector,Tci3_vector,Tco3_vector,Twb3_vector,...
    Tci4_vector,Tco4_vector,Twb4_vector,Tci5_vector,Tco5_vector,...
    Twb5_vector,T_ei,Pressure_tubing,ploss_fric_total_vector,...
    ploss_stat_total_vector,ploss_kin_total_vector,rho_f_t_vector,...
    rho_an1_vector,rho_an2_vector,rho_an3_vector,h_ti_vector,...
    h_ca1_vector,h_ca2_vector,h_ca3_vector,Nu1_vector,Nu2_vector,...
    Nu3_vector,Ra1_vector,Ra2_vector,Ra3_vector,phi_vector,...
    Cj_vector,Uti_vector] = temperature_tubing(flowrate_sc,...
    rho_o_sc,TVD,number_cells,incl,t,csg_shoe1,csg_shoe2,csg_shoe3,...
    csg_shoe4,csg_shoe5)

global r_ti1 r_to1 r_ci1 r_co1 r_wb1 r_ci2 r_co2 r_wb2 r_ci3 r_co3...
    r_wb3 r_ci4 r_co4 r_wb4 r_ci5 r_co5 r_wb5

%================Thermophysical and other parameters:================%

% Produced fluid mass flow rate:                          % [kg/s]
w = flowrate_sc*rho_o_sc;

% Earth temperature at wellhead:                          % [C]
T_e = 15;

% Formation thermal conductivity:                         % [W/m-K]
k_e = 1.42;

% Formation specific heat capacity:                       % [J/kg-K]
c_e = 2127;

% Formation density:                                      % [kg/m^3]
rho_e = 2080;

% Formation average geothermal gradient:                  % [C/m]
g_G = 0.0455;

% Gravitational acceleration:                             % [m/s^2]
g = 9.81;

% Specific gravity of produced fluid at standard
% conditions:
sg_o = rho_o_sc/1000;

%=========================Model Parameters:==========================%
```

```
45
46 % Formation thermal diffusivity:                              % [m^2/s]
47 alpha = k_e/(c_e*rho_e);
48
49 % Dimensionless temperature for the different wellbore
50 % radiuses:
51 T_D1 = dimless_temp(alpha,t,r_wb1);
52 T_D2 = dimless_temp(alpha,t,r_wb2);
53 T_D3 = dimless_temp(alpha,t,r_wb3);
54 T_D4 = dimless_temp(alpha,t,r_wb4);
55 T_D5 = dimless_temp(alpha,t,r_wb5);
56
57 % Element measured length:                                   % [m]
58 dz = csg_shoe1/number_cells;
59
60 % Creating the undisturbed earth temperature vector:
61 [T_ei,Tbom] = geograd(number_cells,T_e,g_G,dz,incl);
62
63 %% Creating empty vectors
64 % Empty vector of cells
65 cells = NaN(number_cells,1);
66
67 % Vectors assigned "NaN" values:
68 [rho_f_t_vector,rho_an1_vector,rho_an2_vector,rho_an3_vector] =...
69     deal(cells);
70
71 [Ra1_vector,Ra2_vector,Ra3_vector] = deal(cells);
72
73 [Nu1_vector,Nu2_vector,Nu3_vector] = deal(cells);
74
75 [h_ti_vector,h_ca1_vector,h_ca2_vector,h_ca3_vector] =...
76     deal(cells);
77
78 [Pressure_tubing,ploss_fric_total_vector,ploss_stat_total_vector,...
79     ploss_kin_total_vector] = deal(cells);
80
81 [Tci2_vector,Tco2_vector,Tci3_vector,Tco3_vector,Tci4_vector,...
82     Tco4_vector,Tci5_vector,Tco5_vector,Twb2_vector,Twb3_vector,...
83     Twb4_vector,Twb5_vector,Ta2_vector,Ta3_vector] = deal(cells);
84
85 [Twb2_vector(end),Twb3_vector(end),Twb4_vector(end),...
86     Twb5_vector(end)] = deal(NaN);
```

```
87
88  Uti_vector = cells; Uti_vector(1)=NaN;
89  phi_vector = cells;
90  Cj_vector = cells;
91
92  % Updating cells vector with boundary condition:
93  cells(end)=Tbom;
94
95  % Empty vectors with boundary conditions for temperature
96  % in production flow,tubing inside wall, tubing outside
97  % wall, annulus, casing inside wall, casing outside wall,
98  % and wellbore wall:
99  [Tf_vector,Tti_vector,Tto_vector,Ta1_vector,Tci1_vector,...
100     Tco1_vector,Twb1_vector] = deal(cells);
101
102
103 %%
104 %=======================Stepwise calculation:=======================%
105
106 % Calculating the temperature from the bottom cell towards
107 % the top:
108
109 for idx = number_cells:-1:1
110
111     if idx > 1;
112         %% Parameter values for the whole length of the well
113
114         % Previous cell produced fluid temp.              % [C]
115         T_f_prev = Tf_vector(idx);
116
117         % Previous cell tubing temp.                      % [C]
118         T_ti_prev = Tti_vector(idx);
119         T_to_prev = Tto_vector(idx);
120
121         % Previous and current cell undisturbed
122         % formation temp.                                 % [C]
123         T_ei_prev = T_ei(idx);
124         T_ei_current = T_ei(idx-1);
125
126         % Previous cell pressure:
127         P_prev(idx == number_cells)...
128             = 1030*g*TVD(number_cells);
```

```
129         P_prev(idx < number_cells)...
130             = Pressure_tubing(idx);
131
132         ploss_fric_prev(idx == number_cells) = 0;
133         ploss_fric_prev(idx<number_cells) =...
134             ploss_fric_total_vector(idx);
135         ploss_stat_prev(idx == number_cells) = 0;
136         ploss_stat_prev(idx<number_cells) =...
137             ploss_stat_total_vector(idx);
138         ploss_kin_prev(idx == number_cells) = 0;
139         ploss_kin_prev(idx<number_cells) =...
140             ploss_kin_total_vector(idx);
141
142         % Convective heat transfer coefficients for
143         % annulus 1, 2 and 3.                              % [W/m-K]
144         h_ca1 = h_ca1_vector(idx);
145
146         if idx == csg_shoe2
147             h_ca2 = h_ca1;
148         else
149             h_ca2 = h_ca2_vector(idx);
150         end
151
152         if idx == csg_shoe3
153             h_ca3 = h_ca2;
154         else
155             h_ca3 = h_ca3_vector(idx);
156         end
157
158         % Previous cell Uti:                               % [W/m-K]
159         U_ti_prev = Uti_vector(idx);
160         U_ti_prev(idx == number_cells) = 60;
161
162         % Produced fluid density [kg/m^3], pressure
163         % losses [Pa/m], viscosity [Pa-s], Reynolds
164         % number, Darcy friction factor, and thermal
165         % expansion coefficient [1/K]:
166         [rho_f_t,visc_t,beta_t,P_current]= dens_visc_t(...
167             Tf_vector(idx),rho_o_sc,P_prev,...
168             ploss_fric_prev,ploss_stat_prev,...
169             ploss_kin_prev);
170
```

```
171         % Reynold's number and friction factor in tubing
172         [~,Re,fmoody] = fricloss_tubing(w,visc_t,r_ti1,...
173             rho_f_t);
174
175         % Previous cell density                             % [kg/m^3]
176         rho_f_t_prev(idx==number_cells) = rho_f_t;
177         rho_f_t_vector(idx(idx==number_cells)) = rho_f_t;
178         rho_f_t_prev(idx<number_cells)...
179             = rho_f_t_vector(idx);
180
181         % Update parameters for produced fluid
182         k_f_t = kf_o(T_f_prev,sg_o);                        % [W/m-K]
183         c_f_t = cf_o(T_f_prev,sg_o);                        % [J/kg-K]
184         k_t = k_tbg((T_ti_prev+T_to_prev)/2);               % [W/m-K]
185
186
187         %% Parameter values from casing shoe 1 and up:
188
189         % Previous cell casings 1, wellbore 1, and
190         % annulus 1 temp.                                   % [C]
191         T_ci1_prev = Tci1_vector(idx);
192         T_co1_prev = Tco1_vector(idx);
193         T_wb1_prev = Twb1_vector(idx);
194         T_a1_prev = Ta1_vector(idx);
195
196         % Current cell parameters evaluated at
197         % Previous cell temperatures:
198         k_f_a1 = kf_a(T_a1_prev);                           % [W/m-K]
199         c_f_a1  = cf_a(T_a1_prev);                          % [J/kg-K]
200         k_c1 = k_csg((T_ci1_prev + T_co1_prev)/2);          % [W/m-K]
201         k_cem1 = k_cement((T_co1_prev + T_wb1_prev)/2);     % [W/m-K]
202
203         % Density [kg/m^3], viscosity [Pa-s], and
204         % thermal expansion coefficient [1/K]:
205         [rho_f_a1,visc_f_a1,beta_an1]...
206             = dens_visc_a(Ta1_vector(idx),TVD(idx));
207
208
209         %% Parameter values from casing shoe 2 and up:
210
211         % Previous cell temperatures:                       % [C]
212         T_ci2_prev = Tci2_vector(idx);
```

```
213         T_co2_prev = Tco2_vector(idx);
214         T_wb2_prev = Twb2_vector(idx);
215         T_a2_prev = Ta2_vector(idx);
216
217         % Current cell parameters evaluated at
218         % Previous cell temperatures:
219         c_f_a2  = cf_a(T_a2_prev);                          % [J/kg-K]
220         k_f_a2 = kf_a(T_a2_prev);                           % [W/m-K]
221         k_c2 = k_csg((T_ci2_prev + T_co2_prev)/2);          % [W/m-K]
222         k_cem2 = k_cement((T_co2_prev + T_wb2_prev)/2);     % [W/m-K]
223
224         % Density [kg/m^3], viscosity [Pa-s], and
225         % thermal expansion coefficient [1/K]:
226         [rho_f_a2,visc_f_a2,beta_an2] ...
227             = dens_visc_a(Ta2_vector(idx),TVD(idx));
228
229         % Assuming parameters for the first cell
230         % in annulus 2 of new section are equal to
231         % parameters of annulus 1:
232         if idx == csg_shoe2;
233             rho_f_a2 = rho_f_a1;                            % [kg/m^3]
234             visc_f_a2 = visc_f_a1;                          % [Pa-s]
235             beta_an2 = beta_an1;                            % [1/K]
236             c_f_a2  = c_f_a1;                               % [J/kg-K]
237             k_f_a2 = k_f_a1;                                % [W/m-K]
238             k_c2 = k_c1;                                    % [W/m-K]
239             k_cem2 = k_cem1;                                % [W/m-K]
240         end
241
242
243         %% Parameter values from casing shoe 3 and up:
244
245         % Previous cell temperatures                        % [C]
246         T_ci3_prev = Tci3_vector(idx);
247         T_co3_prev = Tco3_vector(idx);
248         T_wb3_prev = Twb3_vector(idx);
249         T_a3_prev = Ta3_vector(idx);
250
251         % Current cell parameters evaluated at
252         % Previous cell temperatures:
253         c_f_a3 = cf_a(T_a3_prev);                           % [J/kg-K]
254         k_f_a3 = kf_a(T_a3_prev);                           % [W/m-K]
```

```
255         k_c3 = k_csg((T_ci3_prev + T_co3_prev)/2);          % [W/m-K]
256         k_cem3 = k_cement((T_co3_prev + T_wb3_prev)/2);     % [W/m-K]
257
258         % Density [kg/m^3], viscosity [Pa-s], and
259         % thermal expansion coefficient [1/K]:
260         [rho_f_a3,visc_f_a3,beta_an3] = ...
261             dens_visc_a(Ta3_vector(idx),TVD(idx));
262
263         % Assuming parameters for the first cell
264         % in annulus 3 of new section are equal to
265         % parameters of annulus 2:
266         if idx == csg_shoe3;
267             rho_f_a3 = rho_f_a2;                            % [kg/m^3]
268             visc_f_a3 = visc_f_a2;                          % [Pa-s]
269             beta_an3 = beta_an2;                            % [1/K]
270             c_f_a3  = c_f_a2;                               % [J/kg-K]
271             k_f_a3 = k_f_a2;                                % [W/m-K]
272             k_c3 = k_c2;                                    % [W/m-K]
273             k_cem3 = k_cem2;                                % [W/m-K]
274         end
275
276
277         %% Parameter values from casing shoe 4 and up (cemented):
278
279         % Previous cell temperatures                        % [C]
280         T_ci4_prev = Tci4_vector(idx);
281         T_co4_prev = Tco4_vector(idx);
282         T_wb4_prev = Twb4_vector(idx);
283
284         % Current cell parameters evaluated at
285         % Previous cell temperatures:
286         k_c4 = k_csg((T_ci4_prev + T_co4_prev)/2);          % [W/m-K]
287         k_cem4 = k_cement((T_co3_prev+T_wb4_prev)/2);       % [W/m-K]
288
289         if idx == csg_shoe4;
290             k_c4 = k_c3;                                    % [W/m-K]
291             k_cem4 = k_cem3;                                % [W/m-K]
292         end
293
294         if idx < csg_shoe4;
295             k_cem3 = k_cement((T_co3_prev...
296                 + T_ci4_prev)/2);                           % [W/m-K]
```

```
297         end
298
299
300         %% Parameter values from casing shoe 5 and up (cemented):
301
302         % Previous cell temperatures                          % [C]
303         T_ci5_prev = Tci5_vector(idx);
304         T_co5_prev = Tco5_vector(idx);
305         T_wb5_prev = Twb5_vector(idx);
306
307         % Current cell parameters evaluated at
308         % Previous cell temperatures:
309         k_c5 = k_csg((T_ci5_prev + T_co5_prev)/2);          % [W/m-K]
310         k_cem5 = k_cement((T_co5_prev+T_wb5_prev)/2);       % [W/m-K]
311
312         if idx == csg_shoe5;
313             k_c5 = k_c4;                                    % [W/m-K]
314             k_cem5 = k_cem4;                                % [W/m-K]
315         end
316
317         if idx < csg_shoe5;
318             k_cem4 = k_cement((T_co4_prev...
319                 + T_ci5_prev)/2);                           % [W/m-K]
320         end
321
322
323 %%
324 %============Estimating Overall Heat Transfer Coefficient:==========%
325
326         % Estimating the overall heat transfer
327         % coefficient based on tubing inside area,
328         % U_ti:                                               % [W/m^2-K]
329         [U_ti,T_to,h_ca1,h_ca2,h_ca3,h_ti,Nu1,Nu2,Nu3,...
330             Ra_1,Ra_2,Ra_3] = U_ti_est(idx,incl(idx),...
331             U_ti_prev,T_f_prev,T_ei_current,visc_t,k_e,...
332             Re,fmoody,beta_an1,beta_an2,beta_an3,...
333             visc_f_a1,visc_f_a2,visc_f_a3,rho_f_a1,...
334             rho_f_a2,rho_f_a3,k_f_t,c_f_t,k_f_a1,...
335             k_f_a2,k_f_a3,c_f_a1,c_f_a2,c_f_a3,k_t,...
336             k_c1,k_c2,k_c3,k_c4,k_c5,k_cem1,k_cem2,...
337             k_cem3,k_cem4,k_cem5,T_D1,T_D2,T_D3,...
338             csg_shoe1,csg_shoe2,csg_shoe3,csg_shoe4,...
```

```
339             csg_shoe5,h_ca1,h_ca2,h_ca3);
340
341
342 %%
343 %====================Produced fluid parameters:====================%
344
345         % Calculating the Joul-Thomson coefficient:       % [K/Pa]
346         Cj = JT_coeff(rho_f_t,c_f_t,beta_t,T_f_prev);
347
348         % Calculating pressure drops in tubing:           % [Pa/m]
349         [ploss_fric,ploss_stat,ploss_kin,v,v_prev] =...
350             p_loss_tbg(w,rho_f_t_prev,rho_f_t,visc_t,...
351             r_ti1,incl(idx));
352
353         % Calculating the "phi" parameter:                % [K/m]
354         phi = phi_parameter(Cj,c_f_t,ploss_fric,...
355             ploss_stat,ploss_kin,v,v_prev);
356 %%
357 %=======================Relaxation distance:=======================%
358
359         % Dimensionless time for each section
360         if idx > csg_shoe2;
361             T_D = T_D1;
362         elseif idx <= csg_shoe2 && idx > csg_shoe3;
363             T_D = T_D2;
364         elseif idx <= csg_shoe3 && idx > csg_shoe4;
365             T_D = T_D3;
366         elseif idx <= csg_shoe4 && idx > csg_shoe5;
367             T_D = T_D4;
368         elseif idx <= csg_shoe5;
369             T_D = T_D5;
370         end
371
372         % Relaxation distance                             % [m]
373         A = ((c_f_t)*w/(2*pi))*...
374             (k_e+(r_ti1*U_ti*T_D))/...
375             (r_ti1*U_ti*k_e);
376
377 %%
378 %=====================The temperature model:=====================%
379
380         % The tubing temperature                          % [C]
```

```
381         T_f = T_ei_current+A*(1-exp(-dz/A))...
382             *((g_G*cosd(incl(idx))) + phi...
383             - (g*cosd(incl(idx))/(c_f_t)))...
384             + exp(-dz/A)*(T_f_prev - T_ei_prev);
385 
386 %%
387 %===============Calculating new wellbore temperatures:===============%
388 
389         %%% Wellbore temperatures:
390 
391         if idx > csg_shoe2;
392             % Wellbore 1 temperature
393             T_wb1 = (k_e*T_ei_current...
394                 + r_ti1*U_ti*T_D1*T_f)...
395                 /(k_e+r_ti1*U_ti*T_D1);
396         else T_wb1 = NaN;
397         end
398 
399         if idx <= csg_shoe2 && idx > csg_shoe3;
400             % Wellbore 2 temperature
401             T_wb2 = (k_e*T_ei_current...
402                 + r_ti1*U_ti*T_D2*T_f)...
403                 /(k_e+r_ti1*U_ti*T_D2);
404         else T_wb2 = NaN;
405         end
406 
407         if idx <= csg_shoe3 && idx > csg_shoe4;
408             % Wellbore 3 temperature:
409             T_wb3 = (k_e*T_ei_current...
410                 +r_ti1*U_ti*T_D3*T_f)...
411                 /(k_e+r_ti1*U_ti*T_D3);
412         else T_wb3 = NaN;
413         end
414 
415         if idx <= csg_shoe4 && idx > csg_shoe5;
416             % Wellbore temperature
417             T_wb4 = (k_e*T_ei_current...
418                 + r_ti1*U_ti*T_D4*T_f)...
419                 /(k_e+r_ti1*U_ti*T_D4);
420         else T_wb4 = NaN;
421         end
422         if idx <= csg_shoe5;
```

```
423             % Wellbore 5 temperature:
424             T_wb5 = (k_e*T_ei_current...
425                 + r_ti1*U_ti*T_D5*T_f)...
426                 /(k_e+r_ti1*U_ti*T_D5);
427         else T_wb5 = NaN;
428         end
429
430         %%% Temperatures for interfaces between casing
431         %%% shoe 1 and 2:                                    % [C]
432
433         if idx > csg_shoe2;
434
435             % Tubing inside temperature:
436             T_ti = T_f - ((r_ti1*U_ti)/(r_ti1*h_ti))...
437                 *(T_f-T_wb1);
438
439             % Tubing outside temperature:
440             T_to = T_ti - ((r_ti1*U_ti)/k_t)...
441                 *log(r_to1/r_ti1)*(T_f-T_wb1);
442
443             % Tubing outside temperature:
444             T_ci1 = T_to - ((r_ti1*U_ti)/(r_to1*h_ca1))...
445                 *(T_f-T_wb1);
446
447             % Annulus 1 temperature:
448             T_a1 = (T_to+T_ci1)/2;
449
450             % Casing 1 outer temperature:
451             T_co1 = T_ci1 - ((r_ti1*U_ti)/k_c1)...
452                 *log(r_co1/r_ci1)*(T_f-T_wb1);
453         end
454
455         %%% Temperatures for interfaces between casing
456         %%% shoe 2 and 3:                                    % [C]
457
458         if idx <= csg_shoe2 && idx > csg_shoe3;
459
460             % Tubing inside temperature:
461             T_ti = T_f - ((r_ti1*U_ti)/(r_ti1*h_ti))...
462                 *(T_f-T_wb2);
463
464             % Tubing outside temperature:
```

```
465             T_to = T_ti - ((r_ti1*U_ti)/k_t)...
466                 *log(r_to1/r_ti1)*(T_f-T_wb2);
467 
468             % Casing 1 inside temperature:
469             T_ci1 = T_to - ((r_ti1*U_ti)/(r_to1*h_ca1))...
470                 *(T_f-T_wb2);
471 
472             % Annulus 1 temperature:
473             T_a1 = (T_to+T_ci1)/2;
474 
475             % Casing 1 outer temperature:
476             T_co1 = T_ci1 - ((r_ti1*U_ti)/k_c1)...
477                 *log(r_co1/r_ci1)*(T_f-T_wb2);
478 
479             % Casing 2 inside temperature:
480             T_ci2 = T_co1 - ((r_ti1*U_ti)*(1/(r_co1*h_ca2))...
481                 *(T_f-T_wb2));
482 
483             % Annulus 2 temperature:
484             T_a2 = (T_co1+T_ci2)/2;
485 
486             % Casing 2 outer temperature:
487             T_co2 = T_ci2 - ((r_ti1*U_ti)/k_c2)...
488                 *log(r_co2/r_ci2)*(T_f-T_wb2);
489         end
490 
491         %%% Temperatures of interfaces between casing
492         %%% shoe 3 and 4:                                    % [C]
493 
494         if idx <= csg_shoe3 && idx > csg_shoe4;
495 
496             % Tubing inside temperature:
497             T_ti = T_f - ((r_ti1*U_ti)/(r_ti1*h_ti))...
498                 *(T_f-T_wb3);
499 
500             % Tubing outside temperature
501             T_to = T_ti - ((r_ti1*U_ti)/k_t)...
502                 *log(r_to1/r_ti1)*(T_f-T_wb3);
503 
504             % Casing 1 inside temperature
505             T_ci1 = T_to - ((r_ti1*U_ti)/(r_to1*h_ca1))...
506                 *(T_f-T_wb3);
```

```
507
508             % Annulus 1 temperature
509             T_a1 = (T_to+T_ci1)/2;
510
511             % Casing 1 outer temperature
512             T_co1 = T_ci1 - ((r_ti1*U_ti)/k_c1)...
513                 *log(r_co1/r_ci1)*(T_f-T_wb3);
514
515             % Casing 2 inside temperature
516             T_ci2 = T_co1 - ((r_ti1*U_ti)*(1/(r_co1*h_ca2))...
517                 *(T_f-T_wb3));
518
519             % Annulus 2 temperature:
520             T_a2 = (T_co1+T_ci2)/2;
521
522             % Casing 2 outer temperature
523             T_co2 = T_ci2 - ((r_ti1*U_ti)/k_c2)...
524                 *log(r_co2/r_ci2)*(T_f-T_wb3);
525
526             % Casing 3 inside temperature
527             T_ci3 = T_co2 - ((r_ti1*U_ti)*(1/(r_co2*h_ca3))...
528                 *(T_f-T_wb3));
529
530             % Annulus 3 temperature:
531             T_a3 = (T_co2+T_ci3)/2;
532
533             % Casing 3 outer temperature
534             T_co3 = T_ci3 - ((r_ti1*U_ti)/k_c3)...
535                 *log(r_co3/r_ci3)*(T_f-T_wb3);
536         end
537
538
539         %%% Temperatures of interfaces between casing
540         %%% shoe 4 and 5:                                    % [C]
541
542         if idx <= csg_shoe4 && idx > csg_shoe5;
543
544             % Tubing inside temperature:
545             T_ti = T_f - ((r_ti1*U_ti)/(r_ti1*h_ti))...
546                 *(T_f-T_wb4);
547
548             % Tubing outside temperature
```

```
549             T_to = T_ti - ((r_ti1*U_ti)/k_t)...
550                 *log(r_to1/r_ti1)*(T_f-T_wb4);
551
552             % Casing 1 inside temperature
553             T_ci1 = T_to - ((r_ti1*U_ti)/(r_to1*h_ca1))...
554                 *(T_f-T_wb4);
555
556             % Annulus 1 temperature
557             T_a1 = (T_to+T_ci1)/2;
558
559             % Casing 1 outer temperature
560             T_co1 = T_ci1 - ((r_ti1*U_ti)/k_c1)...
561                 *log(r_co1/r_ci1)*(T_f-T_wb4);
562
563             % Casing 2 inside temperature
564             T_ci2 = T_co1 - ((r_ti1*U_ti)*(1/(r_co1*h_ca2))...
565                 *(T_f-T_wb4));
566
567             % Annulus 2 temperature:
568             T_a2 = (T_co1+T_ci2)/2;
569
570             % Casing 2 outer temperature
571             T_co2 = T_ci2 - ((r_ti1*U_ti)/k_c2)...
572                 *log(r_co2/r_ci2)*(T_f-T_wb4);
573
574             % Casing 3 inside temperature
575             T_ci3 = T_co2 - ((r_ti1*U_ti)*(1/(r_co2*h_ca3))...
576                 *(T_f-T_wb4));
577
578             % Annulus 3 temperature:
579             T_a3 = (T_co2+T_ci3)/2;
580
581             % Casing 3 outer temperature:
582             T_co3 = T_ci3 - ((r_ti1*U_ti)/k_c3)...
583                 *log(r_co3/r_ci3)*(T_f-T_wb4);
584
585             % Casing 4 inner temperature;
586             T_ci4 = T_co3 - ((r_ti1*U_ti)/k_cem3)...
587                 *log(r_ci4/r_co3)*(T_f-T_wb4);
588
589             % Casing 4 outer temperature:
590             T_co4 = T_ci4 - ((r_ti1*U_ti)/k_c4)...
```

```
591                 *log(r_co4/r_ci4)*(T_f-T_wb4);
592         end
593
594
595         %%% Temperatures of interfaces between casing
596         %%% shoe 5 and WH:                                  % [C]
597
598         if idx <= csg_shoe5;
599
600             % Tubing inside temperature:
601             T_ti = T_f - ((r_ti1*U_ti)/(r_ti1*h_ti))...
602                 *(T_f-T_wb5);
603
604             % Tubing outside temperature
605             T_to = T_ti - ((r_ti1*U_ti)/k_t)...
606                 *log(r_to1/r_ti1)*(T_f-T_wb5);
607
608             % Casing 1 inside temperature
609             T_ci1 = T_to - ((r_ti1*U_ti)/(r_to1*h_ca1))...
610                 *(T_f-T_wb5);
611
612             % Annulus 1 temperature
613             T_a1 = (T_to+T_ci1)/2;
614
615             % Casing 1 outer temperature
616             T_co1 = T_ci1 - ((r_ti1*U_ti)/k_c1)...
617                 *log(r_co1/r_ci1)*(T_f-T_wb5);
618
619             % Casing 2 inside temperature
620             T_ci2 = T_co1 - ((r_ti1*U_ti)*(1/(r_co1*h_ca2))...
621                 *(T_f-T_wb5));
622
623             % Annulus 2 temperature:
624             T_a2 = (T_co1+T_ci2)/2;
625
626             % Casing 2 outer temperature
627             T_co2 = T_ci2 - ((r_ti1*U_ti)/k_c2)...
628                 *log(r_co2/r_ci2)*(T_f-T_wb5);
629
630             % Casing 3 inside temperature
631             T_ci3 = T_co2 - ((r_ti1*U_ti)*(1/(r_co2*h_ca3))...
632                 *(T_f-T_wb5));
```

```
633
634             % Annulus 3 temperature:
635             T_a3 = (T_co2+T_ci3)/2;
636
637             % Casing 3 outer temperature:
638             T_co3 = T_ci3 - ((r_ti1*U_ti)/k_c3)...
639                 *log(r_co3/r_ci3)*(T_f-T_wb5);
640
641             % Casing 4 inner temperature;
642             T_ci4 = T_co3 - ((r_ti1*U_ti)/k_cem3)...
643                 *log(r_ci4/r_co3)*(T_f-T_wb5);
644
645             % Casing 4 outer temperature:
646             T_co4 = T_ci4 - ((r_ti1*U_ti)/k_c4)...
647                 *log(r_co4/r_ci4)*(T_f-T_wb5);
648
649             % Casing 5 inner temperature:
650             T_ci5 = T_co4 - ((r_ti1*U_ti)/k_cem4)...
651                 *log(r_ci5/r_co4)*(T_f-T_wb5);
652
653             % Casing 5 outer temperature:
654             T_co5 = T_ci5 - ((r_ti1*U_ti)/k_c5)...
655                 *log(r_co5/r_ci5)*(T_f-T_wb5);
656         end
657
658 %%
659 %==================Gathering values in vectors:====================%
660
661         % If temperature variable undefined, take on
662         % a "NaN" value:
663
664         T_a2(exist('T_a2','var')==0)=NaN;
665         T_ci2(exist('T_ci2','var')==0)=NaN;
666         T_co2(exist('T_co2','var')==0)=NaN;
667         Twb2_vector(exist('Twb2','var')==0)=NaN;
668
669         T_a3(exist('T_a3','var')==0)=NaN;
670         T_ci3(exist('T_ci3','var')==0)=NaN;
671         T_co3(exist('T_co3','var')==0)=NaN;
672         T_wb3(exist('T_wb3','var')==0)=NaN;
673
674         T_ci4(exist('T_ci4','var')==0)=NaN;
```

```
675         T_co4(exist('T_co4','var')==0)=NaN;
676         T_wb4(exist('T_wb4','var')==0)=NaN;
677
678         T_wb5(exist('T_wb5','var')==0)=NaN;
679         T_ci5(exist('T_ci5','var')==0)=NaN;
680         T_co5(exist('T_co5','var')==0)=NaN;
681
682         % Temperatures:                                    % (C)
683         Tf_vector(idx-1) = T_f;
684         Tto_vector(idx-1) = T_to;
685         Tti_vector(idx-1) = T_ti;
686         Ta1_vector(idx-1) = T_a1;
687         Tci1_vector(idx-1) = T_ci1;
688         Tco1_vector(idx-1) = T_co1;
689         Twb1_vector(idx-1) = T_wb1;
690         Tci2_vector(idx-1) = T_ci2;
691         Tco2_vector(idx-1) = T_co2;
692         Ta2_vector(idx-1) = T_a2;
693         Twb2_vector(idx-1) = T_wb2;
694         Tci3_vector(idx-1) = T_ci3;
695         Tco3_vector(idx-1) = T_co3;
696         Ta3_vector(idx-1) = T_a3;
697         Twb3_vector(idx-1) = T_wb3;
698         Tci4_vector(idx-1) = T_ci4;
699         Tco4_vector(idx-1) = T_co4;
700         Twb4_vector(idx-1) = T_wb4;
701         Tci5_vector(idx-1) = T_ci5;
702         Tco5_vector(idx-1) = T_co5;
703         Twb5_vector(idx-1) = T_wb5;
704
705         % Overall heat transfer coefficient:              % [W/m^2-K]
706         Uti_vector(idx-1) = U_ti;
707
708         % CHTC for natural convection in annulus:         % [W/m^2-K]
709         h_ca1_vector(idx-1) = h_ca1;
710         h_ca2_vector(idx-1) = h_ca2;
711         h_ca3_vector(idx-1) = h_ca3;
712
713         % CHTC for tubing                                 % [W/m^2-K]
714         h_ti_vector(idx-1) = h_ti;
715
716         % Density of fluid in tubing:                     % [kg/m^3]
```

```
717         rho_f_t_vector(idx-1) = rho_f_t;
718
719         % Joul-Thomson coeffecient:                          % [K/Pa]
720         Cj_vector(idx-1) = Cj;
721
722         % Phi parameter:                                      % [K/m]
723         phi_vector(idx-1) = phi;
724
725         % Pressure in tubing:                                 % [Pa]
726         Pressure_tubing(idx-1) = P_current;
727
728         % Pressure losses:                                    % [Pa/m]
729         ploss_fric_total_vector(idx-1) = ploss_fric;
730         ploss_stat_total_vector(idx-1) = ploss_stat;
731         ploss_kin_total_vector(idx-1) = ploss_kin;
732
733         % Nusselt numbers for annulus:
734         Nu1_vector(idx-1) = Nu1;
735         Nu2_vector(idx-1) = Nu2;
736         Nu3_vector(idx-1) = Nu3;
737
738         % Rayleigh numbers for annulus:
739         Ra1_vector(idx-1) = Ra_1;
740         Ra2_vector(idx-1) = Ra_2;
741         Ra3_vector(idx-1) = Ra_3;
742
743     end
744
745     % Density of fluid in annulus                           % [kg/m^3]
746     rho_an1_vector(idx) = rho_f_a1;
747     rho_an2_vector(idx) = rho_f_a2;
748     rho_an3_vector(idx) = rho_f_a3;
749 end
750 end
```

```
1  function k_o = kf_o(T,sg)
2
3  % % Model: Mansure (1996): Cragoe correlation,
4  % % thermal conductivity of petroleum based liquids.
5  % % Range: 0.78 to 0.95 sg.
6
```

```
% Convert temperature from Celcius to Fahrenheit:      % (F)
T = T*9/5+32;

% Calculating API gravity of crude oil:                % (API)
API = (141.5/sg)-131.5;

% Calculate thermal conductivity of crude oil
% as fn of T and API:                                  % (BTU/F-hr-ft)
k_o = 1.62*(1-0.0003*(T-32))/API*12;

% Convert thermal conductivity from BTU/F-hr-ft
% to W/m-K:                                            % [W/m-K]
k_o = k_o * 1.7295772056;
```

```
function c_f_t=cf_o(T,sg)

% % Model: Wright (2014): Dead oil specific heat capacity
% % temperature correlation.

% Calculating specific heat capacity as function of T      % [J/kg-K]
 c_f_t = ((2*10^-3*T - 1.429)*sg...
     + (2.67*10^-3)*T + 3.049)*10^3;
```

```
function k = k_tbg(T)

% % Model: Furrer (2010): Thermal conductivity
% % correlation for alloy 316 stainless steel:

% Convert temperature from Celcius to Kelvin:             % [K]
T = T + 273.15;

% Thermal conductivity as function of temperature.        % [W/m-K]
k = 6.31 + 27.2*10^(-3)*T - 7*10^(-6)*T^2;
```

```
function k_a=kf_a(T)

% % Models: Ozbek and Phillips (1979)

```

```
% Pure water conductivity:                                    % [W/m-K]
x = (T + 273.15)/273.15;
k_w = -0.92247 + 2.8395*x - 1.8007*x^2....
    + 0.52577*x^3 - 0.07344*x^4;

% Weight percent NaCl in aqueous solution                     % (Wt%)
Cs = 3.5;

% Thermal conductivity of aqueous NaCl Solution:             % [W/m-K]
k_a = (1 - (2.3434*10^-3 - 7.924*10^-6*T...
 + 3.924*10^-8*T^2)*Cs + (1.06*10^-5....
 - 2*10^-8*T + 1.2*10^-10*T^2)*Cs^2)*k_w;
```

```
function c_f_a = cf_a(T)
% % Model: Jamieson (1969): Specific heat capacity of
% % sea water correlation.

% The salinity for (Cs = 3.5 wt%) NaCl in solution:          % [g/kg]
S = 35;

% Convert temperature:                                       % [K]
T = T+273.15;

% Model coefficients:
a1 = 5.328 - 9.76*10^-2*S + 4.04*10^-4*S^2;
a2 = -6.913*10^-3 + 7.351*10^-4*S - 3.15*10^-6*S^2;
a3 = 9.6*10^-6 - 1.927*10^-6*S + 8.23*10^-9*S^2;
a4 = 2.5*10^-9 + 1.666*10^-9*S - 7.125*10^-12*S^2;

% Calculating the annulus fluid specific heat capacity:     % [J/kg-K]
c_f_a = (a1 + a2*T + a3*T^2 + a4*T^3)*10^3;
```

```
function k = k_csg(T)

% % Model: Furrer (2010): Thermal conductivity correlation for
% % alloy 316 stainless steel:

% Convert temperature from Celcius to Kelvin:                % [K]
T = T + 273.15;
```

```
8
9  % Thermal conductivity as function of temperature.        % [W/m-K]
10 k = 6.31 + 27.2*10^(-3)*T - 7*10^(-6)*T^2;
```

```
1  function k = k_cement(T)
2
3  % % Model: Santoyo et al. (2001b): Thermal conductivity
4  % % temperature correlation for set cement
5  % % ("Cement system D")
6
7  % Convert temperature:                                    % [K]
8  T = T + 273.15;
9
10 % Calculate thermal conductivity of cement:               % [W/m-K]
11 k = 0.50442 + 0.0003125*T;
```

```
1  function Cj = JT_coeff(rho_f_t,c_f_t,beta_o,T_f)
2
3  % Calculating Joul-Thompson coefficient, Cj:              % [K/Pa]
4  Cj = -(1/(rho_f_t*c_f_t))*(1-T_f*beta_o);
```

```
1  function phi = phi_parameter(Cj,c_f_t,deltaP_fric,deltaP_stat,...
2      deltaP_kin,v,v_prev)
3
4  % The pressure loss per length pipe:                      % [Pa/m]
5  deltaP = deltaP_fric+deltaP_stat+deltaP_kin;
6
7  % Calculating the "phi" parameter:                        % [K/m]
8  phi = Cj*deltaP-(v/c_f_t)*(v-v_prev);
```